OTA Performance Evaluation of MIMO Terminals with Multipath Simulator

Gao, Xiang; Wang, Xiaoguang

2010

Document Version:
Other version

LUND UNIVERSITY & SONY ERICSSON MOBILE COMMUNICATIONS AB

OTA Performance Evaluation of MIMO Terminals with Multipath Simulator

Xiang Gao and Xiaoguang Wang

Supervisor: Thomas Bolin
Examiner: Buon Kiong Lau

2010/5/25

Abstract

With the ever growing requirement for higher data rates, terminals supporting multiple-input multiple-output (MIMO) technologies (or MIMO terminals) are being developed for the beyond-3G wireless communication systems such as HSPA and LTE. To ensure that the terminals are capable of delivering the promises of MIMO technology, test systems for the performance evaluation of MIMO devices are needed. In recent years, over-the-air (OTA) testing is adopted as a test system since it is a more realistic way of specifying terminal RF performance than the conventional conductive test method. Whereas the OTA test system for single-antenna terminals has been standardized, the test method for MIMO terminals is currently being developed.

This thesis introduces a test method called Multipath Simulator (MPS) Method, which is one of the currently proposed methodologies for evaluating the OTA performance of MIMO terminals, and analyzes important aspects that need to be considered when this method is used in the development of a MIMO OTA test system. Channel model is one of the most important aspects for the MIMO OTA test system. Spatial channel models including SCM, SCME and WINNER models are described and compared in the thesis. Based on the analysis, a suggestion on the appropriate channel model is given.

According to the MPS Method, the MIMO OTA test system uses both multipath simulator (MPS) and spatial fading emulator (SFE) to generate spatial-temporal multipath propagation channels. To investigate the architecture of MPS and SFE which can satisfy the MIMO OTA test requirements, a MATLAB simulation system is developed. Based on the MATLAB simulations, simplification of the channel models that reduces cost and complexity of the test system is studied. Methods and criteria to simplify the channel models are also described. The configuration for the SFE such as the number of antenna probes and the effective test area are also studied through the simulation system. Lastly, the optimized configuration parameters for MPS and SFE are tabulated and the capacities for the given MIMO terminals in the chosen scenarios are plotted.

Acknowledgements

We would like to express our gratitude to many people who have helped us during the work of our master thesis. First of all, we would like to thank our supervisor Mr. Thomas Bolin at SEMC and examiner Dr. Buon Kiong Lau at Lund University for their instructions on our work and for their time of discussions. Mr. Thomas Bolin has provided us a comfortable working environment and a lot of useful information and suggestion so that we can go on well with our thesis. We are really grateful for this opportunity to work in Sony Ericsson Mobile Communications (SEMC) AB, Lund. We are also deeply thankful to Dr. Buon Kiong Lau, who has spent a lot of time to help us solve the problems we encountered in our work and kept giving us scientific guidance and inspiration throughout our study.

We would like to thank Mr. Paul Hallbjörner and Mr. Jan Welinder from SP Sweden for the enlightening discussions on the thesis work. We would also like to thank Mr. Zhinong Ying and Ms. Vanja Plicanic at SEMC. They have provided us a lot of help, and their kindness and professionalism have greatly impressed us. We appreciate the time to work with them. And many thanks to Mr. Ruiyuan Tian and Mr. Mikael Håkansson for their help and support.

Finally, we would like to express our gratitude to Lund University for the great study environment and chances to communicate with all the wonderful professors. The study life here is a cherishable memory for us.

List of Acronyms and Abbreviations

3GPP	Third Generation Partnership Project
AoA	Angle of Arrival
AoD	Angle of Departure
AS	Angular Spread
ASA	Angular Spread of Arrival
ASD	Angular Spread of Departure
B3G	Beyond-3G
BER	Bit Error Rate
BLER	Block Error Rate
BS	Base Station
CDL	Clustered Delay Line
CIR	Channel Impulse Response
CQI	Channel Quality Indicator
DS	Delay Spread
DUT	Device under Test
FOM	Figure of Merit
FRC	Fixed Reference Channel
GSCM	Geometry-based Stochastic Channel Model
HARQ	Hybrid Automatic Repeat Request
HSPA	High Speed Packet Access
LOS	Line of Sight
LTE	Long Time Evolution
MIMO	Multiple Input Multiple Output
MPC	Multipath Component
MPS	Multipath Simulator
MS	Mobile Station
OTA	Over-the-Air
PAS	Power Azimuth Spectrum
PDP	Power Delay Profile
RAN	Radio Access Network
RF	Radio Frequency
RMS	Root Mean Square
RX	Receiver
SCM	Spatial Channel Model
SCME	Spatial Channel Model Extension
SFE	Spatial Fading Emulator
SNR	Signal-to-Noise Ratio
TDL	Tapped Delay Line
TRP	Total Radiated Power

TRS	Total Radiated Sensitivity
TX	Transmitter
WINNER	Wireless World Initiative New Radio
XPR	Cross Polarization Ratio

Contents

Chapter 1 Introduction

The requirement for higher data transmission rates is constantly promoting the evolution of existing wireless communication systems. On the other hand, multiple-input multiple-output (MIMO) technology, which facilitates array gain, diversity gain, spatial multiplexing and interference reduction [1], can bring about high data rates, reliable wireless communication link and good coverage. Therefore, it is not surprising that it is keenly adopted in many existing and upcoming wireless communication standards, including HSPA, HSPA Evolution, WiMAX, LTE and LTE Advanced.

In MIMO system implementation, the performance evaluation of multiple-antenna terminals (MIMO terminals) is an important aspect, since good terminal performance is necessary to achieve good performance in the overall MIMO system. In order to ensure that a terminal is capable of delivering the promises of MIMO technology in HSPA and LTE systems, the development of test method for MIMO terminals is an ongoing task of 3GPP RAN4, in liaison with CTIA and EU COST Action 2100.

1.1 Background and Motivation

In 2G and 3G communication systems, the performance of single-antenna terminals is assessed through a set of figures of merit (FOMs), such as maximal transmit power, receiver sensitivity and bit error rate (BER), by connecting an RF cable between the device under test (DUT) and the test equipments. Although such a conductive test method is controllable and repeatable, the use of an RF cable fails to emulate the effect of real terminal antennas. Over-the-air (OTA) test is then introduced as a more realistic way of specifying terminal RF performance. OTA test system for single-antenna terminals has been standardized, and FOMs such as total radiated power (TRP) and total radiated sensitivity (TRS) are used for performance evaluation [2].

Although the OTA test system for single-antenna terminals can reflect more realistic performance of the DUTs in the field than the conventional conductive test method, it is not suitable to evaluate the performance of MIMO terminals, since it makes no attempt to introduce an OTA multipath channel with spatial characteristics. Given that MIMO fundamentally relies on the multipath channel and the decorrelation between multiple antennas to improve the capacity of a wireless network [2], the test system for MIMO terminals should include both temporal and spatial characteristics of the propagation channel.

MIMO OTA is defined in [2] as OTA radiated performance measurement of MIMO terminals in active mode in both uplink and downlink. To evaluate the performance of MIMO terminals, a MIMO OTA test is necessary. A MIMO OTA test system should be able to emulate real world channel propagation conditions in a controllable and repeatable fashion and to differentiate between a “good” MIMO mobile terminal and a “bad” MIMO mobile terminal.

1.2 MIMO OTA Measurement Campaign

1.2.1 Methodologies

Currently, scientific research collaboration within the EU COST Action 2100 Subworking Group (SWG) 2.2 is ongoing to determine one or more feasible and realizable methodologies to measure the OTA performance of MIMO terminals. Many companies participate in this collaboration, such as Elektrobit, Spirent Communications, Sony Ericsson Mobile Communications, Agilent, DoCoMo etc. So far, several methodologies have been proposed and extensively discussed in COST2100 SWG 2.2 meetings (see e.g., [3],[4]-[8]). The details of these proposed methodologies are presented in [9]. The names of these methodologies are listed below:

1. Elektrobit-SATIMO-Nokia Stargate Fading Emulator Method
2. Spirent's Joint Channel-Chamber Method
3. SP Sweden-Sony Ericsson MPS Method
4. Werner's 2-stage Method
5. Rohde&Schwarz 2-Channel Method
6. Agilent's 2-stage MIMO OTA Method
7. TIT-Panasonic RF Spatial fading Emulator Method
8. NTT DoCoMo's Simplified MIMO OTA Method
9. Bluetest Reverberation Chamber Method

All the above methodologies, except No. 9, are based on measurements performed inside an anechoic chamber. A tentative MIMO OTA test system configuration is shown in Figure 1.1. It is noted that the blue triangles (representing absorbers) fully cover all sides of the chamber, as in a typical anechoic chamber. However, not all are included in the figure, so that the detailed features of the test setup within the chamber can be more clearly illustrated.

From Figure 1.1, we can see that the test system includes two main parts: a MIMO fading emulator, which emulates the multipath fading channel, and an array of antenna probes inside the anechoic chamber, which replicates the spatial characteristics of the channel. The transmit signals from the base station (BS) emulator are convolved with the MIMO fading channel and then fed to the antenna probes. The antenna probes can then emulate the angles of arrival in the downlink signal. We refer to this part is as spatial fading emulator (SFE).

The design of the MIMO OTA test system in these methodologies can be divided into two categories in terms of whether the multichannel emulator is realized in baseband, or directly in RF, such as the Multipath Simulator (MPS) method proposed by SP Sweden and Sony Ericsson. Likewise, the SFE can be implemented differently, through the use of different multi-probe configurations. One popular configuration of the SFE uses a ring of antenna probes as shown in Figure 1.1.

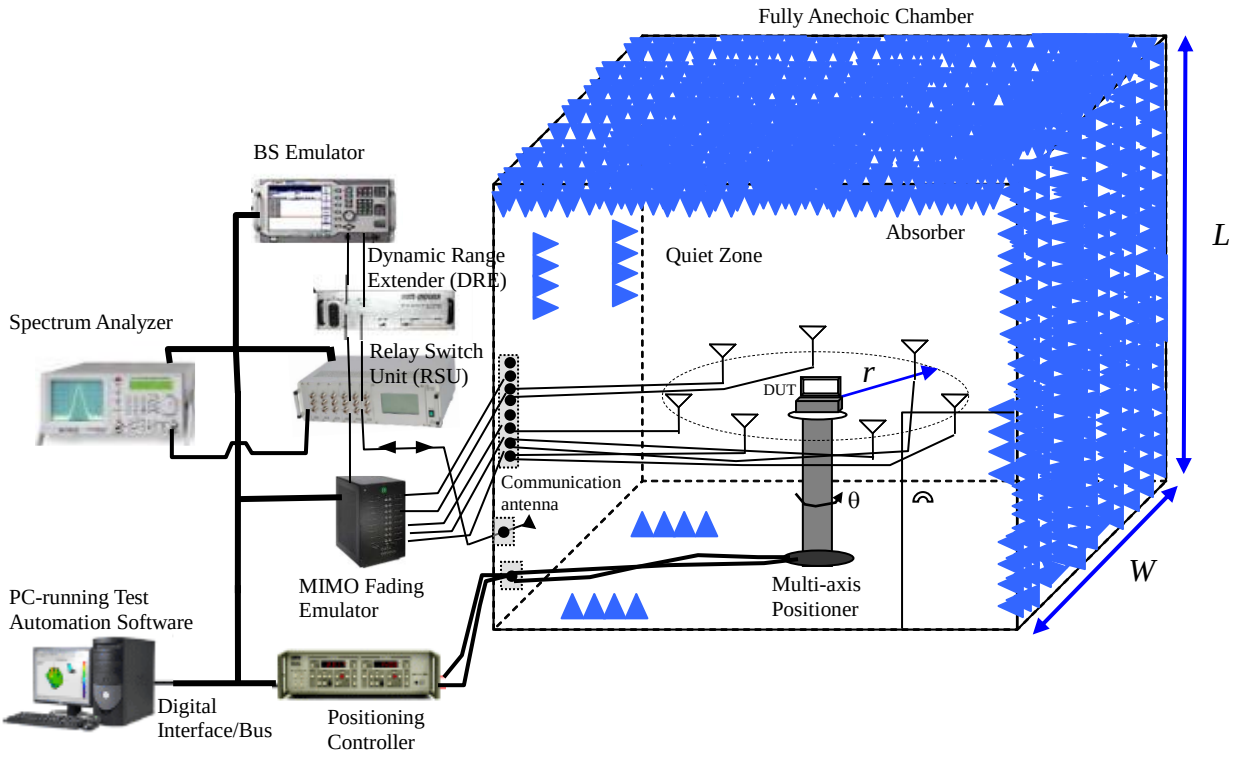

Figure 1.1: Tentative MIMO OTA test system configuration [2].

1.2.2 Guidelines

In order to ensure that consistent MIMO OTA results can be obtained and compared among all the proposed methodologies, these methodologies should meet a set of general guidelines as given in Table 1.1.

The current methodologies have mainly been studied theoretically, although in some cases, preliminary experiments have been performed. Therefore, much work remains in the development of a comprehensive test system. The MIMO OTA measurement campaign, which is a scientific collaboration between members of COST2100 SWG 2.2, is aimed at evaluating and comparing the performance of the aforementioned proposed MIMO OTA measurement methodologies.

1.2.3 Figures of Merit

The MIMO OTA performance is assessed based on a set of measurable FOMs. These FOMs are designed to reflect the user experience when MIMO terminals are used in practical mobile networks [2]. The FOMs to be used for the measurement of MIMO OTA performance are shown in Table 1.2.

Table 1.1: General criteria of MIMO OTA measurement methodology [2].

Guideline No.	Description
1	The MIMO OTA measurement methodology should be able to obtain realistic MIMO performance, and shall capture important aspect of MIMO performance as expected by user or actual field operation.
2	The MIMO OTA measurement methodology should be able to support HSPA MIMO and receive diversity devices, as well as LTE MIMO devices.
3	The MIMO OTA measurement methodology should be able to cover a wide range of carrier frequency range for both HSPA and LTE DUTs operated in MIMO modes.
4	The MIMO OTA measurement methodology should be able to support various scalable HSPA and LTE channel bandwidth.
5	The MIMO OTA measurement methodology should be able to measure the OTA performance of HSPA MIMO devices operating in receive diversity mode.
6	The MIMO OTA measurement methodology should be able to derive the necessary figures of merit (FOMs) using a minimum set of test permutations and MIMO channel models.
7	The MIMO OTA measurement methodology should be able to achieve repeatable figures of merit through the controlled/shielded test environments so that different terminal performance can be compared and verified.
8	The MIMO OTA measurement methodology should achieve fast figures of merit measurement (i.e. fast testing time).
9	The MIMO OTA measurement methodology should be cost effective such that the test cost per terminal can be kept low.
10	The MIMO OTA measurement methodology should be able to perform active MIMO OTA measurement, where DUT can establish active radio connection with the test system.
11	The MIMO OTA measurement methodology should be able to provide end-to-end performance of MIMO devices in active mode.

Table 1.2: Figures of Merit [2].

Category	I	II	III	IV	V
FOMs	MIMO Throughput CQI BLER (FRC)	TRP TRS	Gain Imbalance Spatial correlation MIMO Capacity	Antenna Efficiency MEG	MIMO Throughput (VRC)
Subject	OTA	OTA	MIMO Antennas	MIMO Antennas	OTA
Methodology	Active (with fading)	Active	Passive	Passive/Active	Active (with fading)

The priority level of each category of FOMs decreases from Category I to Category V. We can see that the FOMs of MIMO Throughput, CQI and BLER for the Fixed Reference Channel (FRC) are the most important parameters to evaluate the OTA performance of a MIMO terminal. However, it is difficult to obtain these parameters using a software simulation system since these parameters are not only dependent on the propagation channel, but are also affected by a number of other factors,

including communication protocols, modulation/coding and receiver solutions. As the goal of the software simulation system developed in this thesis is to generate the channel matrix which can be used to interface with software simulator of HSPA or LTE link level simulator *and* provide the parameters such as delays, values of attenuation and phase shifts for the hardware system, we focus on Category III, especially MIMO capacity, to investigate whether candidate channel models for the test system can be simplified but still retain the main characteristics of the original full model. If the change in the capacity by going from the full model to the reduced model lies within a small range, then we consider that the channels are practically the same for our purpose. Consequently, the corresponding reduced channel model can then be employed in the test system.

1.3 Objectives

The primary goal of this thesis is to provide technical support in the development of MIMO OTA test system to evaluate the OTA performance of MIMO terminals in different scenarios for HSPA and LTE systems. The MIMO OTA test system should meet the requirements listed in Table 1.1 and be able to distinguish the performance of different MIMO terminals. The support includes:

1. To develop simulation software which is flexible enough to study the merits of the used channel models with different level of complexity.
2. To optimize parameters of the used channel models in order to reduce the cost and complexity of the MIMO OTA test system.
3. To provide parameters for the hardware configuration, such as the number of delay lines and the values for phase shifters and attenuators.
4. To investigate the appropriate SFE architecture, including the number of antenna probes, the positions of probes and the effective area of the test zone.
5. To produce the channel matrix for a given MIMO terminal with measured 3D radiation patterns.

1.4 Organization

The thesis is organized into five chapters. After the introduction, Chapter 2 gives the description of the MPS Method, including the principles of the method and the system configuration.

In Chapter 3, all spatial channel models related to beyond-3G (B3G) MIMO simulations are introduced and compared. Based on the analysis, a proposal is given on the model(s) to be used in the test system – first in software simulations (as has been done in this thesis), and then in hardware implementation.

Chapter 4 explains the software simulation system, including the system structure, simulation parameters, models and scenarios used in the simulations, and the procedure to generate the channel matrix. Then the simplifications of the channel models are performed and the simulation results are analyzed. Lastly, the simplified model parameters are given in tables.

Chapter 5 concludes the thesis and lists some future work.

1.5 Contributions

The contributions of this thesis are listed below:

- A MATLAB simulation system is built, and it can be used to analyze any clustered delay line (CDL) based channel models as long as the channel parameters are provided in the required format.
- Procedures to simplify the channel models are provided and analyzed. These procedures are generic for any CDL model.
- Channel parameters for the chosen scenarios are optimized and determined for the hardware implementation. Time and cost to develop the MIMO OTA test system are saved by using the results of the software simulations.
- An appropriate SFE architecture is proposed and the effective area of the test zone is determined.
- The channel models for MIMO OTA test are described and compared. This is helpful for choosing proper channel models for the upcoming measurement campaign.
- The channel matrix for a given MIMO terminal is obtained, and it can be used with software simulator of HSPA or LTE system to analyze the system performance.

Chapter 2 Multipath Simulator Methodology

The Multipath Simulator (MPS) Method, which is proposed by SP Sweden and Sony Ericsson, is adopted in this thesis to realize the MIMO OTA test system. This method is conceptually simple, since multipaths are generated via dedicated RF chains. More important, it can be cost-effective, since it performs the multichannel emulation directly in RF, without having to convert the RF signals from BS emulator into baseband signals for processing and converting them back into RF signals for OTA transmission.

2.1 Principle

The principle of the MPS is to emulate the multipath propagation and fading of the transmit signals over the radio channel between a transmitter (TX) and a receiver (RX or DUT). In this method, as illustrated by the hardware setup in Figure 2.1, the MIMO propagation channel is generated by the usage of delay lines, phase shifters, attenuators, and splitters/combiners. The delay lines are used to realize the different delays of the multipath components (MPCs). The base station signals are split into a set of path signals which are transmitted through the delay lines to create the MPCs. Since the runtime difference between the MPCs in the real world changes with time due to the movement of the RX and/or non-stationarity of the surrounding environment, the RX should then "see" time-varying fading, which in this setup is produced by using the phase shifters. The amplitudes of the multipath signals are controlled by the attenuators.

After the above process, the multipath signals are distributed to an array of antenna probes, which are used to create the spatial characteristics of the MIMO propagation channel. The probes are built into an azimuth ring structure to produce the angles of arrival (AoAs) corresponding to the probe directions. When measuring, the DUT is located within a test zone at the center of the antenna ring so that the signals from all the probes reach the DUT over similar OTA distances. The combined multipath signals then emulate a multipath environment where Doppler spectrum, maximum Doppler shift, delay spread and the statistical properties of MIMO channel can be controlled and reproduced.

2.2 Description

The MPS Method consists of the following components as shown in Figure 2.1:

1. Base station simulator to generate the LTE or HSPA RF signal.
2. Splitters/combiners to split and/or combine the RF signals.
3. Delay lines to create the multipath delay effect.
4. Phase shifters to create the Doppler shift effect.
5. Attenuators to control the amplitude of each path.
6. Anechoic chamber, equipped with multiple antenna probes (i.e., the SFE components).

This setup of this method is illustrated in the diagram below.

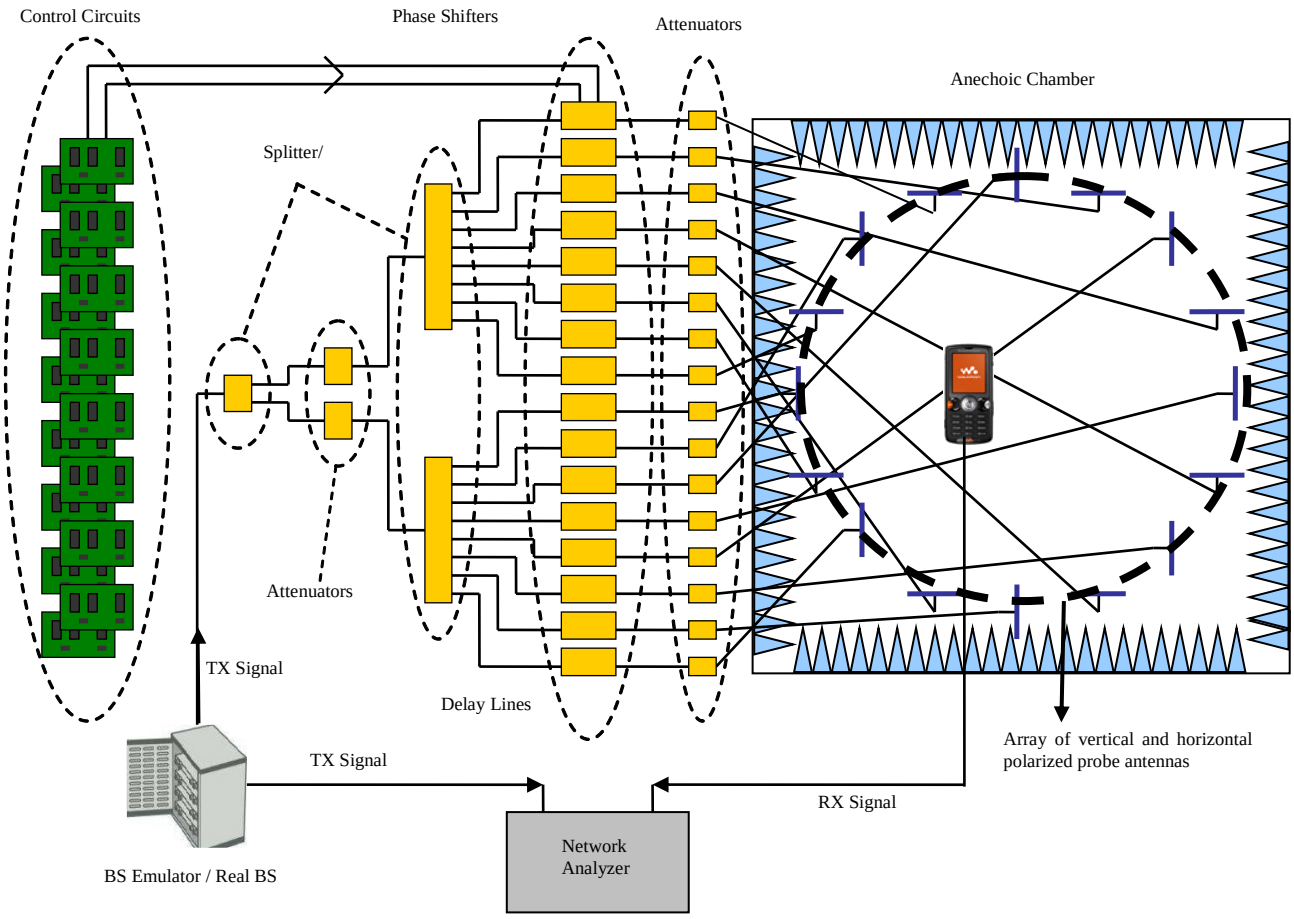

Figure 2.1: System setup and configuration of SP-Sony Ericsson method [9].

In Figure 2.1, the MPS is used to generate the multipath propagation channel of the wireless communication system and works independently from modulations and protocols both for the uplink and the downlink. The original RF signal generated by the BS emulator is split up to a number of rays (i.e. path signal components) which are passed to different delay lines to create the multipath delay effect. Each delay line is connected with a phase shifter for generating the individual phase and Doppler shift for each path signal. Attenuators are used to control the amplitudes of the path signals to realize the given power delay profile.

A set of antenna probes are placed to form a ring structure, where the DUT is located within a test zone at the center of the structure. The radiation field generated at the DUT position is the sum of the direct rays from the probes, together with some contributions from fields scattered from antenna probes, antenna supports, chamber walls, etc. Thus, the radiation field can be controlled by the geometry layout of antenna ring, chamber requirements, attenuation and delay and Doppler shift of each ray. The appearance of an 8-probe realization of the antenna ring in reality is shown in Figure 2.2.

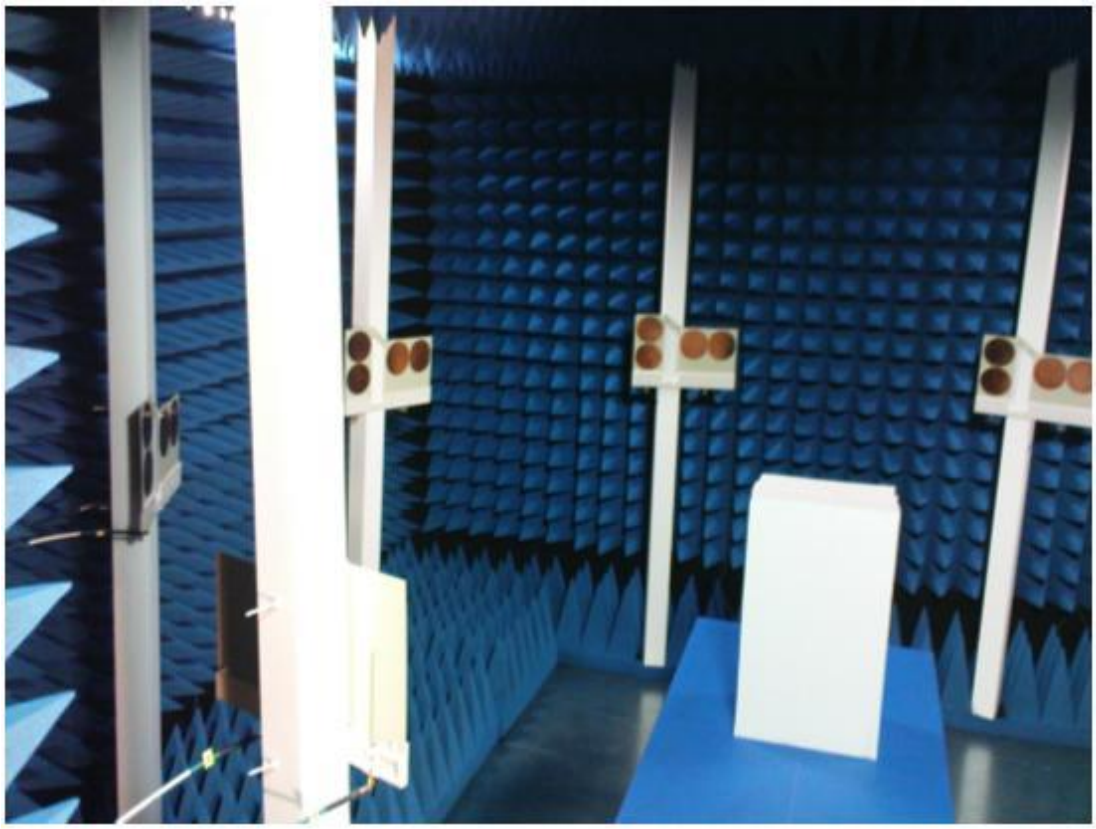

Figure 2.2: Antenna probes in the anechoic chamber.

From Figure 2.2, we can see that several pairs of wideband antenna probes are placed in a circular arrangement inside an anechoic chamber. Each pair consists of a vertical antenna and a horizontal antenna to emulate the two polarizations of the signal path at the receive end of the channel.

The radius of the antenna ring affects the scattering and the scattered fields will decrease as the radius becomes larger. Increasing the number of antennas will make it possible to control the propagation conditions in more detail but will increase cost and scattering.

The optimal geometrical layout of the antenna ring depends on detailed requirements, e.g. angular resolution, statistical properties, uncertainty in the field level and cost. Section 4.3.1 investigates and gives suggestion on the appropriate layout of the antenna probe ring.

Chapter 3 Spatial Channel Model

Propagation channel models play a very important role in the performance evaluation and comparison of MIMO terminals. There are three kinds of spatial channel models considered for beyond-3G (B3G) MIMO simulations: 3GPP Spatial Channel Model (SCM), its extension (SCME), and models developed under the European WINNER project [10]. The basic modeling philosophy behind these models is the same: the sum of specular components is used to describe the changes in the channel impulse response (CIR) between each transmit and receive antenna element (so called sum-of-sinusoid method). All these channel models support the MIMO concept due to the different channel characteristics obtained from different spatial positions of elements inside the transmit/receive antenna array [10]. However, these models have different features/limitations and are suitable for different kinds of simulations. The description and comparison of these models are given in the following sections.

3.1 The Properties of SCM

The SCM was developed in 3GPP/3GPP2 ad hoc group for spatial channel, the scope of which is to develop and specify parameters and methods associated with the spatial channel modeling that are common to the needs of the 3GPP and 3GPP2 organizations [11]. The SCM includes link-level and system-level channel models and only the system-level model can be used to compare the performance of *different* algorithms.

The link-level model is the simple tapped delay line (TDL) model defined only for calibration, which is the comparison of performance results from different implementations of a *given* algorithm. This model cannot be used for algorithm comparison because it reflects only one snapshot of the channel behavior and does not account for system attributes such as scheduling and HARQ (Hybrid Automatic Repeat Request). In [2], the link-level TDL model is suggested for the OTA test of HSPA receive diversity.

The system-level model is the geometry-based stochastic channel model (GSCM) and for use in the system-level simulations. Three environments are defined: Suburban Macro-cell, Urban Macro-cell and Urban Micro-cell. The environment parameters are given in [11]. Every scenario has 6 paths and each path consists of 20 sub-paths. The paths in the SCM are defined by their powers and delays, and the 20 sub-paths of each path have identical powers but different phases and departure/arrival angles. The phases of the sub-paths are i.i.d phases drawn from a uniform distribution within the range of 0 to 2π. The relative angle offsets of the sub-paths are listed in [11].

The procedure to derive the user parameters is provided in [11]. Parameters such as the path delays, powers, and angles of departure (AoDs) and arrival (AoAs) are random variables drawn according to different distributions. These channel parameters evolve in time and undergo fast fading due to

the motion of the mobile stations (MSs) during a drop, where a "drop" is defined as a simulation run for a given number of cells/sectors, BSs, and MSs, over a specified number of frames, while the bulk parameters including angular spread, delay spread, shadowing, and MS location remain fixed.

In addition, the line of sight (LOS) condition is defined in SCM system-level models, but only for the Urban Micro scenario, since the probability of LOS occurrence is very low in the Suburban or Urban Macro cases. The SCM also provides polarization modeling. It defines that each path experiences an independent realization of the cross polarization ratio (XPR) drawn from given distributions and each path has two XPRs, where the V-to-H XPR draws are independent of the H-to-V draws.

3.2 New features of SCME

SCME is the name for the extended version of SCM. The extensions are developed by and used within the European WINNER project, which aims to define the concept of beyond-3G (B3G) wireless communication systems with channel bandwidth of up to 100 MHz and radio frequencies between 2 and 6 GHz [12],[13]. For initial purposes, WINNER selected the 3GPP/3GPP2 SCM and the IEEE 802.11 TGn models [14] respectively for outdoor simulations and indoor simulations. Since the SCM was defined for a 5 MHz bandwidth CDMA system in the 2 GHz band and hence not suitable for WINNER simulations, WINNER Work Package 5 (WP5) performed some modifications and extensions to the SCM. The first extension of the original model was released in 2005 under the name SCME [10]. The SCME is a comprehensive spatial channel model for 2 and 5 GHz frequency bands and supports bandwidths of up to 100 MHz. The detailed description of the extensions is given in [15]. We present here some primary features that make SCME suitable for B3G MIMO simulations.

3.2.1 Bandwidth Extension

To support a bandwidth of 100 MHz, the SCME adds intra-path delay spread (DS), which is zero in the SCM. The path DS is chosen to keep the error in power between an exponential power delay profile (PDP) and the SCM definition (no path DS) to be within an acceptable range. A path DS of 10 ns is set for all paths since the power error is below -20 dB and can be considered reasonably small. Each path in the SCM with 20 sub-paths is subdivided into 3 or 4 zero-delay mid-paths, which are moved to different delays relative to the original path. The number of mid-paths, the power and delay parameters are given in Table 3.1.

Table 3.1: Mid-path power-delay parameters [15].

Scenario		Suburban Macro, Urban Macro		Urban Micro	
No. mid-paths per path		3		4	
Mid-path power and delay relative to paths (ns)	1	10/20	0	6/20	0
	2	6/20	7	6/20	5.8
	3	4/20	26.5	4/20	13.5
	4	-	-	4/20	27.6

Table 3.1 shows that the path in Macro scenarios is split into 3 mid-paths while the path in Urban

Micro scenario is divided into 4 mid-paths, but both with the constraint of 10 ns path DS.

3.2.2 Frequency Range

The SCME is for the 2 and 5 GHz frequency bands while the SCM is only for the 2 GHz frequency band. It is found that the different frequency ranges contribute to different gains in the free-space path-loss. The path-loss at 5 GHz frequency band is 8 dB higher than that at 2 GHz frequency band. Thus, the SCME proposed a 5 GHz path-loss model that has an offset of 8 dB relative to the 2 GHz model. Additionally, the COST-Walfish-Ikegami-Model (COST-WI) [18], which is only used for the Urban Micro scenario in the SCM, is applied for all the SCME scenarios, since the usage of higher frequencies decreases the coverage area. The path-loss model used in SCME is detailed in [15].

Besides the effect on the path-loss, the 5 GHz frequency band also causes different decay rate of the PDP compared to 2 GHz in Urban and Suburban Macro scenarios. Therefore, the SCME proposes RMS delay spread values based on a 5 GHz measurement analysis. Other parameters, such as the K-factor and the shadowing parameters are kept the same as those of the 2 GHz band.

3.2.3 LOS for All Scenarios

In the SCM, the LOS condition is only an option for the Urban Micro scenario. The SCME extended the K-factor option to cover both Macro scenarios. Urban and Suburban Macro are assigned the same parameters. The probability of having LOS is given by [15]

$$P_{LOS} = \left(1 - \frac{h_B}{h_{BS}}\right) \cdot \left(1 - \frac{d}{d_{co}}\right), d_{co} < 300, h_{BS} > h_B \,,$$

and is zero otherwise. h_{BS} is the BS height, h_B is the average height of the rooftops, and $d_{co}$is the cut-off distance. The K-factor model is $K = 15.4 - 5.0 \cdot \log_{10}(d)$, where d is the BS-MS distance and the following parameters are assumed: MS antenna height of 1.5 m, MS beamwidth of 360°, and selected season is summer.

3.2.4 Tapped Delay Line (TDL) Model

The SCME provided a reduced variability TDL model with fixed path powers, path delays, departure/arrival angles of cluster and intra-cluster taps. This model is similar to the SCM link-level model, but it is close to the system-level model and can be used to compare the performance of different algorithms. The parameters of the TDL model are given in Table 3.2.

.

The TDL model defines 6 paths, as in the SCM. It is backward-compatible with the original SCM, which means that when its results are down-sampled to 5 MHz, the channel characteristics are equivalent to those retrieved from the SCM. In other words, if this model is used in systems with bandwidth greater than 5 MHz, up-sampling should be performed and the intra-cluster delay spread should be added. With intra-cluster delay spread, each path will have 3 mid-paths in Macro scenarios and 4 mid-paths in Urban Micro scenario.

Table 3.2: Tap delay line parameters [15].

Scenario		Suburban Macro		Urban Macro				Urban Micro	
Power-delay parameters: relative path power [dB] / delay [μs]	1	0	0	0		0		0	0
	2	-2.67	0.14	-2.22		0.36		-1.27	0.28
	3	-6.21	0.06	-1.72		0.25		-2.72	0.20
	4	-10.41	0.40	-5.19		1.04		-4.30	0.66
	5	-16.47	1.38	-9.05		2.73		-6.01	0.81
	6	-22.19	2.83	-12.50		4.60		-8.43	0.92
Resulting total DS [μs]		0.231		0.841				0.294	
Path AS at BS, MS [°]		2.35		2.35				5.35	
Angular parameters: AoA /AoD [°]	1	156.15	-101.34	65.75	81.97	76.48	-127.28	0.70	6.61
	2	-137.2	-100.86	45.65	80.54	-11.87	-129.97	-13.23	14.13
	3	39.34	-110.96	143.19	79.62	-14.57	-136.81	146.07	50.83
	4	115.16	-112.99	32.51	98.63	17.71	-96.22	-30.55	38.40
	5	91.19	-115.51	-91.06	102.13	167.66	-159.60	-11.44	6.67
	6	4.68	-118.07	-19.17	107.06	139.08	173.19	-1.06	40.28
Resulting total AS at BS, MS [°]		4.70, 64.78		7.87, 62.35		15.76, 62.19		18.21, 67.80	

3.3 WINNER Models

Although WINNER Work Package 5 (WP5), which is focused on multi-dimensional radio channel modeling, performed some modifications and implemented the extended SCM model (SCME), it is still not good enough for the more advanced simulations [16]. To meet the requirements of the evaluation of B3G systems, the WINNER channel models were then developed. The development of the WINNER models was performed in two phases: WINNER Channel Model-Phase I (WINNER I) and WINNER Channel Model-Phase II (WINNER II). The channel models from the two phases follow the same channel modeling approach (i.e., geometry-based stochastic channel modeling approach) and both are based on measurement data.

The WINNER II models are evolved from the WINNER I models and it includes new features such as frequency range extension, addition of new scenarios, treatment of the LOS component as a random variable, and scatterer movement in fixed connections. Model parameters of WINNER I have been revised and updated according to new results and proposals from partners within the WINNER II work package and various standardization bodies. The features of the WINNER I models and the WINNER II models are compared in Table 3.3.

Since WINNER II models have extended features and support more scenarios, we choose these models in this thesis for the simulation study.

Table 3.3: Comparison of Features of WINNER I and WINNER II models

Feature	**WINNER I**	**WINNER II**
Frequency range	5 GHz	2-6 GHz
Bandwidth	100 MHz	100 MHz
Number of sub-paths per cluster	10	20
Number of main scenarios	7	14
Indoor-to-outdoor and outdoor-to-indoor models	No	Yes
Time evolution	No	Yes
Reduced variability CDL model for calibration, comparisons and fast simulations	Yes	Yes
CDL analyzed from measured PDP	Yes	No
CDL based on expectation values of generic model	No	Yes
Intra-cluster delay spread	No	Yes
LOS as random variable	No	Yes
Moving scatterers	No	Yes

3.3.1 Generic Model

The WINNER II Generic Model is a system level model. It can describe an arbitrary number of propagation environment realizations for single or multiple radio links for all the defined scenarios for desired antenna configurations by different parameter sets [17]. The generic model is a stochastic model controlled by two levels of parameters: large-scale parameters and small-scale parameters.

Parameters such as delay and angular spreads, shadow fading standard deviation and Rician K-factor are called large-scale parameters, since they are considered as an average over a typical channel segment, i.e., a distance of some tens of wavelengths. These parameters are drawn randomly from tabulated distribution functions. Small-scale parameters like delays, powers and directions of arrival and departure are drawn randomly according to tabulated distribution functions and random large-scale parameters. All of these parameters have been specified from measurement results or found from existing literature.

WINNER II continues to use the name “cluster” for a one-path signal. In the terminology of [17], a cluster is defined to be a propagation path diffused in space, either or both in delay and angle domains. Number of rays per cluster has been selected to be 20, as in SCM and SCME.

The geometrical setup in WINNER II is fixed and only the initial phases of the scatterers are free random variables. By randomly picking different initial phases, a number of different realizations of the model can be generated.

The parameters for generic model are given in [17]. For simplicity, these parameters are assumed not to depend on distance.

3.3.2 Clustered Delay Line (CDL) Model

The WINNER Generic Model is the most accurate model aiming to be applicable for many different simulations and to cover a large number of scenarios with several combinations of large-scale and small-scale parameters. However, in some simulations, simplification or approximation of the channel models can be done to reduce the simulation complexity and save simulation time.

The clustered delay line (CDL) model is reduced-complexity channel model that has fixed large-scale and small-scale parameters. It is created for calibration and rapid comparison of different simulations. The CDL model does not only have the characteristics of the well-known TDL class of fading channel models, but it also has the multipath AoD and AoA information to address the needs of MIMO channel modeling. The parameters of the CDL model are based on expectation values of the generic model.

In the CDL model, a cluster is centered at each tap (or each nominal signal path) and each cluster is comprised of the vector of equal-powered MPCs (sinusoids) that have the same, or close to same, delay. The MPCs within one cluster have varying phases but fixed AoA and AoD offsets, which depend on the angular spreads at the MS and the BS, respectively. The offset angles of each cluster are defined by the Laplacian power azimuth spectrum (PAS), values of which for 1° root mean square (RMS) angular spread are shown in Table 3.4.

Table 3.4: Ray offset angles within a cluster, given for 1° RMS angular spread [17].

Ray index	Basis vector of offset angles
1,2	± 0.0447
3,4	± 0.1413
5,6	± 0.2492
7,8	± 0.3715
9,10	± 0.5129
11,12	± 0.6797
13,14	± 0.8844
15,16	± 1.1481
17,18	± 1.5195
19,20	± 2.1551

Doppler information is not specified explicitly for the CDL models, since it is determined by the AoAs of the MPCs, MS speed and direction, and the specified antenna patterns at the MS and BS.

3.4 Comparison of the Spatial Channel Models

The MIMO OTA test system in this thesis aims to evaluate the performance of MIMO terminals in HSPA and LTE systems, thus supported bandwidth of up to 20 MHz is required. The SCME and WINNER models both satisfy this requirement. The SCM is not suitable, due to its 5 MHz bandwidth. The feature and parameter comparisons of these models are shown in Table 3.5 and Table 3.6.

Table 3.5: Comparison of features.

Feature	**SCM**	**SCME**	**WINNER II**
Bandwidth ≥ 100 MHz	No	Yes	Yes
Indoor scenarios	No	No	Yes
Outdoor-to-indoor scenario	No	No	Yes
AoA/AoD elevation	No	No	Yes
Intra-cluster delay spread	No	Yes	Yes
TDL model based on the generic model	No	Yes	Yes
Time evolution of model parameters	No	Yes	Yes

Table 3.6: Comparison of parameters.

Parameter	**SCM**	**SCME**	**WINNER II**
Max. bandwidth [MHz]	5	100*	100**
Frequency range [GHz]	2	2-5	2-6
No. of scenarios	3	3	12
No. of clusters	6	6	8-20
No. of mid-paths per cluster	1	3-4	1-3
No. of sub-paths per cluster	20	20	20
No. of taps	6	18-24	12-24
BS angle spread [º]	5-19	4.7-18.2	2.5-53.7
MS angle spread [º]	68	62.2-67.8	11.7-52.5
Delay spread [ns]	170-650	231-841	16-630
Shadow fading standard deviation [dB]	4-10	4-10	2-8

* artificial extension from 5 MHz bandwidth

** based on 100 MHz measurements

Currently, the SCME has been considered as the primary channel model for the MIMO OTA test by the COST2100 community, even though some scenarios from WINNER II CDL model that are not available in the SCME may also be used. However, there exist some limitations in SCME which need to be taken into account when it is used in MIMO performance evaluation:

- To keep backward compatibility with the SCM, the number of clusters and total number of MPCs are not increased. In addition, the introduced intra-cluster delay spread (10 ns) is not based on the targeted 100 MHz bandwidth, but on PDP matching, so that the bandwidth dependence cannot be well reflected [10].
- The SCME is extended from the SCM, but the number of scenarios is not extended and the indoor channel model is not included, so that the scenarios are not sufficient for advanced simulations.
- Although the SCME provides LOS condition for all scenarios, there is no definite K-factor in the SCME TDL model. The K-factor is calculated based on the distance between the MS and BS.
- XPR is not provided in the SCME TDL model. Although the TDL model given in the SCME is simple and can be used for comparison simulations, the lack of the XPR makes it incapable of handling polarized situations.

Due to the above reasons, we use the CDL model of WINNER II in this thesis for the development of MIMO OTA test based on the MPS Method. The WINNER II CDL model supports more scenarios and is based on real channel measurements.

Chapter 4 MATLAB Simulation and Results

As described in Chapter 3, the MIMO OTA test system uses multipath simulator (MPS) and spatial fading emulator (SFE) to generate spatial-temporal multipath propagation channels. A MATLAB simulation platform is developed in this thesis to determine the architecture of MPS and SFE that satisfies the MIMO OTA test requirements without unnecessary complexity.

The MATLAB simulation platform is very flexible. MIMO systems with an arbitrary number of transmit and receive antennas can be simulated. Any CDL channel model can be studied through the simulation. Many important aspects of the MIMO OTA test system can be first investigated in software before involving any hardware.

In our study, we focus on 2×2 MIMO systems, which is the current requirement for testing HSPA and LTE terminals. The simulation is divided into two parts:

- Study of MPS, mainly on the generation and simplification of spatial channel models.
- Study of SFE, mainly on the antenna probe placement and the effective test area in the probe ring.

The study based on MATLAB simulations is described in detail in this chapter.

4.1 Simulation Structure

Figure 4.1 shows the high-level structure of the MATLAB simulation platform.

The CDL channel parameters are obtained from predefined local files. These files follow a predefined format and record channel parameters in different scenarios, such as delay values, cluster ray power, K-factor of LOS ray, angles of departure (AoDs), angles of arrival (AoAs), cluster angular spread of AoDs and AoAs, and XPR.

Then, the CDL channel parameters are converted into a new set of parameters. Together with MS and probe antenna patterns, the new set of parameters is used to generate channel matrix.

Based on the MIMO channel matrices of transfer functions and impulse responses, capacities and channel characteristics including power delay profile, frequency correlation and spatial correlation are calculated for analysis.

Simulation parameters are defined to control the simulation process. The parameters can be classified into four major groups as below:

- System simulation parameters
  System-level simulation parameters are defined in this group, and they include system bandwidth, center frequency, sampling frequency in delay domain, number of time samples and SNR range.
- Channel simulation parameters
  These parameters control the MIMO channel generation and the process of channel simplification. Channel characteristics such as LOS ray, intra-cluster delay spread, number of rays within a cluster, spatial correlation, etc., are considered here. A change of the parameters in this group causes different channel behavior.
- Antenna simulation parameters
  Simulation parameters for the BS, MS and probe antennas are defined in this group. These include the number of BS and MS antennas, antenna spacing and whether MS and probe antennas are isotropic.
- Spatial fading emulator parameters
  Spatial fading emulator consists of the positions of the antenna probes and the DUT. Number of probe antennas and radius of the ring, DUT position and angle of rotation are defined in this group.

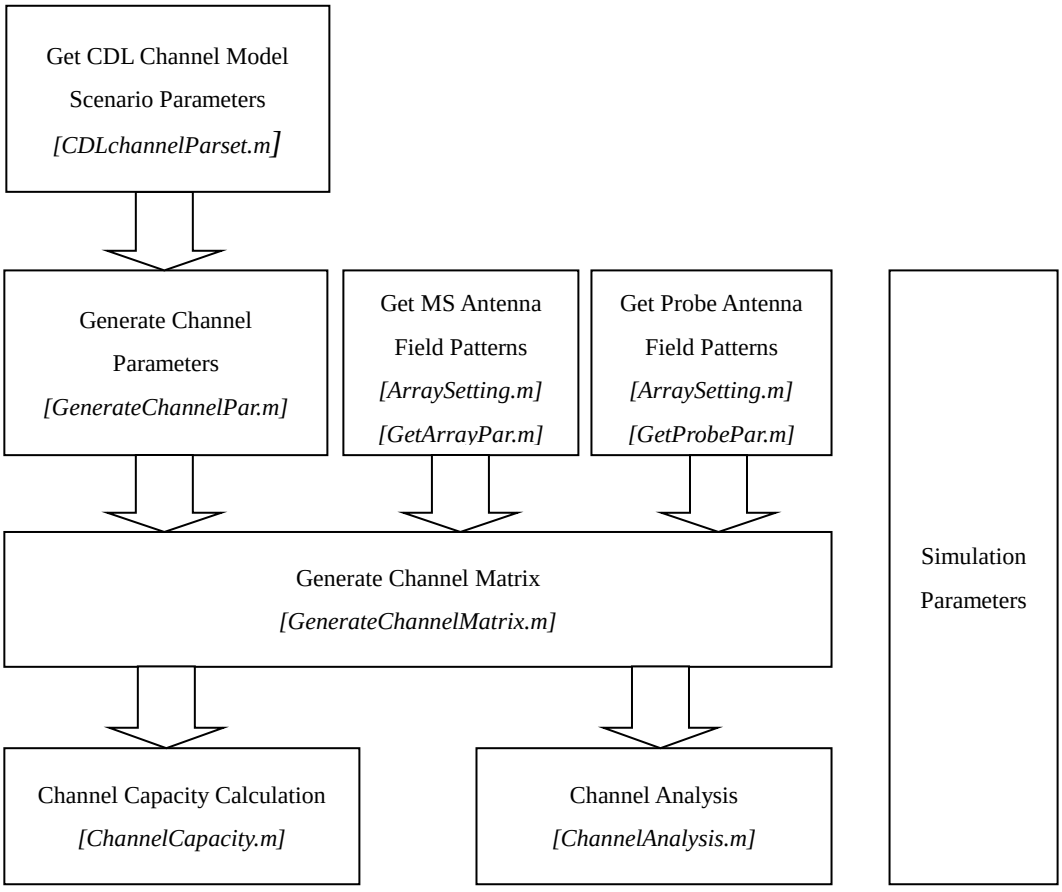

Figure 4.1: High-level structure of the MATLAB simulation platform.

4.2 Multipath Simulator (MPS)

The study of the MPS Method in this thesis mainly focuses on the channel simplifications. In this section, the simplification methods and their evaluations are described in detail.

4.2.1 CDL Channel Models

The implementation of channels in the MIMO OTA test system is based on the CDL concept, which represents the *average* channel characteristics. According to the planning document of the COST2100 measurement campaign [2], the following scenarios in WINNER II CDL channel models are selected for this study:

- Large indoor hall: B3
- Outdoor to indoor: B4
- Typical urban micro-cell: B1
- Suburban: C1
- Rural macro-cell: D1

Except for B4, these scenarios are defined for both LOS and NLOS cases. For B4, the probability of LOS occurrence is approximated as zero. For indoor and urban micro-cell scenarios, whether there is the LOS component depends on the MS location with respect to the street grid or the floor plan [17]. For other outdoor scenarios, the LOS probability decreases with the distance between MS and BS. In WINNER II channel models, LOS probability models for some scenarios are provided. Although these models are not exact, we can make a rough estimation on LOS probability in order to decide which cases should be simulated for the scenarios of interest. LOS probabilities for these scenarios are listed in Table 4.1 [17].

Table 4.1: Line of sight (LOS) probabilities.

Scenarios	LOS probability as a function of distance d [m]
B3	$P_{LOS} = \begin{cases} 1, & d \le 10 \\ \exp(-\frac{d-10}{45}), & d < 10 \end{cases}$
B1	$P_{LOS} = \min(18/d, 1) \cdot \left(1 - \exp(-d/36)\right) + \exp(-d/36)$
C1	$P_{LOS} = \exp\left(-\frac{d}{200}\right)$
D1	$P_{LOS} = \exp\left(-\frac{d}{1000}\right)$

Based on the probabilities of LOS, we choose NLOS case for C1 and D1 scenarios, and both LOS and NLOS cases for B1 and B3 scenarios, in our simulation study. The parameters for the chosen scenarios in WINNER II CDL models are provided in Tables 1 to 7 in the Appendix.

4.2.2 MIMO Channel Generation

The CDL channel models include a comprehensive list of parameters, such as delays, powers, AoAs, AoDs, and XPRs. In order to analyze the channels used in an OTA test system, MIMO

channel matrices should be generated from these parameters. In [17], the procedure of channel coefficient generation is given. However, the generation procedure in [17] is intended for the WINNER II generic model. In our simulation, the procedure can be much simpler, as CDL models are used.

The channel of a MIMO system with M_T transmit antennas and M_R receive antennas is given by the $M_R \times M_T$ matrix $\mathbf{H}(\tau, t)$ with

$$\mathbf{H}(\tau, t) = \begin{bmatrix} h_{1,1}(\tau, t) & h_{1,2}(\tau, t) & \cdots & h_{1,M_T}(\tau, t) \\ h_{2,1}(\tau, t) & h_{2,2}(\tau, t) & \cdots & h_{2,M_T}(\tau, t) \\ \vdots & \vdots & \ddots & \vdots \\ h_{M_R,1}(\tau, t) & h_{M_R,2}(\tau, t) & \cdots & h_{M_R,M_T}(\tau, t) \end{bmatrix},$$

$h_{i,j}(\tau, t)$ is the impulse response between the jth transmit antenna and the ith receive antenna. For the CDL channel models, the impulse response can be calculated as follows

$$h_{i,j,n}(t) = \sum_{m=1}^{M} \sqrt{P_m} \begin{bmatrix} F_{BS,j,V}(\varphi_{n,m}) \\ F_{BS,j,H}(\varphi_{n,m}) \end{bmatrix}^T \begin{bmatrix} \exp(j\Phi_{n,m}^{vv}) & \sqrt{\kappa}\exp(j\Phi_{n,m}^{vh}) \\ \sqrt{\kappa}\exp(j\Phi_{n,m}^{hv}) & \exp(j\Phi_{n,m}^{hh}) \end{bmatrix} \begin{bmatrix} F_{MS,i,V}(\phi_{n,m}) \\ F_{MS,i,H}(\phi_{n,m}) \end{bmatrix}. \quad (4\text{-}2)$$

In Eq. (4-2), n denotes the nth cluster, and m is the ray index within the nth cluster. P_m denotes the ray power, so $\sqrt{P_m}$ is the amplitude of the ray. $F_{MS,i,V}$ and $F_{MS,i,H}$ are the ith MS antenna patterns for vertical and horizontal polarizations, respectively. $F_{BS,j,V}$ and $F_{BS,j,H}$ are the jth BS antenna patterns for vertical and horizontal polarizations respectively. $\varphi_{n,m}$ and $\phi_{n,m}$ denote the ray AoD and AoA respectively. κ is the cross-polarization power ratio (XPR), which is the same for all the rays in the WINNER II CDL models. $\{\Phi_{n,m}^{vv}, \Phi_{n,m}^{vh}, \Phi_{n,m}^{hv}, \Phi_{n,m}^{hh}\}$ are the randomly generated phases for each ray m in each cluster n for the four different polarization combinations. The ray phases of the signals from different BS antennas are different. Note that the delay domain is denoted by the cluster index, as different clusters usually have different delays. For the case that different clusters have the same delay, the CIR taps are added as complex numbers. $h_{i,j}(\tau, t)$ is then obtained.

In our MIMO OTA test system, the base station emulator is used to produce HSPA or LTE transmit signals, so it is difficult for the BS antenna patterns and spatial information at BS side to be emulated directly. To solve the problem, one idea is to pre-correlate the signals from different BS antennas. Therefore, the Kronecker model with transmit correlation only can be used to get the channel matrix. In [1], the Kronecker model is given by

$$\mathbf{H} = \mathbf{R}_r^{1/2} \mathbf{H}_0 \mathbf{R}_t^{1/2}. \quad (4\text{-}3)$$

$\mathbf{R}_r$ and $\mathbf{R}_t$ denote receive correlation and transmit correlation matrices, respectively. Both $\mathbf{R}_r$ and $\mathbf{R}_t$ are positive semi-definite Hermitian matrices. $\mathbf{H}_0$ is the uncorrelated i.i.d. Rayleigh

fading channel matrix. This model represents the special case when angular spectra at the receive antenna array are identical for signals from any transmit antenna. This is exactly the assumption in the WINNER II CDL channel models. For the channels "seen" from different BS antennas, all the channel parameters are the same except for phases of the rays. Recent studies show that the Kronecker model is often good enough for small MIMO systems, such as the 2×2 MIMO systems in this thesis.

Receive correlation is contained in the MS antenna patterns and the power azimuth spectrum (PAS), which can be generated directly by antenna probes in the OTA test system. Therefore, only transmit correlation is needed to get channel matrix

$$\mathbf{H} = \mathbf{H}_r \mathbf{R}_t^{1/2} .$$

(4-4)

In $\mathbf{H}_r$ the impulse response is calculated as Eq. (4-5), in which the BS antenna patterns are removed in comparison with Eq. (4-2)

$$h_{i,j,n}(\mathrm{t}) = \sum_{m=1}^{M} \sqrt{P_m} \begin{bmatrix} \exp\left(j\Phi_{n,m}^{vv}\right) & \sqrt{\kappa}\exp\left(j\Phi_{n,m}^{vh}\right) \\ \sqrt{\kappa}\exp\left(j\Phi_{n,m}^{hv}\right) & \exp\left(j\Phi_{n,m}^{hh}\right) \end{bmatrix} \begin{bmatrix} F_{MS,i,V}\left(\phi_{n,m}\right) \\ F_{MS,i,H}\left(\phi_{n,m}\right) \end{bmatrix}.$$

(4-5)

The transmit correlation matrix can be calculated as [19]

$$[\mathbf{R}_t]_{i,j} = \sum_{n=1}^{N} \sum_{m=1}^{M} P_{n,m} \exp\left(j2\pi(j-i)d_t \sin\left(\varphi_{n,m}\right)\right) \Big/ \sum_{n=1}^{N} \sum_{m=1}^{M} P_{n,m} ,$$

where d_t is the BS antenna spacing in wavelength, N is the number of clusters and M is the number of rays per cluster.

The above discussion is for the case that the LOS ray does not exist. In the LOS case, MIMO channel should be modeled as the sum of the LOS component and a fading component, as in Eq. (4-7). The Kronecker model is valid for the fading component [20], which can be obtained by Eq. (4-3), Eq. (4-4) and Eq. (4-6)

$$\mathbf{H} = \mathbf{H}_{LOS} + \mathbf{H}_{Fading} = \mathbf{H}_{LOS} + \mathbf{R}_r^{1/2} \mathbf{H}_0 \mathbf{R}_t^{1/2} .$$

That is to say, in the LOS case, only signals in the fading component are pre-correlated for different BS antennas.

For simplicity in our simulations, we assume that the BS antennas are only vertically polarized, so

only two polarization combinations (*vv, vh*) are considered.

At the MS side, three types of MS antenna patterns are used for our simulation study – isotropic antennas, high-correlation antennas and low-correlation antennas. In the case of isotropic MS antennas, the antenna spacing is usually set as half wavelength. For high-correlation and low-correlation MS antennas, the magnitudes of the 3D antenna patterns are shown in Figure 4.2 and Figure 4.3, respectively.

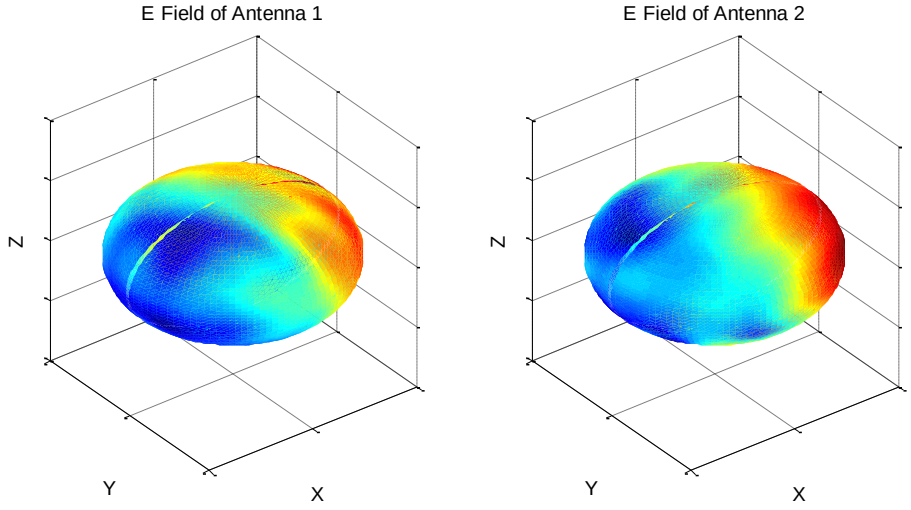

Figure 4.2: E-field of high-correlation MS antennas.

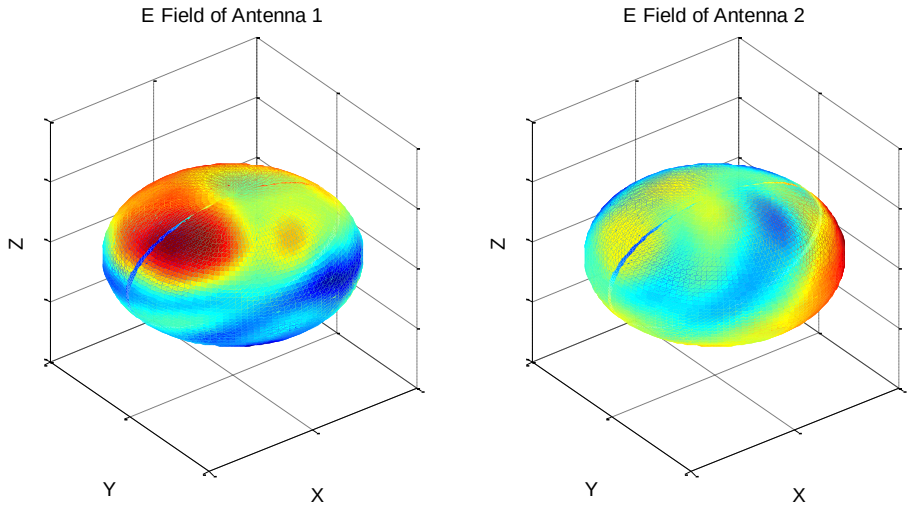

Figure 4.3: E-field of low-correlation MS antennas.

4.2.3 Channel Model Simplification and Analysis

In this section, channel simplification methods and their evaluations are described in detail. Results are given for all the chosen CDL models.

4.2.3.1 Simplification Methods and Criteria

As discussed in previous sections, there are between 8 and 20 clusters in the WINNER II CDL models, and each cluster contains 20 rays for generating Rayleigh fading and intra-cluster angular spread. To implement the entire set of parameters in hardware will result in a very complicated and high-cost MPS in the OTA test system. Therefore, some simplifications of the CDL channel models are needed. And as long as the FOMs from the simplified channels can still closely resemble those of the full channel models, they can be used to reflect real user experience [2]. The simplification steps are shown below:

- Down-scale the bandwidth supported by the channel models.
- Reduce the number of rays in one cluster.
- Remove intra-cluster angular spread.
- Discard some clusters with relatively low powers.

In order to ascertain the extent to which the simplifications can be performed, several criteria are used to evaluate the simplification process. The capacity of MIMO channel is the dominant criterion, since the trend of capacity can reflect the trend of throughput [21], which is a FOM with the highest priority in MIMO OTA measurements. In the simplification process, if the maximal change in capacity at the SNR range of 10 dB to 30 dB is under 10%, the throughput can be regarded as unchanged, so that the simplified channel is considered acceptable.

The capacity of frequency flat and deterministic MIMO channel in absence of channel knowledge at transmitter side is given by [1]

$$C = \log_2 \det\left(\mathbf{I}_{M_R} + \frac{E_s}{M_T N_0}\mathbf{H}\mathbf{H}^H\right),$$

where E_s is the *total* energy available at the transmitter over a symbol period, and E_s/N_0 is the signal-to-noise ratio, which is set to the range of 10 dB to 30 dB in our simulations.

For frequency selective MIMO channel, capacity can be calculated by dividing the interested frequency band into many narrow sub-channels such that each sub-channel is frequency flat [1]. Then capacity of frequency selective channel is obtained by averaging the capacities of the frequency flat sub-channels.

$$C_{FS} \approx \frac{1}{N}\sum_{i=1}^{N} \log_2 \det\left(\mathbf{I}_{M_R} + \frac{E_s}{M_T N_0}\mathbf{H}_i\mathbf{H}_i^H\right),$$

Note that E_s in Eq. (4-9) is the *total* energy available at the transmitter over a symbol period *per* frequency subchannel. Since temporal fading is considered in OTA measurements, a large number of realizations will be generated in order to get the average performance of a DUT. In our simulations, we randomly generate ray phases for each realization to keep the MIMO channel random. For random channel, ergodic capacity and outage capacity are used to characterize the

statistics. The ergodic capacity for the frequency selective MIMO channel is given by [1]

$$\bar{C}_{FS} \approx \mathcal{E}\left\{\frac{1}{N}\sum_{i=1}^{N}\log_2 \det\left(\mathbf{I}_{M_R} + \frac{E_s}{M_T N_0}\mathbf{H}_i\mathbf{H}_i^H\right)\right\}.$$

Outage capacity is used to quantify the reliability of performance. In our simulations, the 10% outage rate is used for the performance evaluation. In the process of channel simplification, the change in both ergodic capacity and outage capacity should be kept under 10%.

Channel properties, such as delay spread, angular spread and MS spatial correlation, are used in the analysis of the simplification process. Changes in these channel properties result in a change in capacity (with high probability), so capacity is taken as the dominant criterion to assess channel simplification.

Delay spread causes frequency selective fading. Frequency selectivity is measured by the coherence bandwidth which is inversely proportional to the delay spread. The RMS delay spread is defined as [1]

$$\tau_{RMS} = \sqrt{\frac{\int_0^{\tau_{max}}(\tau-\overline{\tau})^2\,\Psi_{De}(\tau)\,\mathrm{d}\tau}{\int_0^{\tau_{max}}\Psi_{De}(\tau)\mathrm{d}\tau}},$$

where $\Psi_{De}(\tau)$ is the multipath intensity profile or spectrum, τ_{max} is the maximum delay, and $\overline{\tau}$ is the mean delay given in Eq. (4-12)

$$\overline{\tau} = \frac{\int_0^{\tau_{max}}\tau\,\Psi_{De}(\tau)\,\mathrm{d}\tau}{\int_0^{\tau_{max}}\Psi_{De}(\tau)\,\mathrm{d}\tau}.$$

Angular spread causes space selective fading, which means that the signal amplitude depends on the location of the antenna. Space selective fading is characterized by the coherence distance, which is inversely proportional to the angular spread. Angular spread is given as [22]

$$\theta_{RMS} = \sqrt{\frac{\int\left|\exp(j\theta)-\overline{\theta}\right|^2\Psi_A(\theta)\mathrm{d}\theta}{\int\Psi_A(\theta)\mathrm{d}\theta}},$$

where $\Psi_A(\theta)$ denotes the PAS and $\overline{\theta}$ is the mean angle as

$$\overline{\theta} = \frac{\int\exp(j\theta)\,\Psi_A(\theta)\mathrm{d}\theta}{\int\Psi_A(\theta)\mathrm{d}\theta}.$$

MS spatial correlation describes the independence of the arrival signals at the MS antennas. Spatial

correlation can be calculated as Eq. (4-6). However, for the MS antenna patterns, a more explicit way of calculating spatial correlation is given in [23] as

$$\rho_e \approx |\rho_c|^2 = \frac{\left(\oint \left(XPR\ E_{\theta X}(\Omega)E^*_{\theta Y}(\Omega)\mathrm{P}_\theta(\Omega) + E_{\phi X}(\Omega)E^*_{\phi Y}(\Omega)P_\phi(\Omega)\right)\mathrm{d}\Omega\right)^2}{\oint \left(XPR\ G_{\theta X}(\Omega)\mathrm{P}_\theta(\Omega) + G_{\phi X}(\Omega)P_\phi(\Omega)\right)\mathrm{d}\Omega \cdot \oint \left(XPR\ G_{\theta Y}(\Omega)\mathrm{P}_\theta(\Omega) + G_{\phi Y}(\Omega)P_\phi(\Omega)\right)\mathrm{d}\Omega},$$

where ρ_c is the complex correlation, E_θ and E_ϕ are the field patterns of two polarizations, and X, Y denotes the two antennas.

When the spatial property of the channel changes in the simplification process, the capacities of the MS with high-correlation antennas change greater than the capacities of the MS with isotropic antennas or low-correlation antennas. Keeping the capacity change of the high-correlation MS under 10% can therefore guarantee the capacity change of both the isotropic MS and the low-correlation MS to be under 10%. Therefore, the capacity change of the high-correlation MS is used as the criterion to evaluate the simplified channel when the spatial property changes.

4.2.3.2 Bandwidth Down-scaling

The WINNER II channel models are designed for a bandwidth of 100 MHz. However, HSPA and LTE systems support a bandwidth of up to 5 MHz and 20 MHz respectively, which is much smaller than 100 MHz. Therefore, the resolution in the delay domain does not need to be as high as that for 100 MHz system bandwidth. The procedure for down-scaling the bandwidth is briefly described in [17].

In the WINNER II CDL channel models, 5 ns is the default minimum delay sample spacing in the channel impulse response (CIR) and thus it defines the delay resolution for the CIR taps. If the system bandwidth is smaller than 100 MHz, the minimum delay sample spacing is longer than 5 ns. Down-scaling can be performed in delay domain as follows [17]:

- Create the new delay grid according to the system bandwidth.
- Move the original delay samples to the nearest location in the new grid.
- If there are two nearest locations, the delay tap should be moved to the one that has smaller delay value.
- If more than one delay taps are placed at the same location, sum them up as complex numbers.

In general, resolution in the delay domain is the inverse of system bandwidth. For 20 MHz systems, the resolution is 50 ns. And for 100 MHz, resolution is 10 ns. In the WINNER II channel models, up-sampling is performed, thus the delay sample spacing is 5 ns. However, in our OTA test system and MATLAB simulations, up-sampling is not needed, so we can set the delay sample spacing to 50 ns, which is the inverse of the 20 MHz bandwidth.

According to the down-scaling procedure above, we can simplify the channel by merging some adjacent clusters in the delay domain, so that less delay lines are needed in the OTA test system.

Note that channel spatial properties such as AoAs and AoDs are not changed in this process.

Figure 4.4 shows the power delay profile of the WINNER II B1 NLOS channel after bandwidth down-scaling to 20 MHz. It can be seen that the number of delay taps is greatly reduced from 19 to 8. Due to delay mergence, RMS Delay spread becomes 80 ns, which is a little larger than the 77 ns delay spread of the original channel that supports the 100 MHz bandwidth. The change of delay spread also has influence on the frequency correlation; however, the small change can be ignored.

Figure 4.5 and Figure 4.6 show the ergodic capacity and 10% capacity in the process of bandwidth down-scaling. In Figure 4.5, ergodic capacity does not change. However, it can be seen in Figure 4.6 that the outage capacity of 20 MHz channel is lower than the outage capacity of 100 MHz channel. This is because the channel becomes less frequency selective in the process of bandwidth down-scaling.

In the above simulation, the center frequency is set to 2.48 GHz. The MS antenna patterns are assumed to be isotropic and the spatial fading emulator including the probe ring is not considered, such that the AoAs can be arbitrary.

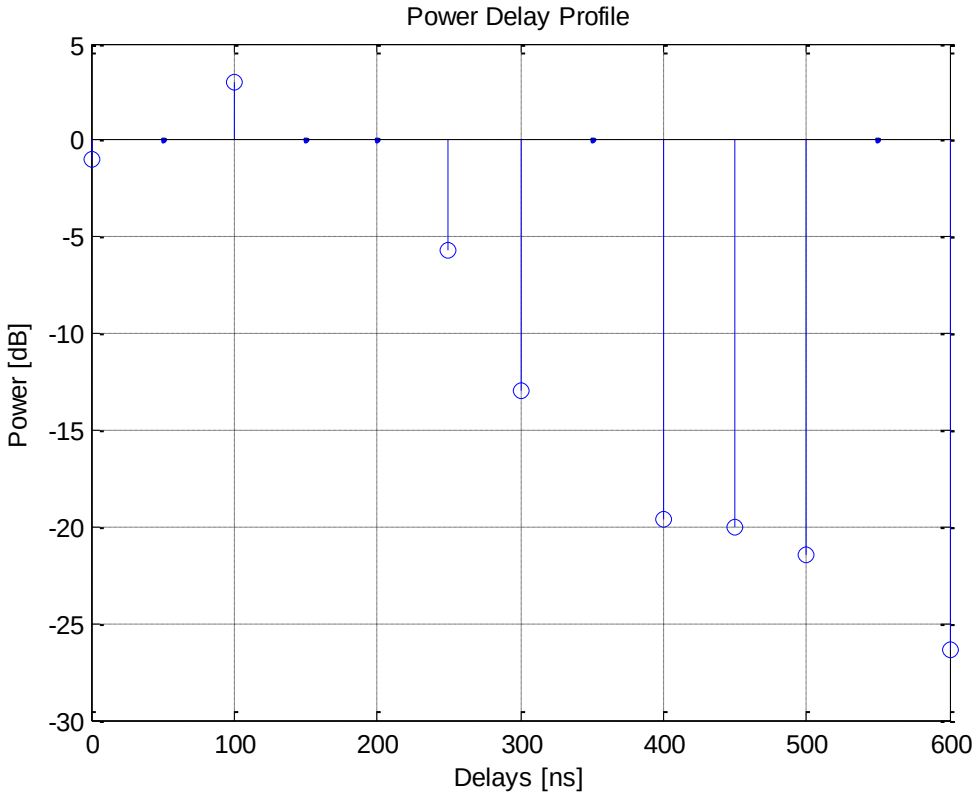

Figure 4.4: Channel impulse response after bandwidth down-scaling to 20 MHz.

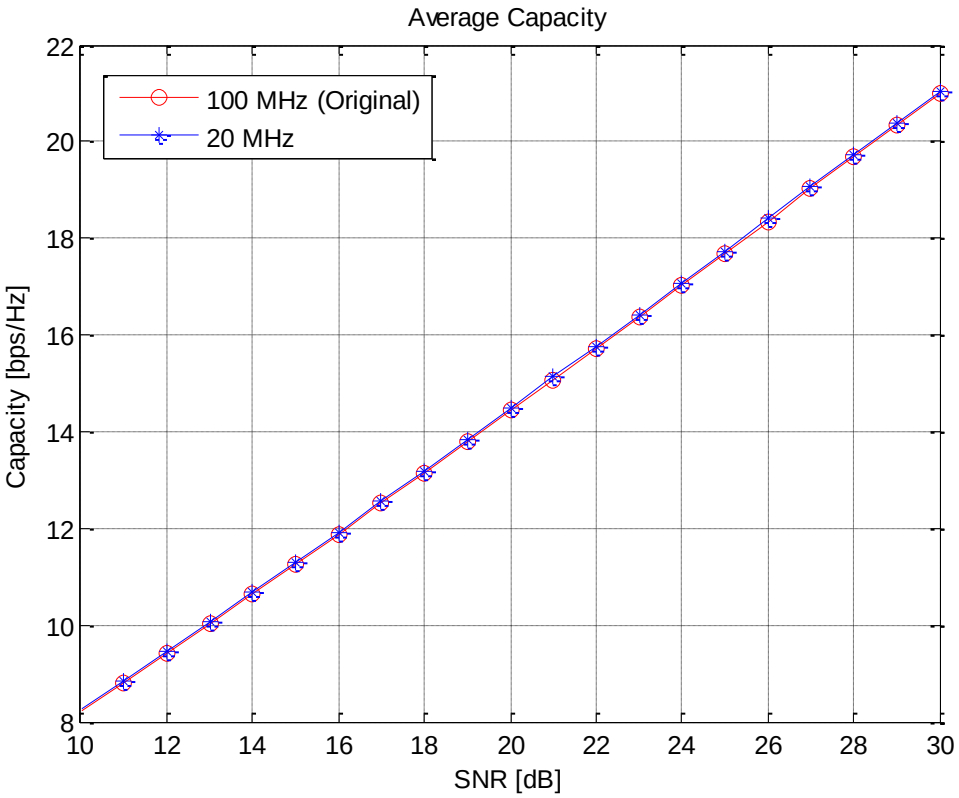

Figure 4.5: Ergodic capacity of MIMO channel supporting 100 MHz and 20 MHz bandwidth.

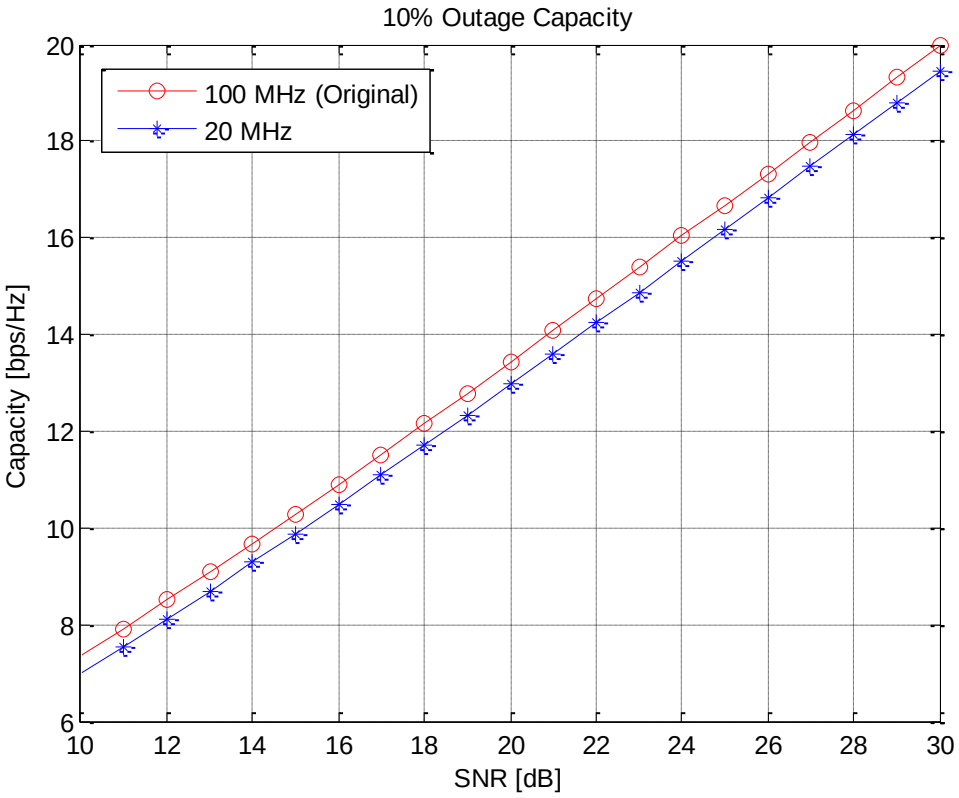

Figure 4.6: Outage capacity of MIMO channel supporting 100 MHz and 20 MHz bandwidth.

Bandwidth down-scaling is the first step of channel model simplification. Although the outage capacity becomes lower, it is reasonable for channels supporting the 20 MHz bandwidth. Therefore, in the following simplification process, the change in capacity will be calculated in comparison with the channel after bandwidth down-scaling to 20 MHz.

4.2.3.3 Rayleigh Fading

In the CDL models, fading process for each CIR tap is modeled by the sum-of-sinusoid approach. Each cluster is composed of 20 rays with the same power and different phases chosen from uniform distribution. The rays have the same delay but different AoDs and AoAs. In other words, 20 rays per cluster can model Rayleigh fading and intra-cluster angular spread. In this section, the number of rays per cluster is to be reduced while Rayleigh fading is maintained. In the next section, intra-cluster angular spread is to be removed or to be modeled in another way.

In order to keep the fading distribution close to Rayleigh, 4 is the minimum number of sinusoids that may be used [15]. It can be seen from Figure 4.7, Figure 4.8 and Figure 4.9, which illustrate the distribution of 0 ns CIR tap amplitudes in the WINNER II B1 NLOS channel model when the number of intra-cluster rays is 20, 4 and 3 respectively. 1000 realizations are generated in the simulation.

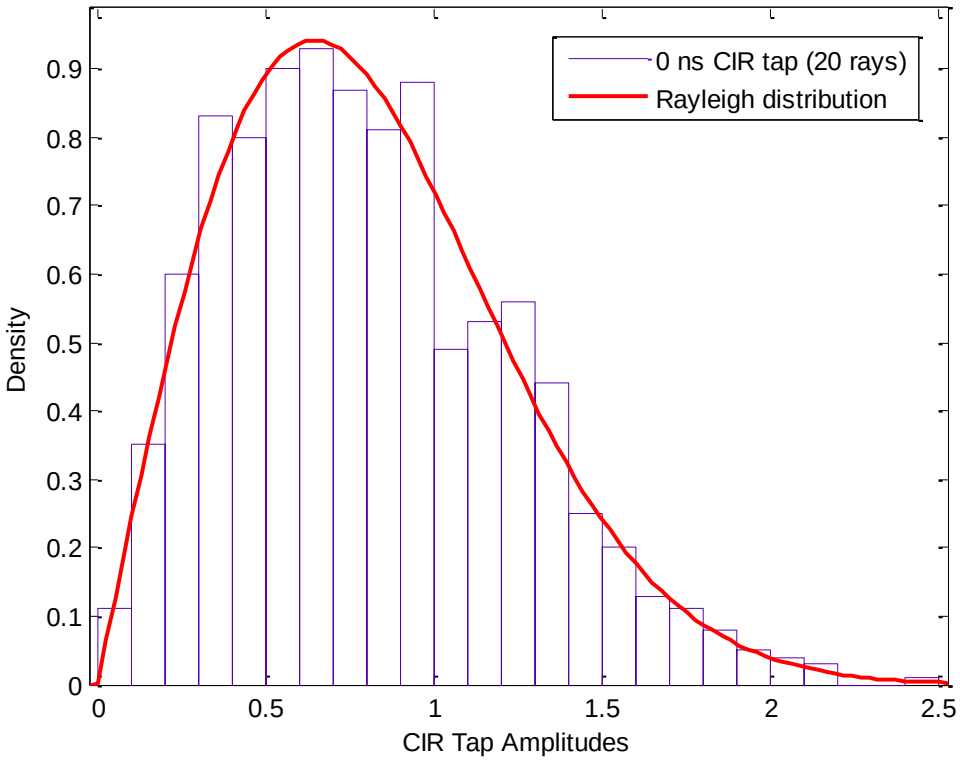

Figure 4.7: CIR tap amplitudes follow Rayleigh distribution when the number of rays per cluster is 20.

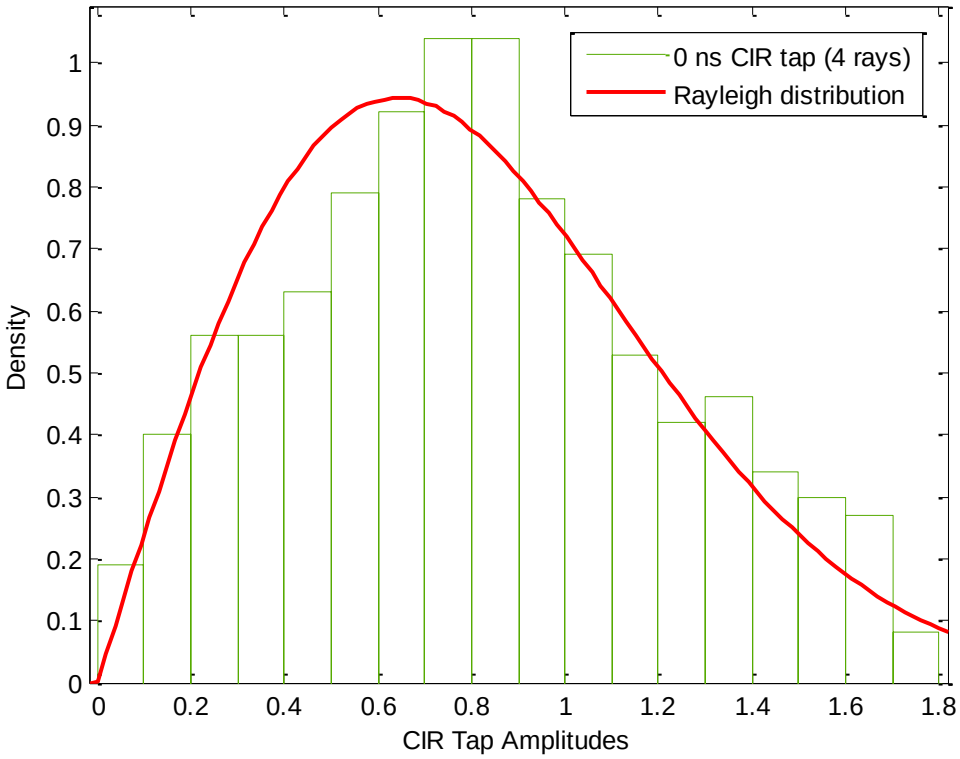

Figure 4.8: Distribution of CIR tap amplitudes is close to Rayleigh when the number of rays per cluster is 4.

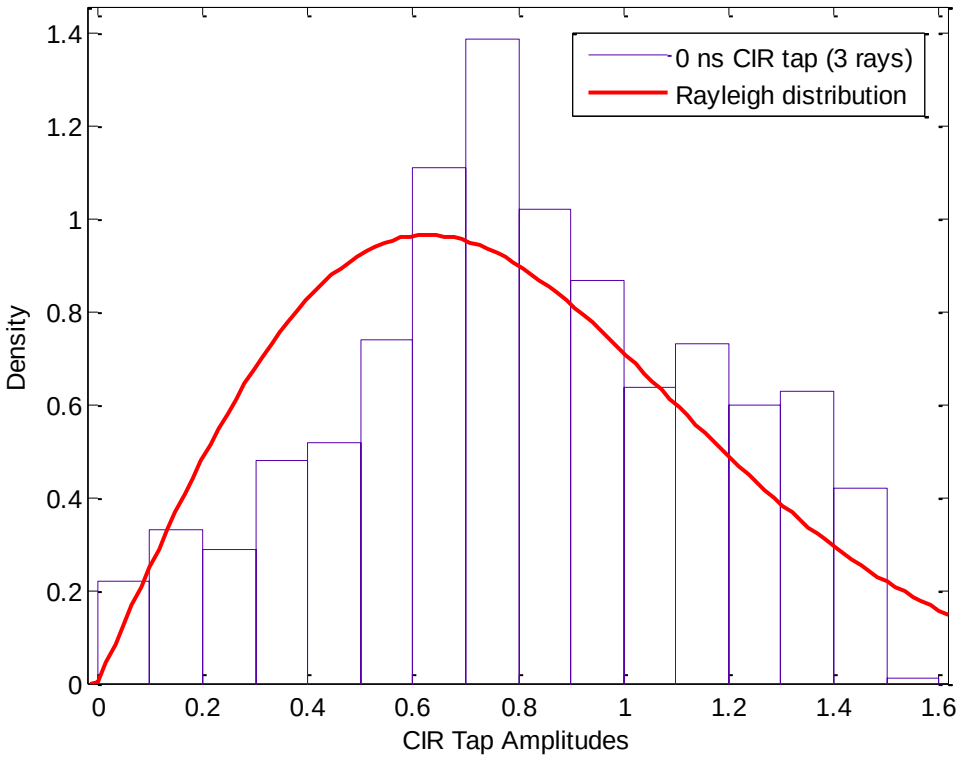

Figure 4.9: Distribution of CIR tap amplitudes is significantly different from Rayleigh when the number of rays per cluster is 3.

If the sum-of-sinusoid approach is used to generate Rayleigh fading, at least 4 rays per cluster are needed. However, it still makes our OTA test system very complicated. Therefore, we consider another approach to model Rayleigh fading. In particular, the amplitude of each cluster is pre-faded through attenuator in the OTA test system to follow Rayleigh distribution. Then only 1 ray per cluster is needed, so that the MPS becomes much simpler. In addition, the phase of the single ray is randomly generated to follow the uniform distribution.

Figure 4.10 shows the distribution of CIR tap amplitudes (over multiple channel realizations) when the pre-fading method is applied. It can be seen that Rayleigh fading can be modeled perfectly in this way. And the average power of this tap is -1.14 dB, which is approximate the power of the first cluster in the WINNER II B1 NLOS model.

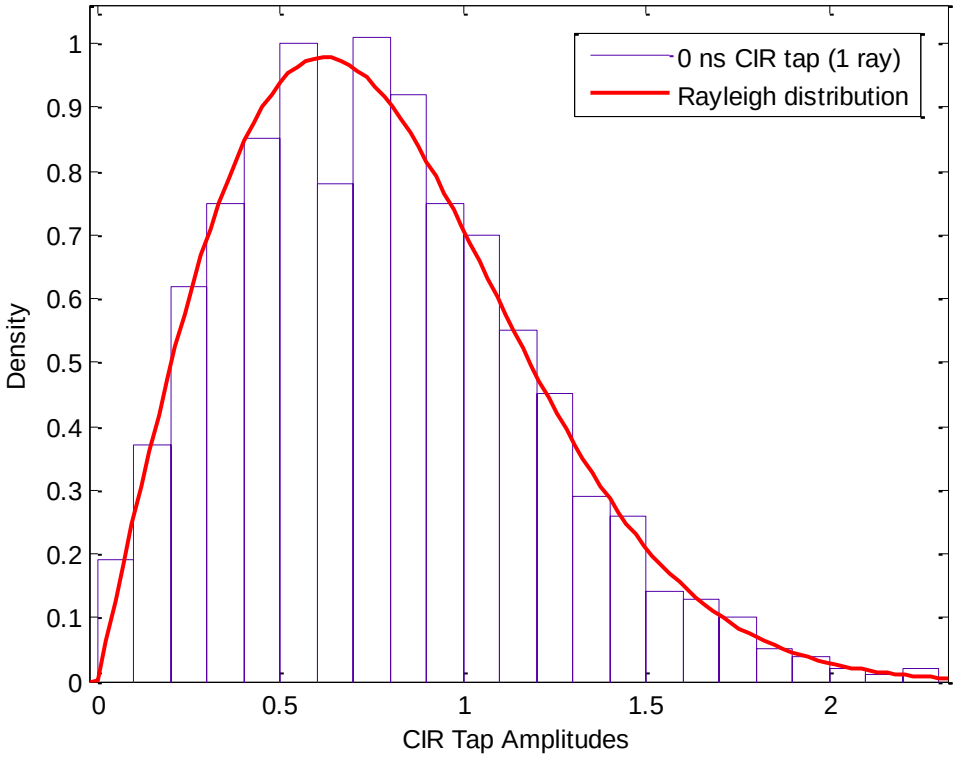

Figure 4.10: The CIR tap amplitudes follow the Rayleigh distribution perfectly when the pre-fading method is applied.

After down-scaling the bandwidth, the delays of different clusters are merged together to form one CIR tap. In this case, the amplitudes of the merged CIR tap are still Rayleigh distributed, when each cluster is pre-faded. The 100 ns tap in the WINNER II B1 NLOS model after the bandwidth down-scaling is taken as an example. This CIR tap contains 3 clusters. Figure 4.11 shows the amplitude distribution. The average power of this tap is 2.98 dB which is approximate the sum of the power of the 3 clusters.

When the LOS ray exists, the 0 ns tap may contain the dominant ray and some clusters. In this case, the 0 ns tap amplitudes are Rician distributed. It can be seen from Figure 4.12 which shows the 0 ns

tap amplitudes in the WINNER II B1 LOS model after the bandwidth down-scaling.

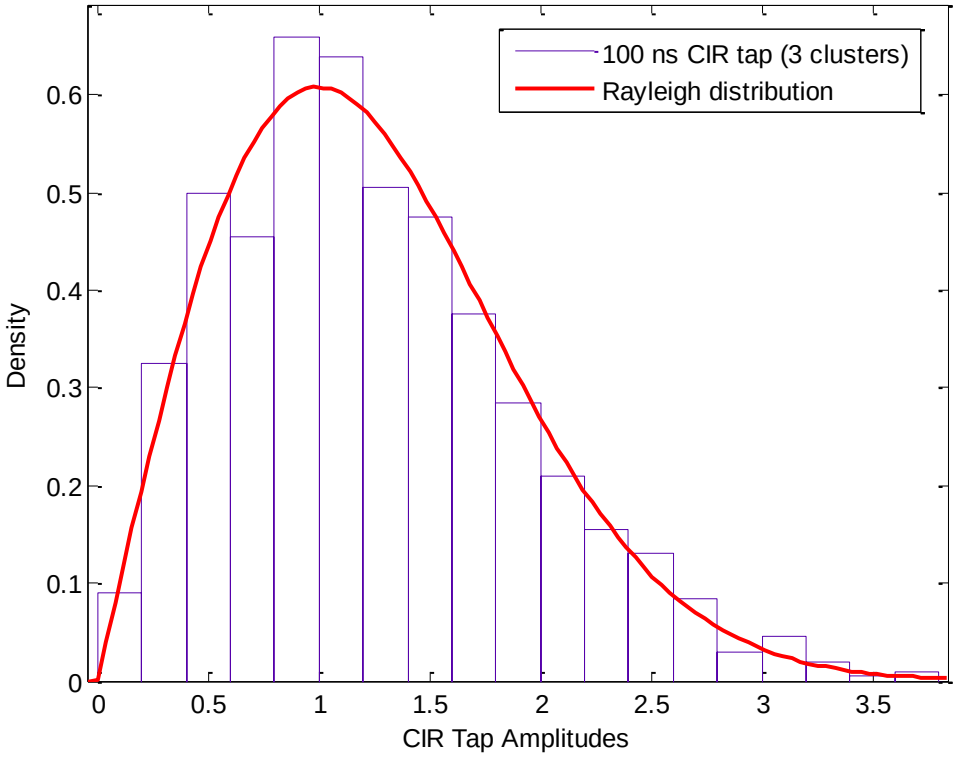

Figure 4.11: Distribution of CIR tap amplitudes follows the Rayleigh distribution when bandwidth down-scaling is performed.

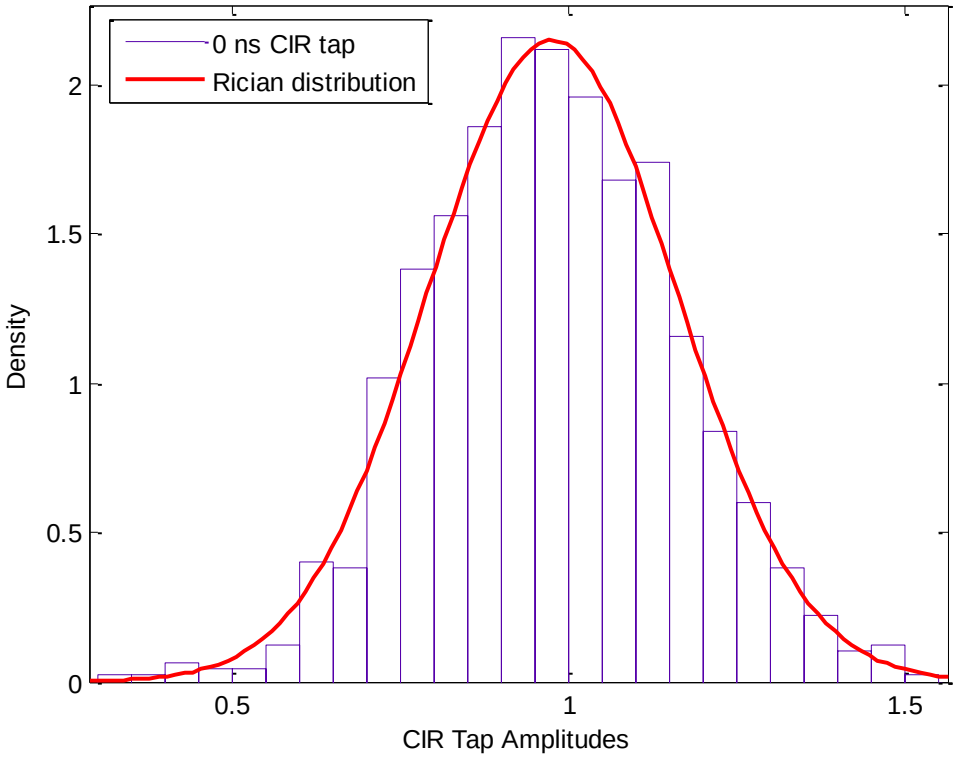

Figure 4.12: CIR tap amplitudes follow the Rician distribution when the LOS ray exists.

Now we compare the capacities derived from the fading channel through sum-of-sinusoid method and pre-fading method. Since there is only 1 ray per cluster in pre-fading method, intra-cluster angular spread cannot be modeled. Therefore, for comparison between the two methods, in the simulation the cluster angular spread is removed for the case of 20 rays per cluster. Taking WINNER II B1 NLOS model as an example, ergodic capacity and outage capacity obtained from the two fading methods are shown in Figure 4.13 and Figure 4.14. As can be observed on these figures, the ergodic capacities are the same, whereas outage capacities are slightly different. The outage capacity from the pre-fading method is 2% lower than the outage capacity from the sum-of-sinusoid method. We consider that the slight change in the outage capacity is acceptable. Therefore, the pre-fading method can be an alternative way to model Rayleigh fading.

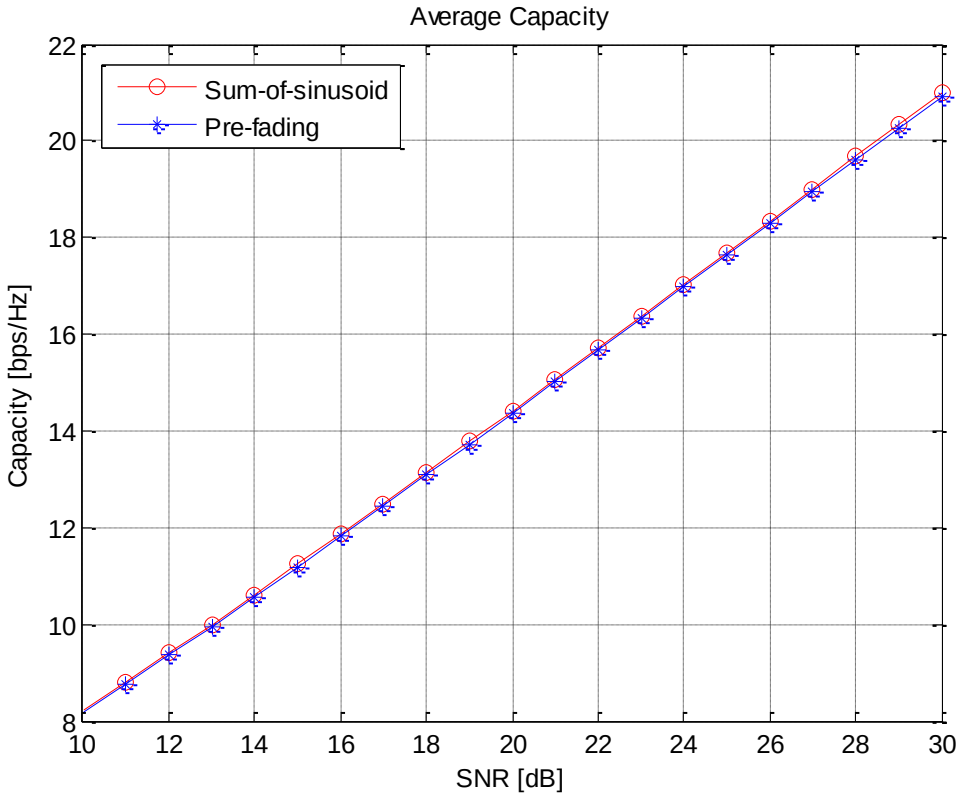

Figure 4.13: Ergodic capacities from two different fading generation methods.

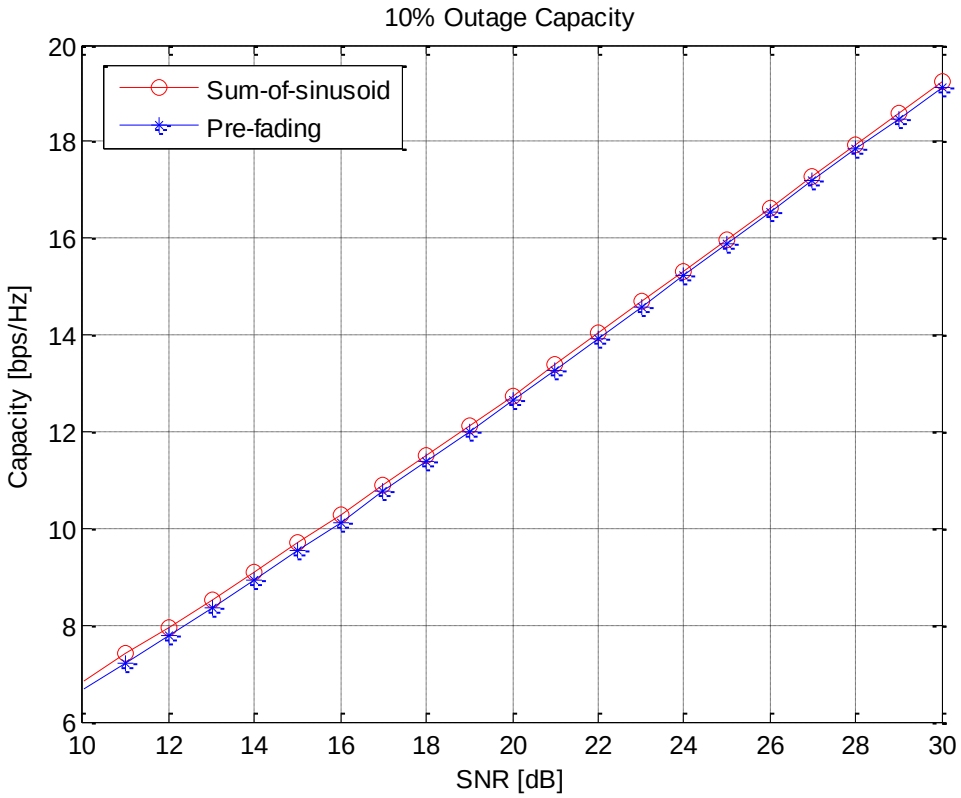

Figure 4.14: 10% outage capacities from two different fading generation methods. Capacity from the pre-fading method is 2% lower than capacity from the sum-of-sinusoid method.

4.2.3.4 Intra-cluster Angular Spread

In the CDL models, intra-cluster angular spreads of departure and arrival (cluster ASD and cluster ASA) are modeled by a number of rays with offset angles within each cluster. The offsets angles form the Laplacian PAS for each cluster [17]. As discussed in previous section, 1 ray per cluster can model Rayleigh fading; however, it is impossible for 1 ray per cluster to model intra-cluster angular spread. Intra-cluster angular spread of departure (ASD) is used in the calculation of BS correlation, which is for pre-processing the transmit signals. Only the spatial effect surrounding the MS should be considered in our OTA test system. Intra-cluster angular spread of arrival (ASA) is relevant to the implementation of our OTA test system, since the number of rays that are needed per cluster has to be determined. In this section, whether the intra-cluster angular spread can be removed is discussed first, and then the method of modeling cluster ASA through 3 rays per cluster is described.

If the intra-cluster angular spread is narrow, the DUT antennas may be unable to resolve it. Based on this hypothesis, we consider removing the intra-cluster ASA. Among all the chosen scenarios in the WINNER II CDL models, B1 NLOS model has the largest intra-cluster ASA, which is 22°, so we take it as an example here to discuss whether the intra-cluster angular spread can be removed. In the simulation, the center frequency is 2.48 GHz, and the isotropic MS antennas are assumed. The MS is rotated 360° in steps of 30°, and the average capacity is obtained from these orientations.

Figure 4.15, Figure 4.16 and Figure 4.17 show the simulation results. In Figure 4.15, spatial

correlation at MS side is shown for the cases with and without intra-cluster ASA respectively. We can see that the spatial correlation changes, with the maximum value occurring at the boresight direction of around 110° (and at 110°+180°=290°, due to rotational symmetry in the two-element isotropic antennas). Figure 4.16 and Figure 4.17 show the change in the ergodic capacity and the outage capacity, respectively. The ergodic capacity of the channel without intra-cluster ASA is 1% lower than the capacity of the channel with intra-cluster ASA, whereas the outage capacity decreases by 3% when the intra-cluster ASA is removed. The decrease of capacities is due to the increase in spatial correlation, which can be seen from Figure 4.15.

Furthermore, the total angular spread with intra-cluster ASA is 39°; the total angular spread without intra-cluster ASA becomes 35°. As discussed in Section 4.2.3.1, decrease in angular spread causes the increase in coherence distance. From our analysis, the performance of the MS with high correlation antennas will decrease even greater, since the antenna spacing may not be able to sufficiently decorrelate the incoming signals at different antennas. Figure 4.18, Figure 4.19 and Figure 4.20 show the results when the high correlation MS antenna patterns are used in the simulations. It can be seen that the ergodic capacity decreases by 3% and outage capacity decreases by 11%.

For the MS with high correlation antennas, the decrease in outage capacity slightly exceeds our limit of the change in capacity of 10%. While the capacity decrease may be good for product differentiation, since the performance gap between the low correlation MS and the high correlation MS can become larger. However, for the high correlation MS, the performance derived from the channel without intra-cluster ASA is less likely to reflect the real user experience (of throughput, which has a similar trend to capacity [21]). Based on this consideration, the intra-cluster ASA in B1 NLOS model should not be completely removed.

An interesting observation when comparing between Figure 4.15 and Figure 4.18 is that the gap between the with and without intra-cluster ASA cases appear to be larger on average in Figure 4.15, even though the difference in capacity is smaller in this case (i.e., the MS with the isotropic antennas). This apparent contradiction can be explained by capacity being a non-linear function of correlation. The increment drop in capacity due to the increase in correlation increases with correlation, and phenomenon is particularly severe when the magnitude of the complex correlation exceeds 0.7. 0.7 is generally accepted as the threshold in correlation for good diversity gain to be obtained from a diversity antenna setup.

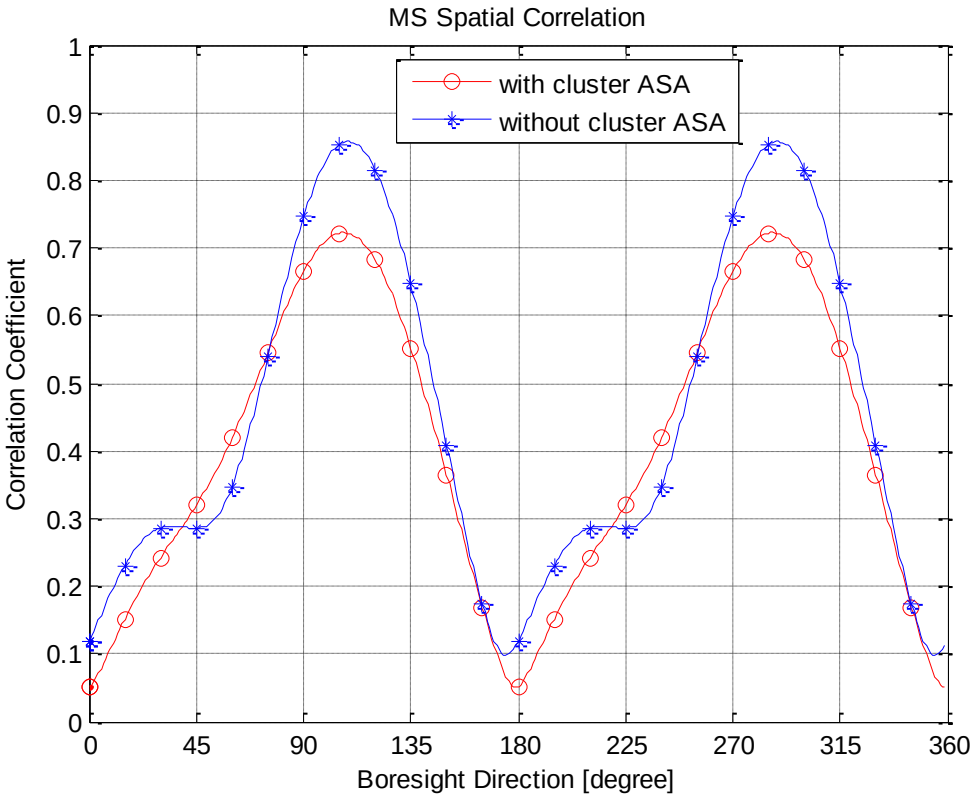

Figure 4.15: Spatial correlation at the MS side for the B1 NLOS channel.

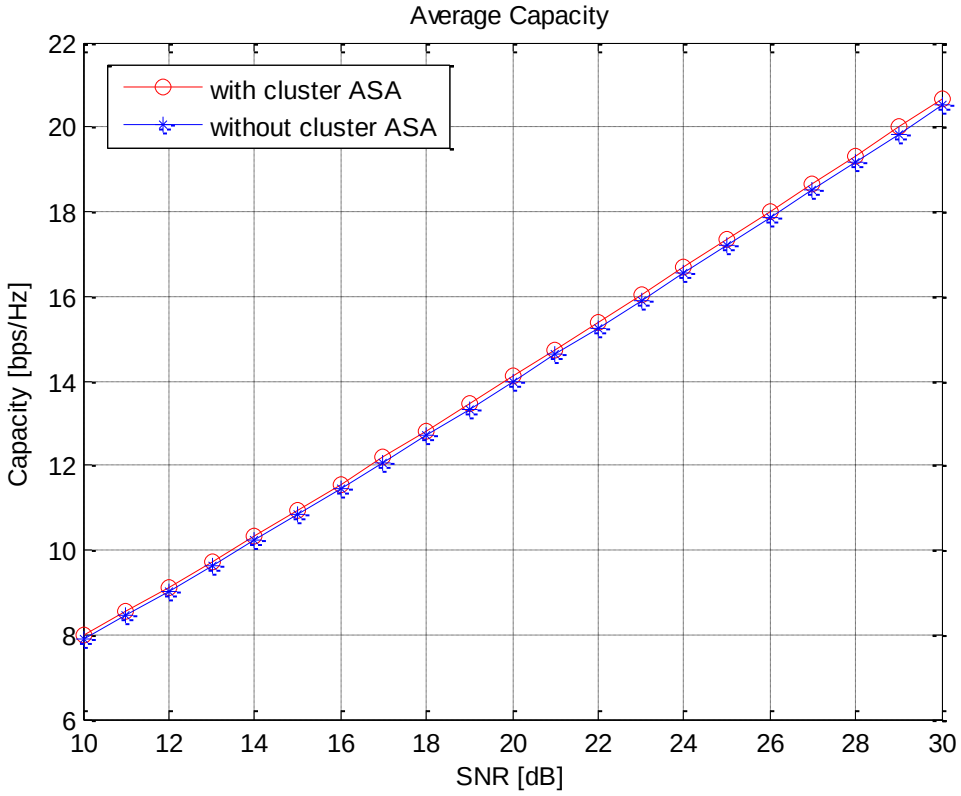

Figure 4.16: Ergodic capacities for the B1 NLOS channel with and without cluster ASA, respectively.

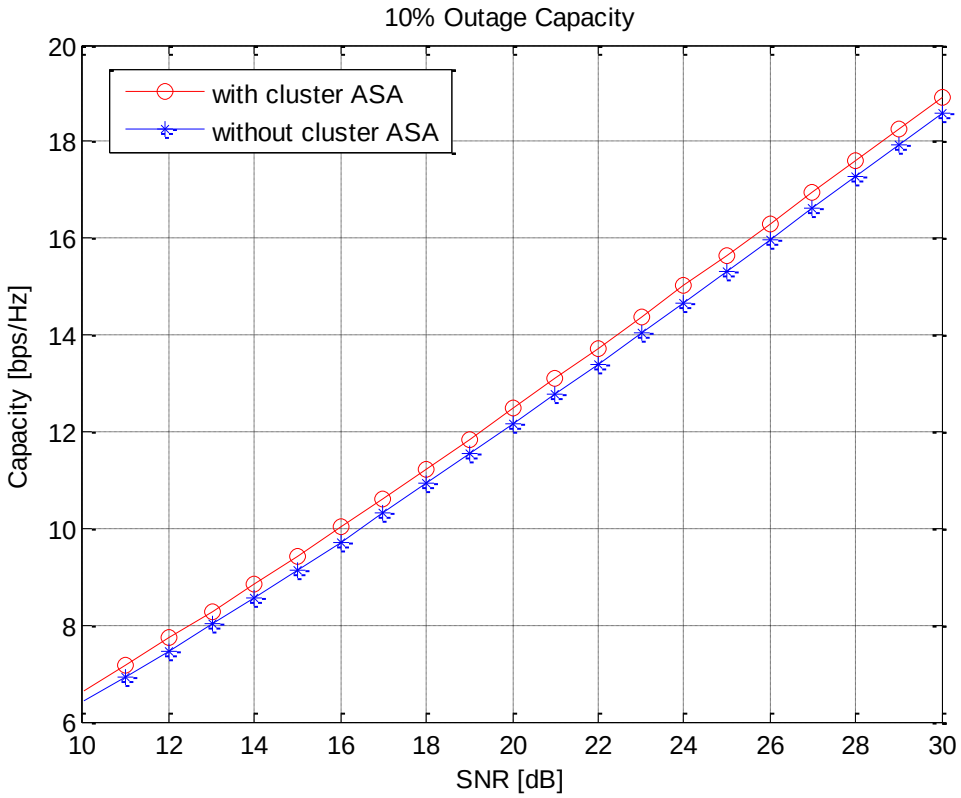

Figure 4.17: 10% outage capacities for the B1 NLOS channel with and without cluster ASA, respectively.

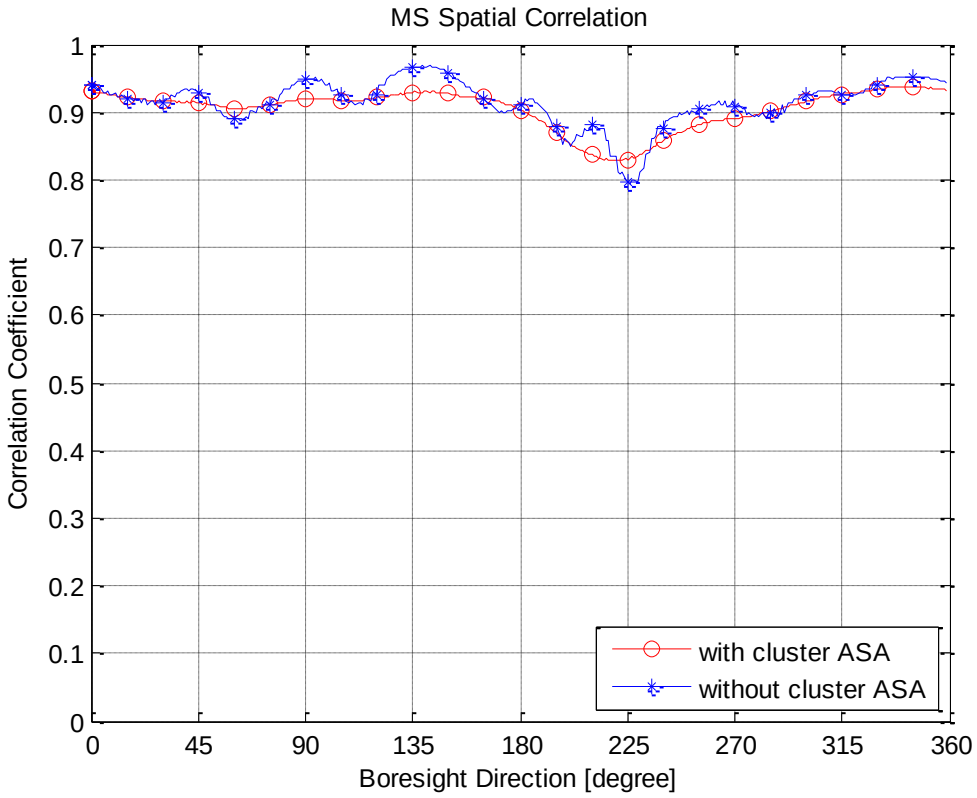

Figure 4.18: Spatial correlation at the MS side for the B1 NLOS channel. The MS with high correlation antennas is simulated.

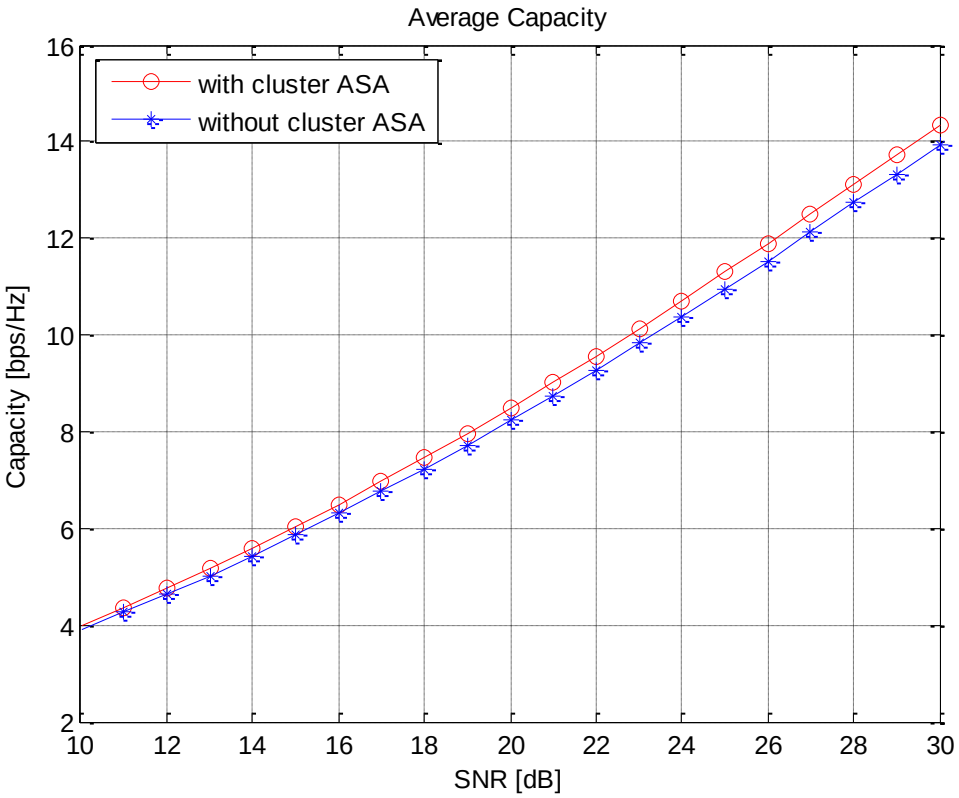

Figure 4.19: Ergodic capacities for the B1 NLOS channel with and without cluster ASA. The MS with high correlation antennas is simulated.

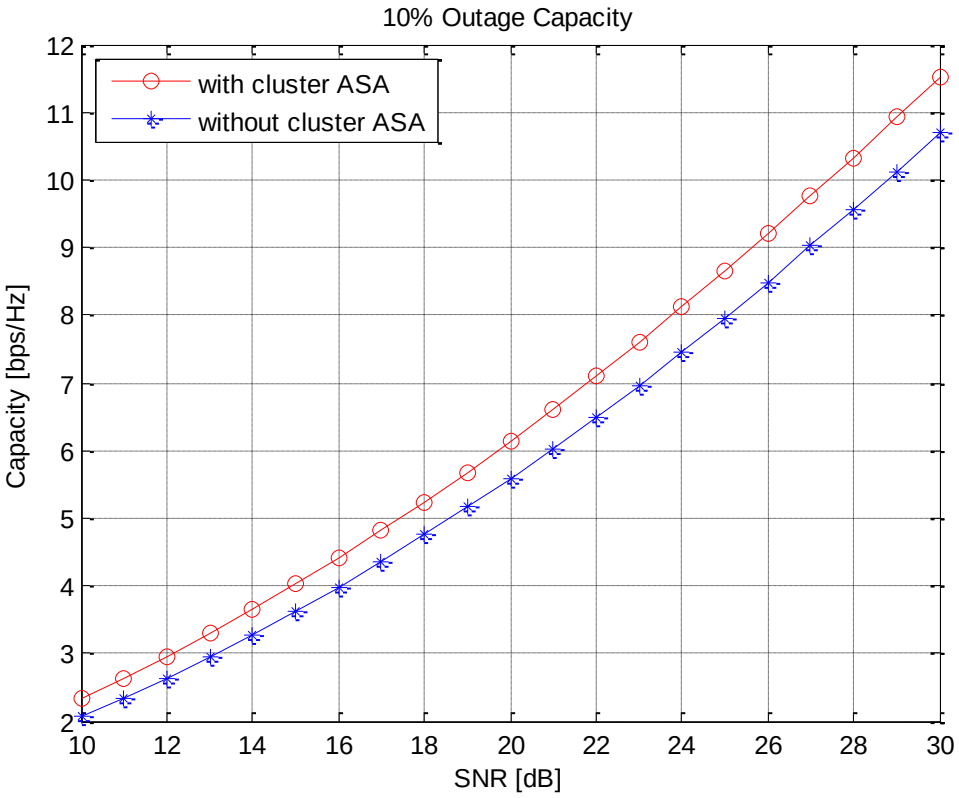

Figure 4.20: 10% Outage capacities for the B1 NLOS channel. The MS with high correlation antennas is simulated.

The B1 LOS model has the second largest intra-cluster ASA (of 18°) among all the chosen scenarios. However, due to the presence of the LOS ray, the total angular spread decreases by only 1° when the intra-cluster ASA is removed. As a result, the ergodic capacity and outage capacity decrease by 1% and 3%, respectively. As in the previous case, the high correlation MS is assumed.

In the case of B3 NLOS model with the high correlation MS, the intra-cluster ASA is 13°. After the cluster ASA is removed, the decrease in the total angular spread is less than 1°. The ergodic capacity and outage capacity of the B3 NLOS channel are plotted in Figure 4.21 and Figure 4.22, respectively. The decreases in the ergodic capacity and outage capacity are 1% and 3%, respectively, which we consider to be acceptable.

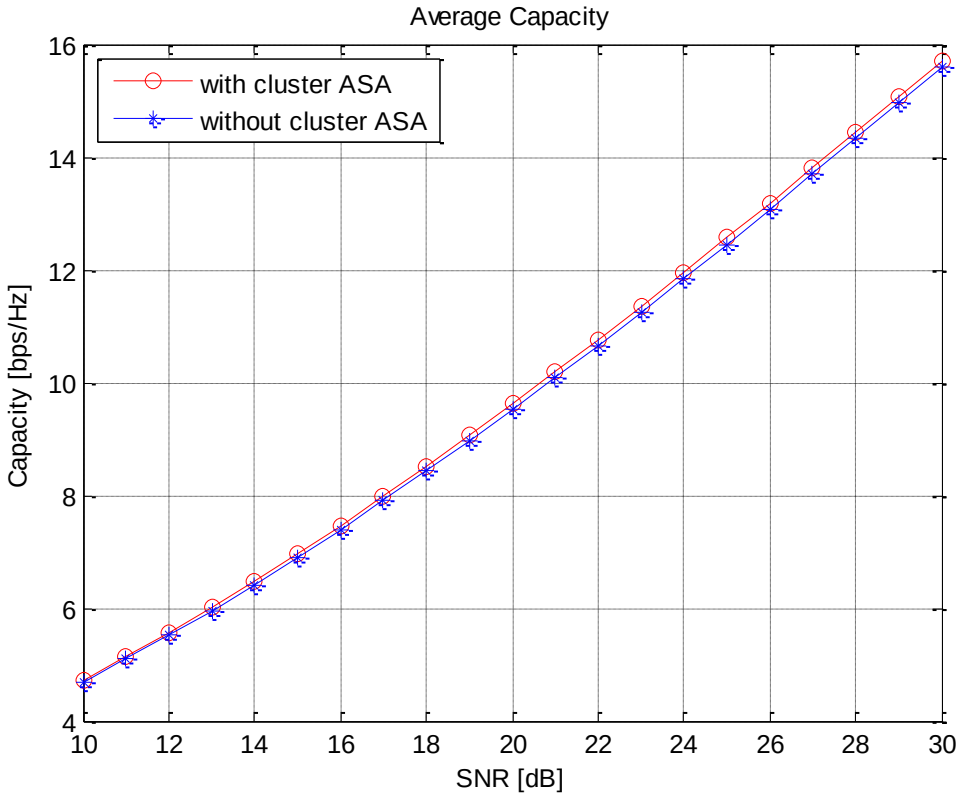

Figure 4.21: Ergodic capacities for the B3 NLOS channel with and without cluster ASA. The MS with high correlation antennas is simulated.

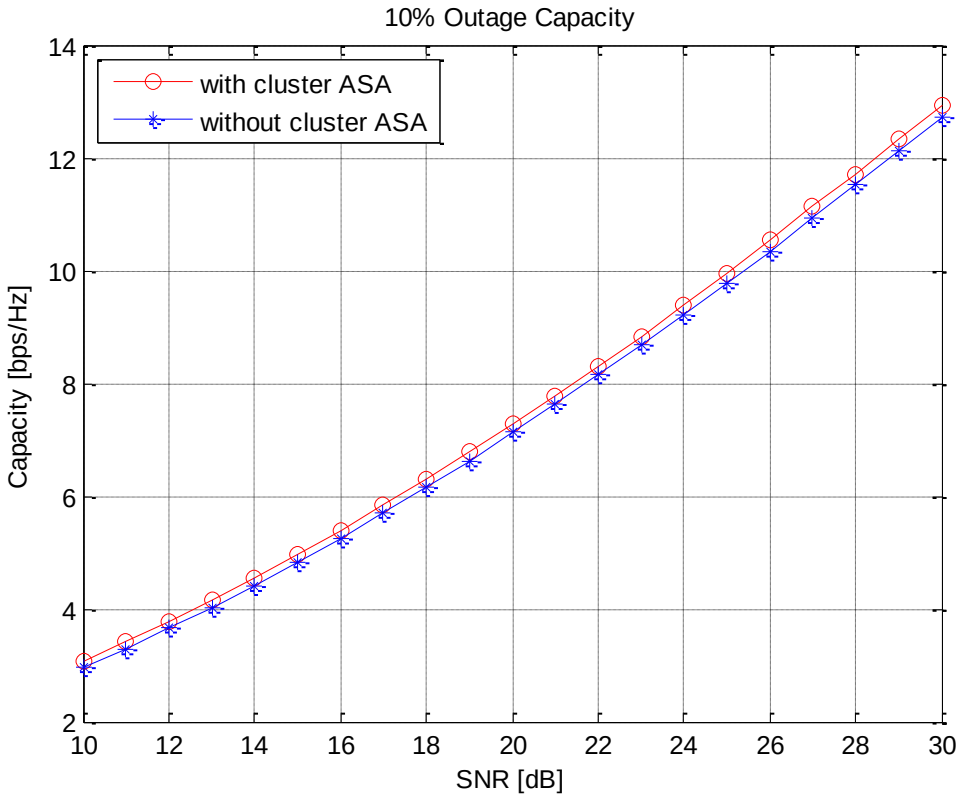

Figure 4.22: 10% outage capacities for the B3 NLOS channel with and without cluster ASA. The MS with high correlation antennas is simulated.

Table 4.2 concludes whether the intra-cluster ASA can be removed in each scenario. The MS with high correlation antennas is used as the DUT to evaluate this simplification method. However, whether the high correlation MS is adequate as the limiting case for this evaluation still requires further study.

Table 4.2: Cluster ASA for all the chosen scenarios in the WINNER II CDL model.

Scenario		Cluster ASA [°]	Total ASA with Cluster ASA [°]	Total ASA w/o Cluster ASA [°]	Cluster ASA Removable
B3	LOS	5	34.7	34.6	Yes
	NLOS	13	46.3	45.6	Yes
B4	NLOS	5	57.0	57.0	Yes
B1	LOS	18	28.2	27.2	Yes
	NLOS	22	39.0	35.2	No
C1	NLOS	10	41.3	40.8	Yes
D1	NLOS	3	35.4	35.3	Yes

Only in the B1 NLOS channel, the intra-cluster ASA is not (completely) removable. Since it is not practical to model intra-cluster ASA using 20 rays, which will result in a very complicated MPS and a large number of probe antennas in the OTA test system, a method of using 3 rays to model the intra-cluster Laplacian PAS in [4] is examined here. The principle of the method is to match the intra-cluster spatial correlation at the MS side between the 20-ray and the 3-ray cluster models. In

other words, by allocating the 3 rays with specific powers and offset angles, we can get a good match to the spatial correlation derived from the original 20-ray model.

In [4], the algorithm of the method is not described in detail. Therefore, we devised an algorithm to model the intra-cluster PAS with 3 rays: we place one ray with relatively larger power at the mean angle of the cluster AoA; the other two rays with lower identical power are placed at the same offset angles around the mean AoA. Using Eq. (4-13) for angular spread calculation, we get the relationship between the power distribution and the offset angles of the 3 rays in determining the angular spread. Then, by matching the spatial correlation derived from the 20 rays, we get the best power distribution and offset angles. The concept of Euclidean distance is used to find the best matching. The cluster spatial correlation is given by

$$\rho_c = \frac{\sum_{m=1}^{M} P_m \exp\left(j2\pi d_t \sin(\theta_m)\right)}{\sum_{m=1}^{M} P_m},$$

where θ_m and P_m are the ray angle and power, respectively, M is the number of rays per cluster, d_t is the antenna spacing in wavelength.

Here, an example is given for the use of 3 rays to model the 22° intra-cluster ASA in the B1 NLOS channel. The MS antenna spacing (i.e., isotropic antennas) is set to half-wavelength. The power distribution and offset angles of the 3 rays are shown in Figure 4.23. One ray with 62% of the total cluster power is placed at the mean AoA, whereas the other two rays, each with 19% of the total power, are placed at offset angles to mean AoA. It can be seen in Figure 4.24 that a good match to intra-cluster spatial correlation can be obtained. When applying the 3-ray method in our simulation, we find that the decreases in ergodic capacity and outage capacity are only 1% and 2% respectively, if the MS with high-correlation antennas is used as the DUT. Figure 4.25 and Figure 4.26 compare the capacities of the 3-ray method and the original 20-ray method. Figure 4.27 compares the MS spatial correlation derived from all the clusters. The difference in the total spatial correlation is much smaller than the difference in Figure 4.18.

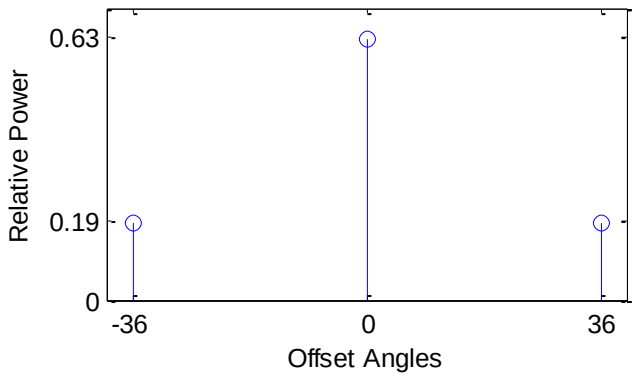

Figure 4.23: Relative power distribution and offset angles of the 3 rays used to model the 22° cluster ASA in B1 NLOS. Antenna spacing is assumed to be half-wavelength.

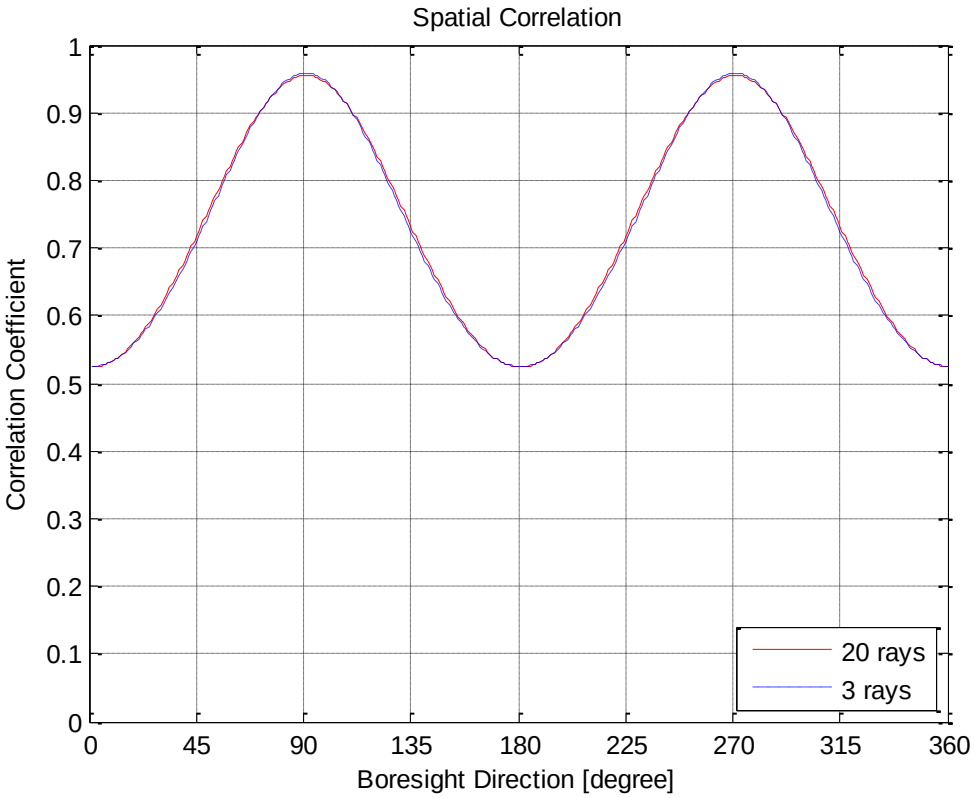

Figure 4.24: 3 rays to match the intra-cluster spatial correlation at MS side. Antenna spacing is assumed to be half-wavelength.

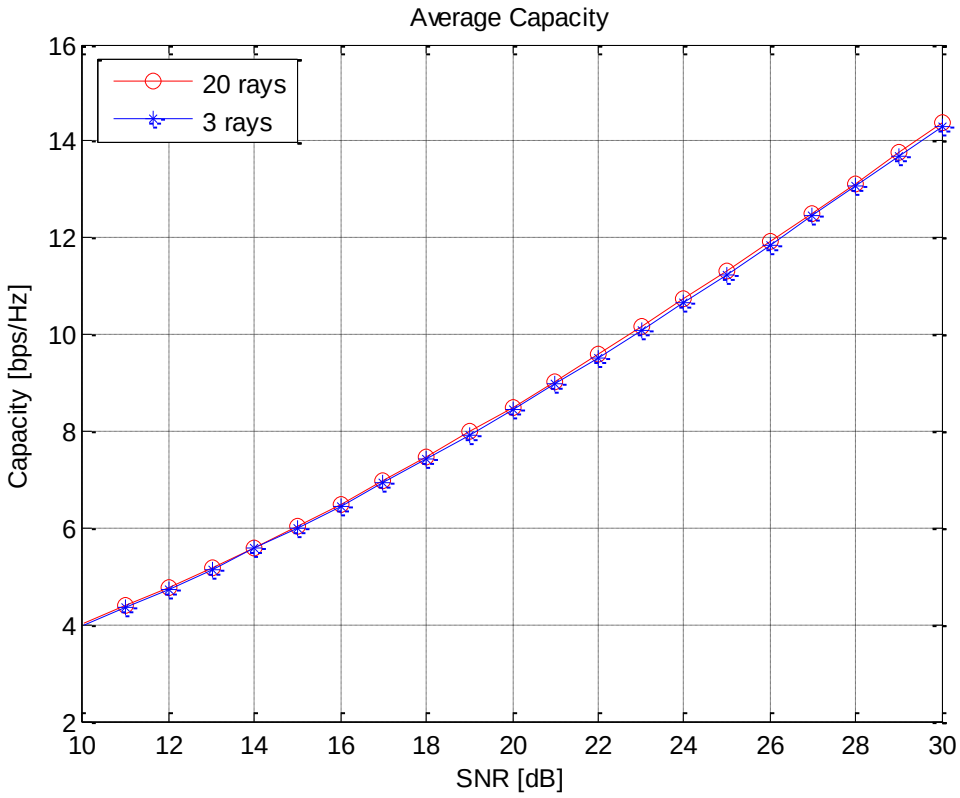

Figure 4.25: Ergodic capacities of the B1 NLOS channel using 20 rays and 3 rays, respectively, to model the cluster ASA. The MS with high correlation antennas are simulated.

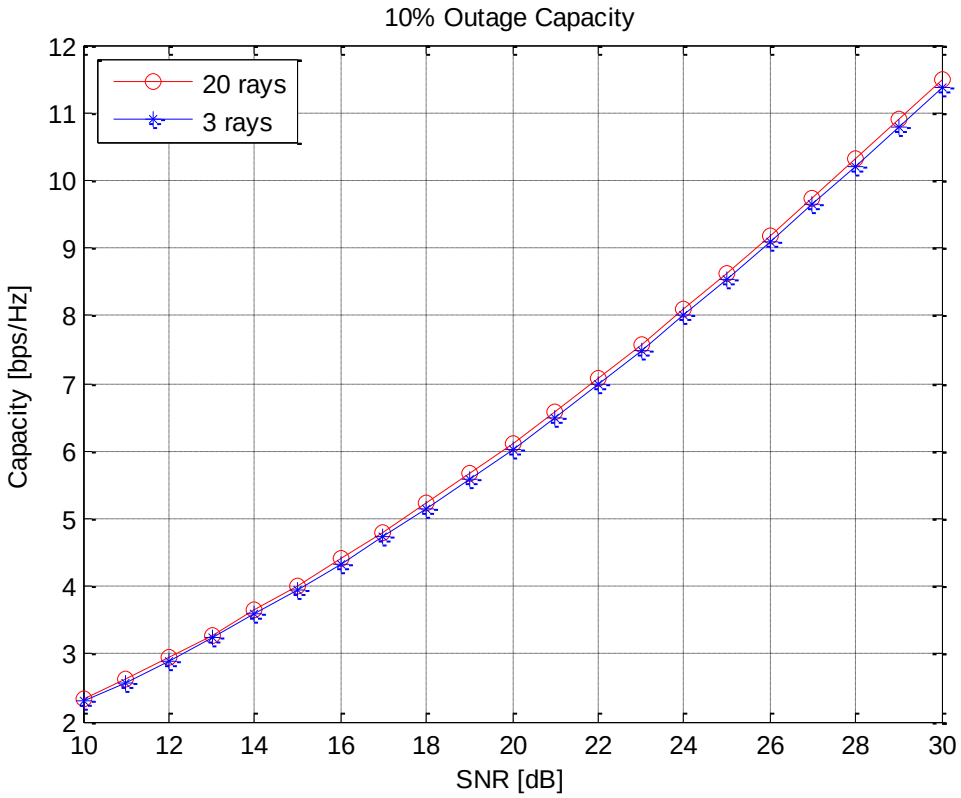

Figure 4.26: 10% outage capacities of the B1 NLOS channel using 20 rays and 3 rays, respectively, to model cluster ASA. The MS with high correlation antennas are simulated.

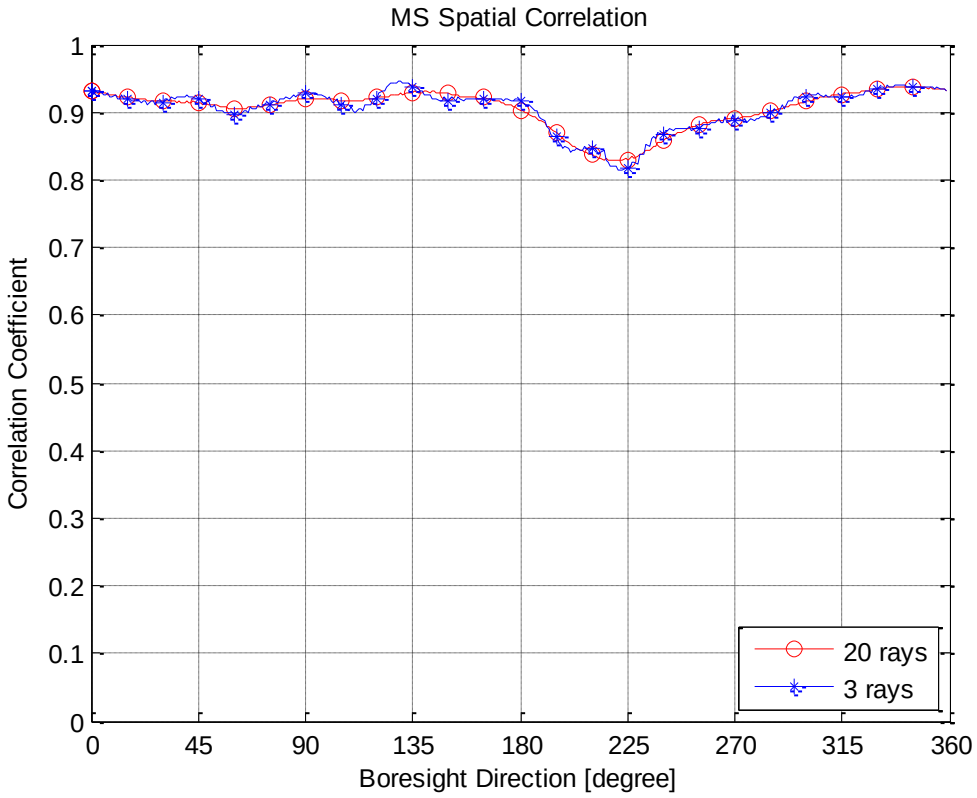

Figure 4.27: MS spatial correlation derived from the B1 NLOS channel using 20 rays and 3 rays to model cluster ASA. The MS with high correlation antennas are simulated.

Arbitrary intra-cluster ASA can be modeled using this method. To some extent, it is a good way to replace the 20-ray method, which is impractical in the OTA test system.

However, we find that degree of matching depends on the MS antenna spacing. Figure 4.28 shows the matching when antenna spacing is 3 wavelengths. It can be seen that the agreement between the two cases is quite poor. In this case, the power distribution and offset angles of the 3 rays are different from that shown in Figure 4.23. Although the matching is not good, the total angular spread of the 3-ray model is the same with original 20-ray model, and the changes in ergodic capacity and outage capacity are only 1% and 2% respectively. Therefore, the 3-ray matching method can be used to model the cluster ASA for isotropic antennas with 3 wavelengths spacing. However, tuning the 3-ray model to (the antenna spacing of) a given DUT is impractical. Moreover, OTA test systems should not need to know the antenna configurations of the DUTs in general. Nevertheless, for a given channel model, it may be possible to match to some extent the 3-ray model to the original 20-ray model for an expected range of antenna spacings of the DUTs. This issue is left for further study.

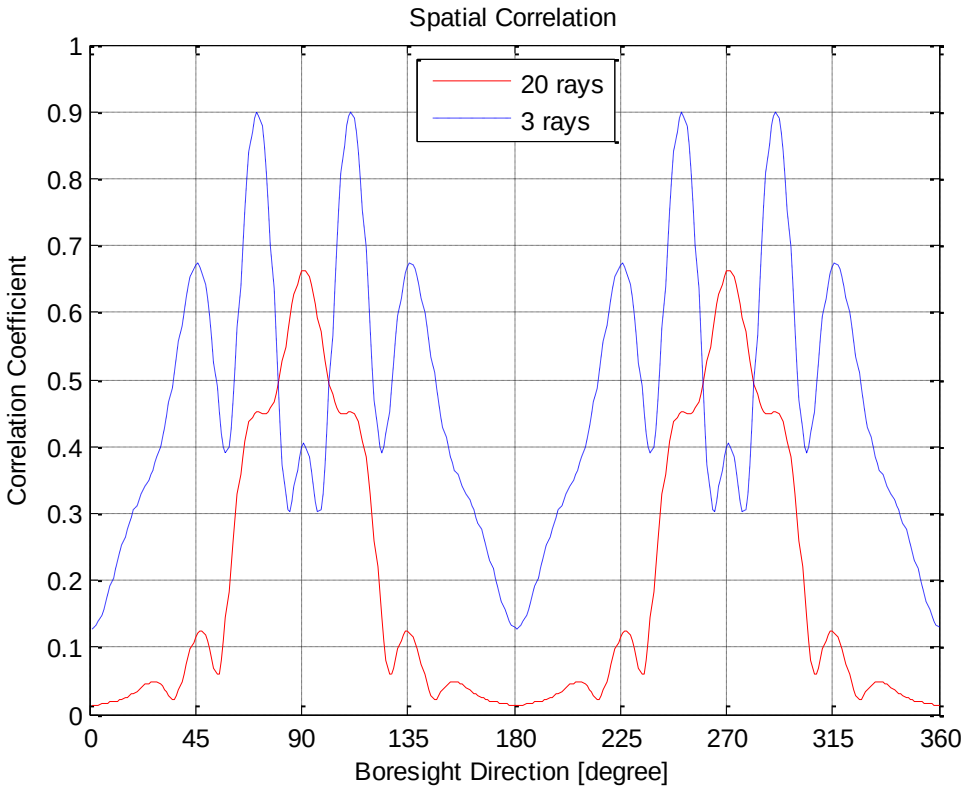

Figure 4.28: Using 3 rays to match the intra-cluster spatial correlation at the MS side. Antenna spacing is assumed to be 3 wavelengths.

4.2.3.5 Cluster Discarding

The number of clusters in the CDL channel model determines how many attenuators and phase shifters are needed in the MIMO OTA test system. For simple implementation in MPS, we consider in the following the possibility to discard the clusters with relatively low powers, as long as the DUT performance does not change appreciably in the simplified channel.

Discarding low power clusters leads to the changes in the delay distribution and the angle distribution surrounding the MS. Thus, the capacity will change correspondingly. Our study confirms the simple intuition that both delay spread and angular spread will decrease after cluster discarding. This is because the discarded clusters have lower powers, which tend to have larger delays. As discussed previously, the decrease in the delay spread leads to the decrease in the outage capacity; and the decrease in the angular spread has a significant influence on the capacity of the MS with high-correlation antennas. If the changes in both the ergodic capacity and the outage capacity do not exceed 10%, we regard that the clusters can be discarded. To evaluate the channel simplification method of cluster discarding, the antenna patterns of the high-correlation MS are used in the simulations. We also take the spatial correlation at the MS side as a reference in our analysis.

Due to cluster discarding, the total power of all the clusters in a CDL model will decrease. In order to eliminate the effect of power decrease on the capacity, we spread the power of the discarded clusters to all the preserved clusters, so that the total power of all clusters in the model remains the same.

The ray power threshold is defined in the simulation. Clusters with ray power lower than the threshold are discarded. The object is to find the threshold upper limit with which the channel can have the least clusters while the change in capacities can be kept within 10%. Here, the WINNER II C1 NLOS channel model is taken as an example to explain the process of cluster discarding and threshold determination. Figure 4.29, Figure 4.30 and Figure 4.31 illustrate the ergodic capacity, the outage capacity and the MS spatial correlation, respectively, with different ray power thresholds for cluster discarding. Compared to the channel without cluster discarding, the ergodic capacities decrease 2% for both -21.0 dB and -20.5 dB thresholds; outage capacities experience greater changes, which are 7% and 10%, respectively. Therefore, -21.0 dB is the upper limit of thresholds for cluster discarding in C1 NLOS. Using the upper threshold, the number of clusters is reduced to from 14 to 10 without sacrificing the performance appreciably.

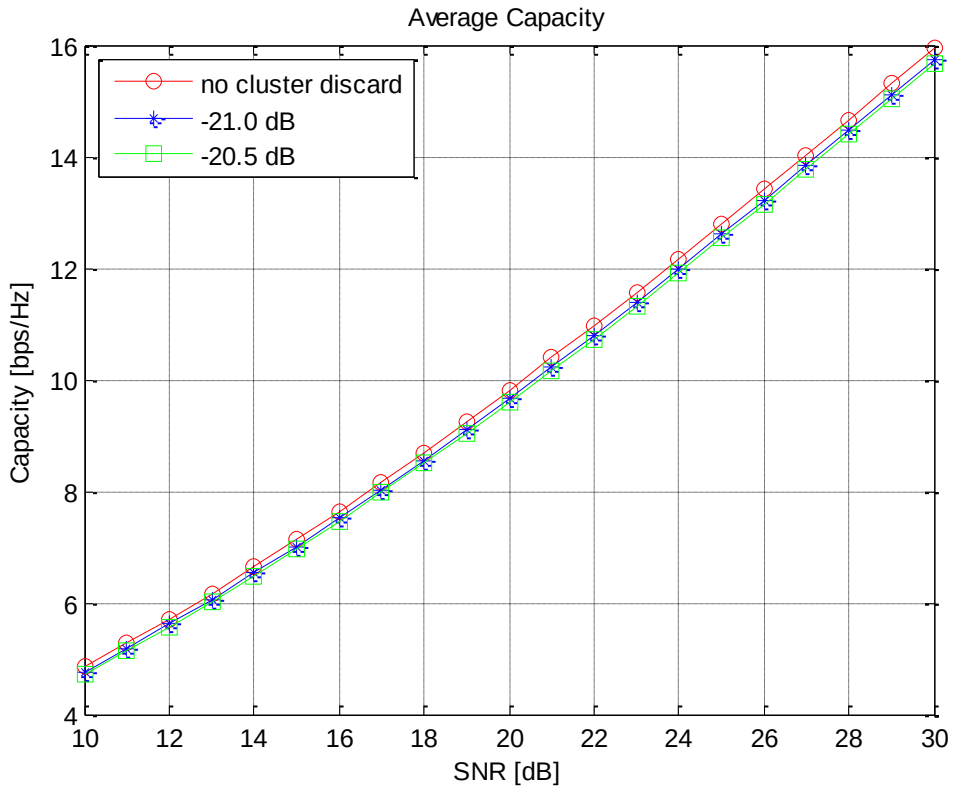

Figure 4.29: Ergodic capacities of the C1 NLOS model with different ray power thresholds for cluster discarding.

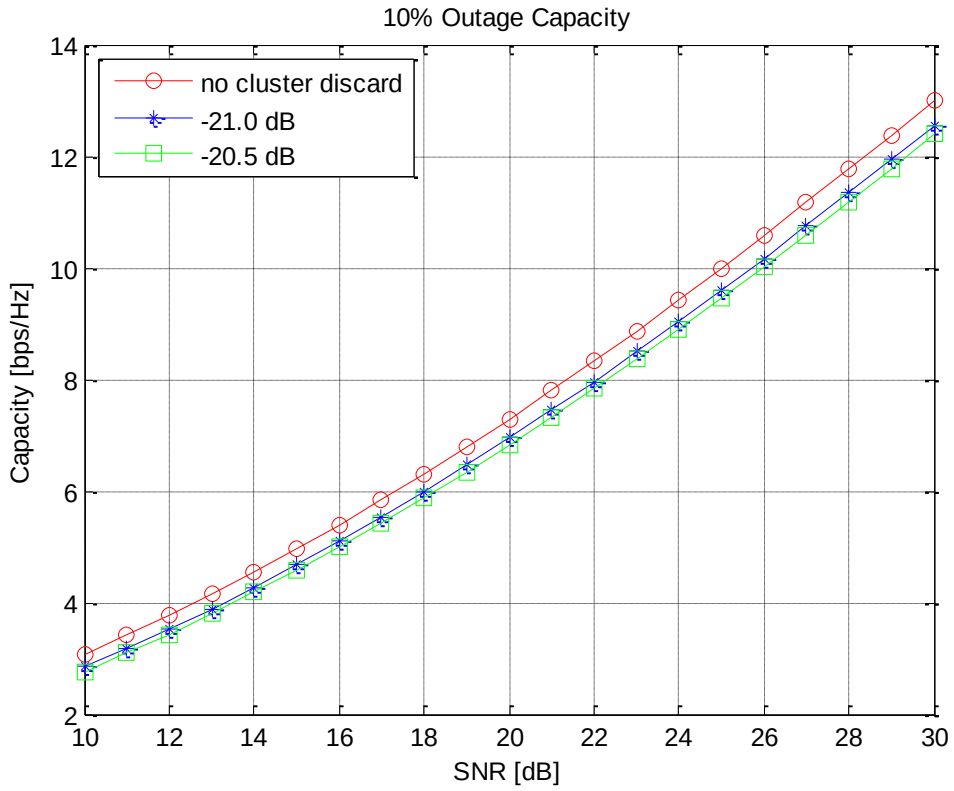

Figure 4.30: 10% outage capacities of the C1 NLOS model with different ray power thresholds for cluster discarding.

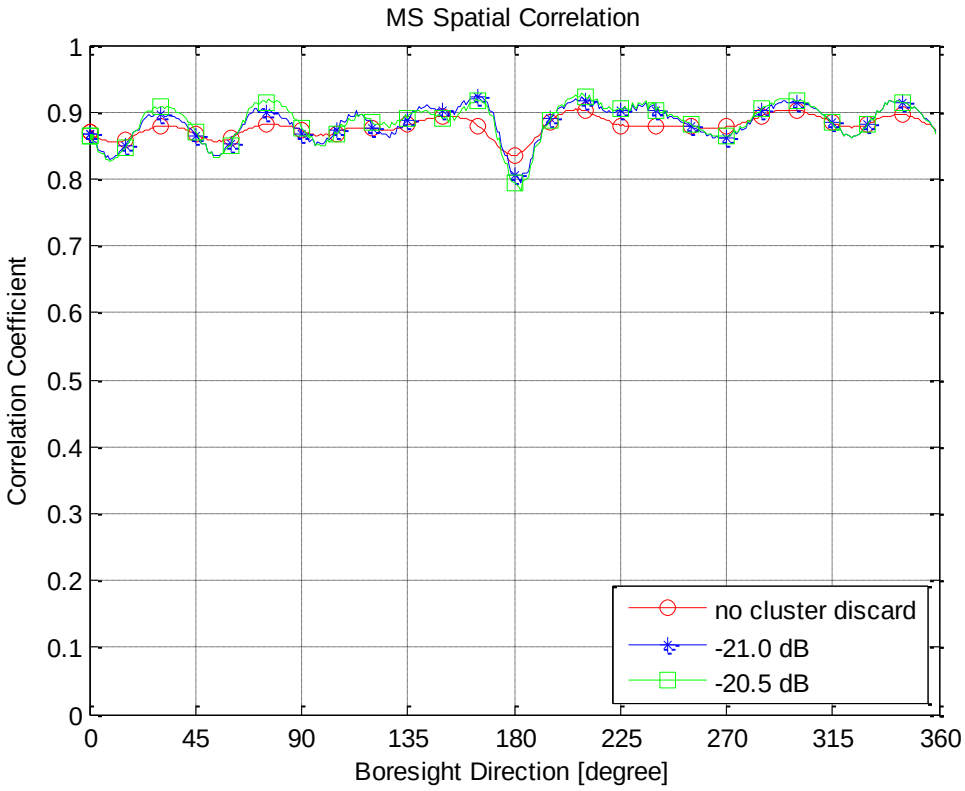

Figure 4.31: MS spatial correlations of the C1 NLOS model with different ray power thresholds for cluster discarding.

Through simulations for all the chosen scenarios, the ray power threshold upper limits are found and listed in Table 4.3. In all the scenarios except B1 NLOS, the cluster ASAs are removed.

Table 4.3: Results of cluster discarding for all the chosen scenarios.

Scenarios		Ray Power Threshold Upper Limit [dB]	Number of Preserved Clusters
B3	LOS	-26.8	6
	NLOS	-24.1	11
B4	NLOS	-19.9	4
B1	LOS	-26.9	4
	NLOS	-21.1	4
C1	NLOS	-21.0	10
D1	NLOS	-17.2	5

The threshold upper limits and number of preserved clusters are not the final results for cluster discarding. When SFE is applied in the simulation, for example, the shifting of the AoAs to the positions of the antenna probes is considered, and as a result the number of clusters that can be discarded may change. The final results of the simplified channels for all the scenarios are given in Section 4.4. However, the results in Table 4.3 can be a reference for channel simplification in the delay domain, if other SFE implementation methods are used.

4.3 Spatial Fading Emulator (SFE)

In this thesis, SFE is taken to mean the part of the MIMO OTA test setup that replicates the spatial characteristics of the channel model, which consists an array of probe antennas inside an anechoic chamber. Currently, an azimuth ring structure, with uniform spacing between adjacent probe antennas, is the most commonly used configuration. The following study of SFE involves the determination of the number of antenna probes needed and the effective test area within the emulator.

4.3.1 Antenna Probes

The radius of the emulator is restricted by the size of the anechoic chamber. In our study, the radius is set to be 1.4 m, which corresponds to Sony Ericsson's test configuration. The emulator size restricts the number of antenna probes that may be used, as the spacing between adjacent probes needs to be large enough to mitigate coupling effect. In addition, the size of the antenna probes also affects the spacing and placement. For example, the dual-polarized wideband antenna probes as shown in Figure 2.2 have the benefit of covering multiple mobile frequency bands, including the bands that are lower than 1 GHz. However, they are physically large. Therefore, how many antenna probes are needed to model AoAs should be determined, such that the implemented SFE can fulfill its function.

According to Table 4.3, we collect the AoAs of preserved clusters in all the scenarios. Each cluster has only one AoA in all the scenarios, except for B1 NLOS. For B1 NLOS, 3 rays are used to model intra-cluster ASA, so each cluster has 3 AoAs. Table 4.4 lists the AoAs of preserved clusters after cluster discarding. Note that the angles are converted from (-180°, 180°) in the original CDL models to (0°, 360°).

Table 4.4: AoAs of preserved clusters after cluster discarding in Table 4.3.

Scenario		AoAs [°]
B3	LOS	0, 307, 286, 76, 80, 287
	NLOS	287, 0, 266, 314, 75, 314, 301, 71, 86, 67, 95
B4	NLOS	0, 294, 91, 157
B1	LOS	0, 45, 291, 61
	NLOS	304, 340, 16, 324, 0, 36, 21, 57, 93, 269, 305, 341
C1	NLOS	0, 289, 46, 294, 294, 314, 304, 73, 70, 314
D1	NLOS	0, 28, 38, 305, 42

As illustrated in Table 4.4, there are 38 AoAs in total. However, it is not feasible to place 38 antenna probes in the emulator when the radius is in the order of 1.4 m, while retaining low coupling between adjacent antennas (for the mobile bands of interest). Furthermore, it will add additional hardware complexity into the setup. However, it can be observed in Table 4.4 that some of the AoAs are very close to one another, for example 36° and 38°, 70° and 71°. Therefore, to reduce the number of angles in total, we can shift some angles to the nearest probe locations, as long as the performance of the modified channel is still close to that of the original channel. If at most 5° is allowed for shifting the AoAs, the total number of AoAs can be greatly reduced to 13 (i.e.

nearly a three-fold reduction).

This method of determining the number of probes and their placements is restricted to the chosen scenarios. If different groups of scenarios are chosen, the number of probes and their placements are likely to be different. Thus this approach is not flexible enough for SFE to model AoAs. Only when the channel models in the MIMO OTA measurement are finalized, this method can be more readily applied. In order to model AoAs in any scenario, evenly distributed probes are commonly used in the proposed OTA test methodologies. Arbitrary AoA can be shifted to the nearest angle that is represented by an antenna probe. In [24], the number of antenna probes is determined by the spatial fading correlation of the MS antenna array. At least 15 probes are proposed. In our study, we determine the number of probes based on channel capacity.

The maximum shifting angle equals 180° divided by the number of probes. The more probes used, the more accurately the discretized AoAs reflect the original AoAs. To reduce the complexity of the SFE, the least number of probes that fulfills the performance requirement needs to be determined. A shift in the AoA of a ray influences the overall angular spread. Thus, we compare the angular spread after AoA shifting with the angular spread of the original channel (in this case, the original channel implies the one obtained after cluster discarding, i.e., Table 4.3). Table 4.5 shows the comparison of angular spread in each scenario. We consider four cases of the number of probes, i.e., being 18, 15, 12 and 9, and the corresponding maximum shifting angles are 10°, 12°, 15° and 20°.

Table 4.5: Total angular spread in the channel simplification process.

Scenario		Original AS [°]	AS after Cluster Discarding [°]	AS after Angle Shifting [°] / Number of Probes			
				18	15	12	9
B3	LOS	34.7	33.3	35.2	31.4	34.5	32.2
	NLOS	46.3	44.1	44.0	44.4	45.4	43.5
B4	NLOS	57.1	56.7	56.8	57.1	56.1	57.0
B1	LOS	28.2	25.8	23.5	27.5	27.7	27.6
	NLOS	39.0	36.4	38.3	35.1	38.2	30.3
C1	NLOS	41.3	40.0	39.3	40.9	41.4	41.2
D1	NLOS	35.4	31.9	32.5	31.6	31.6	29.5

The decrease in angular spread after cluster discarding *and* AoA shifting should not be too large, so that the change in capacity can be kept within 10%. We calculate the capacity change for all the cases in Table 4.5. The MS with high correlation antennas is simulated.

When the number of probes is 18, the decrease in capacity exceeds 10% only in B1 LOS. The ergodic capacity and outage capacity decrease 3% and 12% respectively.

When the number of probes is 15, the decrease in capacity exceeds 10% only in B1 NLOS. The ergodic capacity and outage capacity decrease 3% and 13% respectively.

When the number of probes is 12, only in B4 NLOS scenario the capacity decreases out of 10%. The change in ergodic capacity and outage capacity are 3% and 10% respectively.

When the number of probes is 9, the decrease in capacity exceeds 10% in B1 NLOS and D1 NLOS. In B1 NLOS, the ergodic capacity and outage capacity decrease 5% and 19% respectively. In D1 NLOS, the ergodic capacity and outage capacity decrease 3% and 13% respectively.

Since the decrease in capacity is also due to cluster discarding, in order to keep the capacity change within 10% for a given number of probes, we can lower the upper limit of ray power threshold to retain more clusters. For example, when the probe number is 9, the capacity change in B1 NLOS can be kept within 10% if the cluster discarding threshold is set to -32.6 dB. Five more clusters are retained in this case. When the probe number is 15, to keep the change in capacity in B1 NLOS within 10%, we can set the threshold to -21.6 dB. One more cluster is retained, and the change in the outage capacity reduces to 8%.

When the number of probes is 12, 15 or 18, the change in capacity marginally exceeds our limit in only one scenario; when the number of probes is 9, there are two scenarios in which the capacity decreases more than 10%, with B1 NLOS experiencing a more severe decrease in the outage capacity of 19%. Therefore, we choose to focus on the cases of 12, 15 or 18 probes. If 15 probes are used, one more cluster needs to be retained in B1 NLOS; however, considering that the cluster ASA cannot be removed in B1 NLOS, adding one cluster means adding three more rays. Thus we suggest 12 antenna probes to be used in the emulator. In this case, the cluster threshold in B4 NLOS is set to -23.3 dB.

From the discussion above, there is a tradeoff between the number of RF chains and the number of antenna probes in the MIMO OTA test system. RF chain is more expensive than antenna probes. To keep the MPS simple, the optimal number of antenna probes should be 12.

In [24], 15 probes are needed with regards to the effective test area of the DUT. And for uniform placement of probes in a ring configuration, an odd number of probes is suggested to avoid wave reflection from the probe on the opposite end, across the center of the ring from the transmitting probe. However, these proposals need to be studied further and verified in the real MIMO OTA test system.

4.3.2 Effective Test Area in SFE

In [24], effective area is defined with regard to the wave power ratio P/P_0 of less than 2 dB, where P is the power received at the observation point, and P_0 is the power received at the center of the emulator. The effective area is obtained to be within a radius of $0.2r$, r is the radius of the emulator.

In the emulator, the far field concept should also be considered. In general, the far field distance of an antenna is considered to be a distance larger than 10 wavelengths from the phase center of the antenna. That is to say, the distance between probe antenna and MS antenna should be larger than 10 wavelengths. In our simulation, the system frequency is 2.48 GHz, so 10 wavelengths is about 1.2 m. And the radius of the emulator is 1.4 m, so the far field area has the radius of about 0.2 m, which is shown in Figure 4.32. In our study, the performance of the DUT antennas at different

locations in the far field area is simulated. Effective area is found with regard to the change in capacity within 10%. Vertical and horizontal probe antenna patterns are added in the simulation. The free-space path-loss from the probe antenna to the MS antenna is also considered. The effective area is found for the simplified channel after cluster discarding and AoA shifting to 12 or 15 probes. We place one MS isotropic antenna on the negative y-axis and the other isotropic antenna on the positive y-axis. Table 4.6 and Table 4.7 list the effective test area for all the chosen scenarios when probe number is 12 and 15, respectively.

Note that the decrease in capacity is not only due to the change in the DUT location, but also due to the channel simplification that is done before. If the radius of the effective area is only 0.8 wavelengths, it is impossible to place DUTs with antenna spacing of over 0.8 wavelengths within the test area, which can be the case for larger DUTs, such as laptops with antenna spacing of up to 3 wavelengths. To have a larger effective area, more clusters should be preserved in the simplification process of cluster discarding. However, when the number of probe is 12, even if no cluster discarding is performed, the radius of the effective area for B3 LOS is less than 1.5 wavelengths.

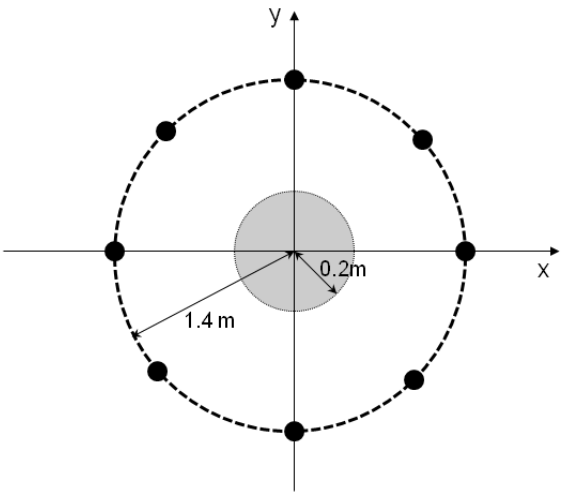

Figure 4.32: Far field area in the spatial fading emulator.

Table 4.6: Effective area when the number of probes is 12.

Scenario		Ray Power Threshold Upper Limit [dB]	Radius of Effective Area [wavelength]
B3	LOS	-26.8	0.8
	NLOS	-24.1	1.5
B4	NLOS	-23.3	1.5
B1	LOS	-26.9	1.3
	NLOS	-21.1	1.5
C1	NLOS	-21.0	1.5
D1	NLOS	-17.2	1.3

Table 4.7: Effective area when the number of probes is 15.

Scenario		Ray Power Threshold Upper Limit [dB]	Radius of Effective Area [wavelength]
B3	LOS	-26.8	1.5
	NLOS	-24.1	1.5
B4	NLOS	-19.9	1.5
B1	LOS	-26.9	0.8
	NLOS	-21.6	1.5
C1	NLOS	-21.0	1.5
D1	NLOS	-17.2	1.5

When the number of probes is 15, all the scenarios except B1 LOS can support an effective area with a radius of 1.5 wavelengths. To enlarge the effective area for the B1 LOS scenario, we can lower the threshold of cluster discarding to -27.8 dB.

From above analysis, the effective area of 15 probes is larger than the area of 12 probes. In order to support DUTs with antenna spacing of 3 wavelengths, 15 probes are needed.

4.4 Results

From the above analysis, the chosen CDL model can be simplified to fit the MIMO OTA test system. Considering the number of antenna probes and the effective area in SFE, the cluster discarding threshold and the corresponding number of preserved clusters for each scenario are listed in Table 4.8. The delays, powers and AoAs of the simplified channel are listed in Table 4.9 to Table 4.15.

Table 4.8: Results of cluster discarding for all the chosen scenarios. Number of antenna probes and effective test area are considered.

Scenario		Ray Power Threshold Upper Limit [dB]	Number of Preserved Clusters
B3	LOS	-26.8	6
	NLOS	-24.1	11
B4	NLOS	-19.9	4
B1	LOS	-27.8	5
	NLOS	-21.6	5
C1	NLOS	-21.0	10
D1	NLOS	-17.2	5

It is noted that the AoDs and the cluster ASDs are kept the same as the original channel model to generate the transmit correlation matrix for the simplified model. The K-factors for LOS cases and the XPRs are also unchanged. There is only one ray per cluster in all scenarios except for B1 NLOS. Since the cluster ASA in B1 NLOS cannot be removed, 3 rays per cluster are used to model the cluster ASA. However, this method has limitations, which are described in Section 4.2.3.4. The AoAs are shifted to the 15 evenly placed antenna probes.

The changes in the ergodic capacity and the 10% outage capacity are shown in Figure 4.33 to Figure 4.46, for MS with low-correlation antennas and high-correlation antennas. It can be seen from these figures, the changes in capacity are all within 10%, which means the simplified channel can deliver almost the same performance as the original channel. Thus, we propose that the simplified channel can be used in the MIMO OTA test system.

Table 4.9: WINNER II B3 LOS simplified model.

Cluster #	Delay [ns]	Power [dB]	AoA [°]
1	0	-10.9	0
2	0	-6.0	312
3	0	-12.2	288
4	50	-13.2	72
5	50	-10.5	72
6	100	-12.0	288

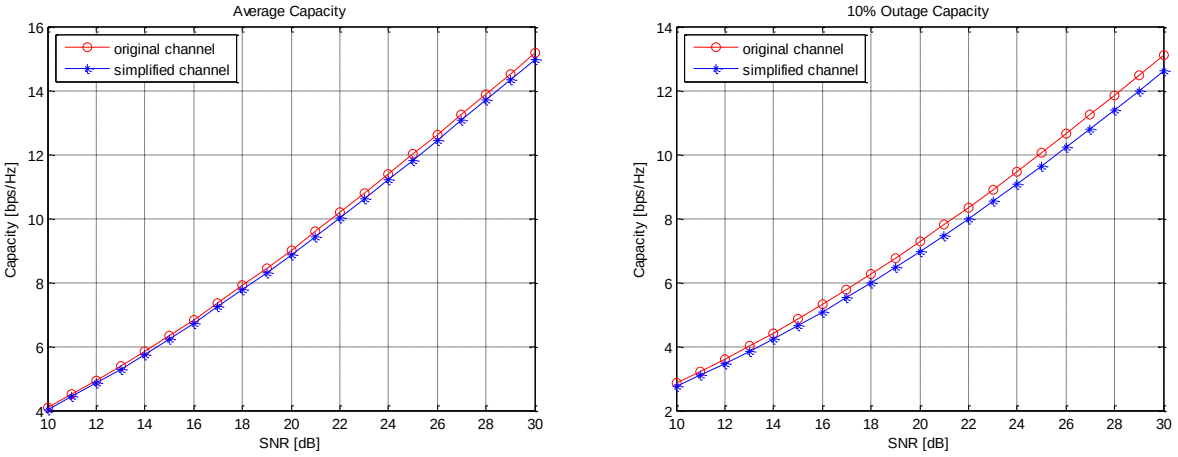

Figure 4.33: Capacities of the original channel and the simplified channel in B3 LOS. The MS with low-correlation antennas are used. In comparison with the original channel, the ergodic capacity and the outage capacity in the simplified channel decrease by 2% and 4%, respectively.

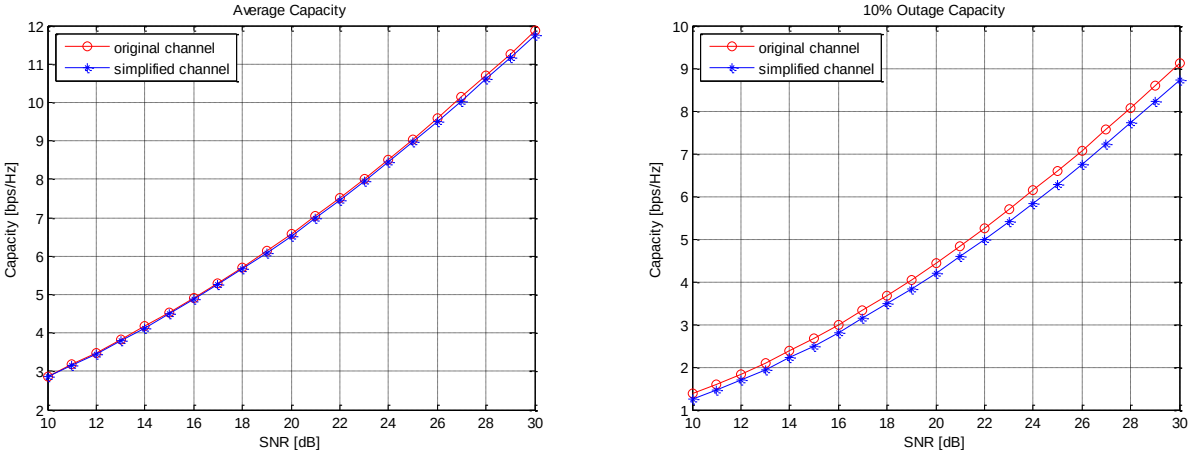

Figure 4.34: Capacities of the original channel and the simplified channel in B3 LOS. The MS with high-correlation antennas are used. In comparison with the original channel, the ergodic capacity and the outage capacity in the simplified channel decrease by 1% and 9%, respectively.

Table 4.10: WINNER II B3 NLOS simplified model.

Cluster #	Delay [ns]	Power [dB]	AoA [°]
1	0	-6.5	288
2	0	0.1	0
3	0	-10.9	264
4	0	-1.2	312
5	0	-7.0	72
6	0	-2.6	312
7	50	-4.2	312
8	50	-6.1	72
9	50	-9.0	96
10	50	-5.4	72
11	100	-11.0	96

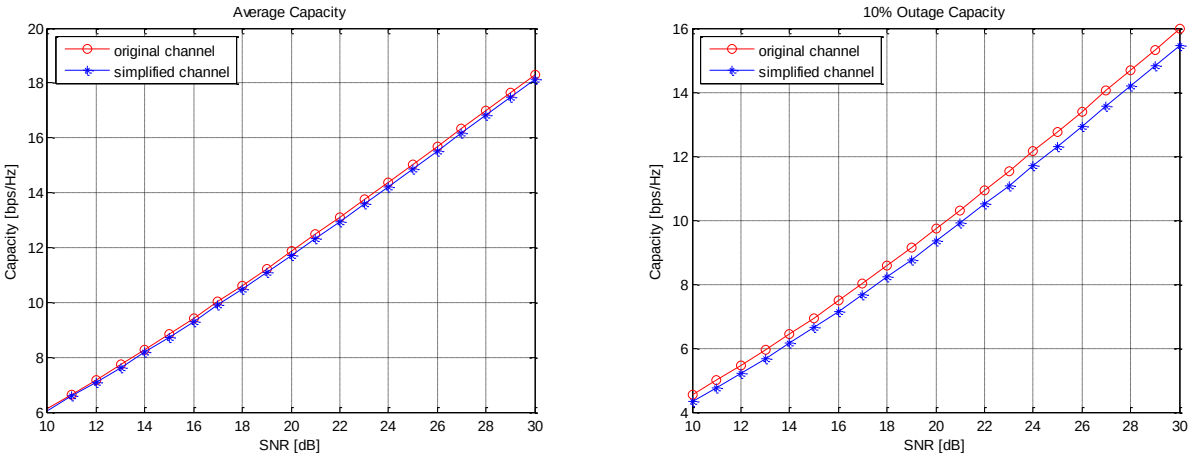

Figure 4.35: Capacities of the original channel and the simplified channel in B3 NLOS. The MS with low-correlation antennas are used. In comparison with the original channel, the ergodic capacity and the outage capacity in the simplified channel decrease by 2% and 6%, respectively.

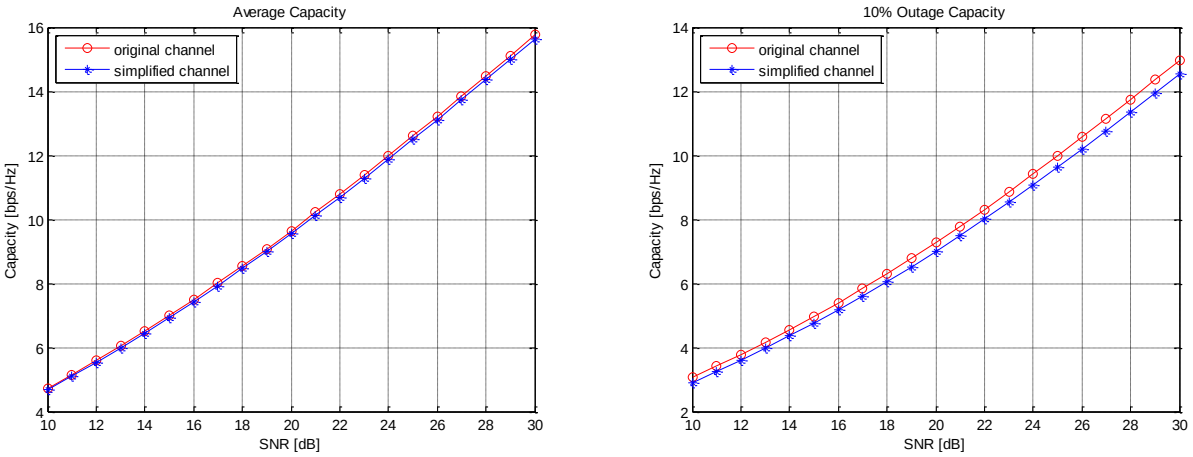

Figure 4.36: Capacities of the original channel and the simplified channel in B3 NLOS. The MS with high-correlation antennas are used. In comparison with the original channel, the ergodic capacity and the outage capacity in the simplified channel decrease by 2% and 7%, respectively.

Table 4.11: WINNER II B4 NLOS simplified model.

Cluster #	Delay [ns]	Power [dB]	AoA [°]
1	0	0.6	0
2	0	-3.1	288
3	50	-6.3	96
4	50	0.2	168

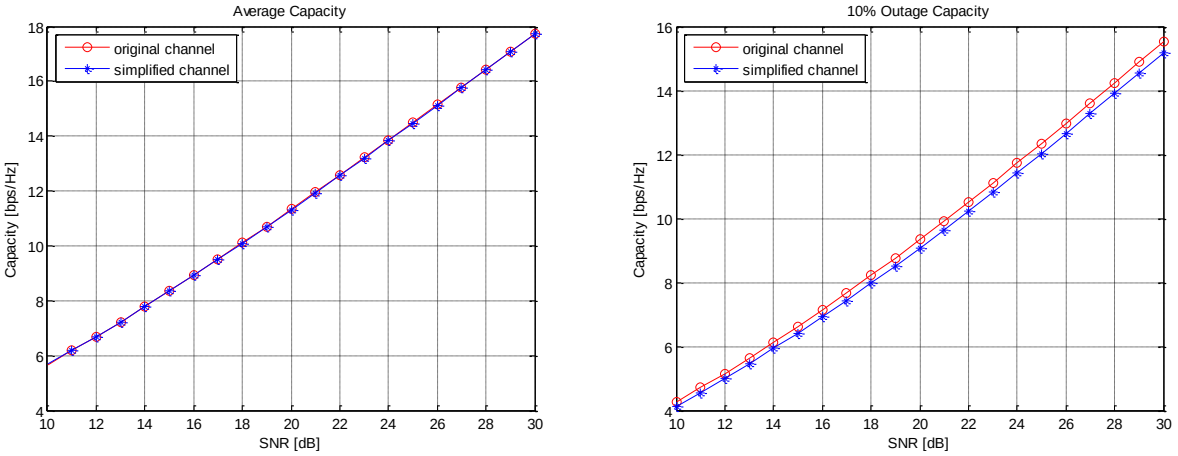

Figure 4.37: Capacities of the original channel and the simplified channel in B4 NLOS. The MS with low-correlation antennas are used. In comparison with the original channel, the ergodic capacity and the outage capacity in the simplified channel decrease by 0% and 3%, respectively.

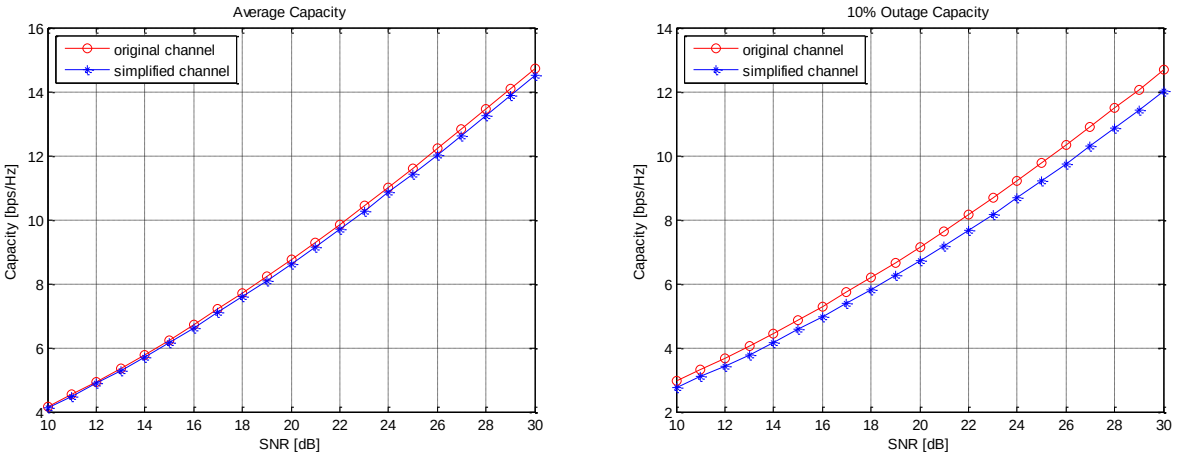

Figure 4.38: Capacities of the original channel and the simplified channel in B4 NLOS. The MS with high-correlation antennas are used. In comparison with the original channel, the ergodic capacity and the outage capacity in the simplified channel decrease by 2% and 7%, respectively.

Table 4.12: WINNER II B1 LOS simplified model.

Cluster #	Delay [ns]	Power [dB]	AoA [°]
1	0	-11.0	0
2	50	-6.8	48
3	50	-14.8	72
4	50	-9.9	288
5	100	-13.2	72

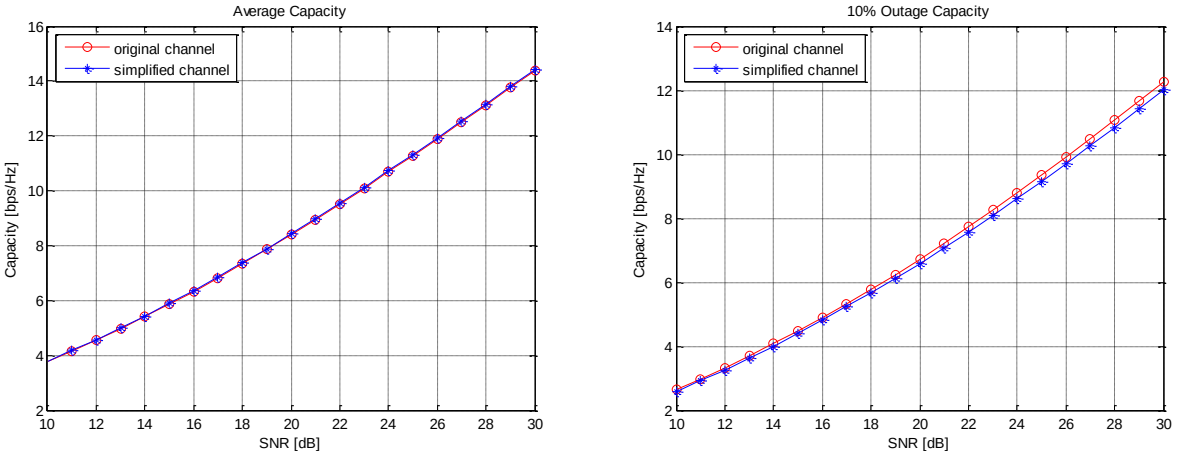

Figure 4.39: Capacities of the original channel and the simplified channel in B1 LOS. The MS with low-correlation antennas are used. In comparison with the original channel, the ergodic capacity and the outage capacity in the simplified channel decrease by 1% and 2%, respectively.

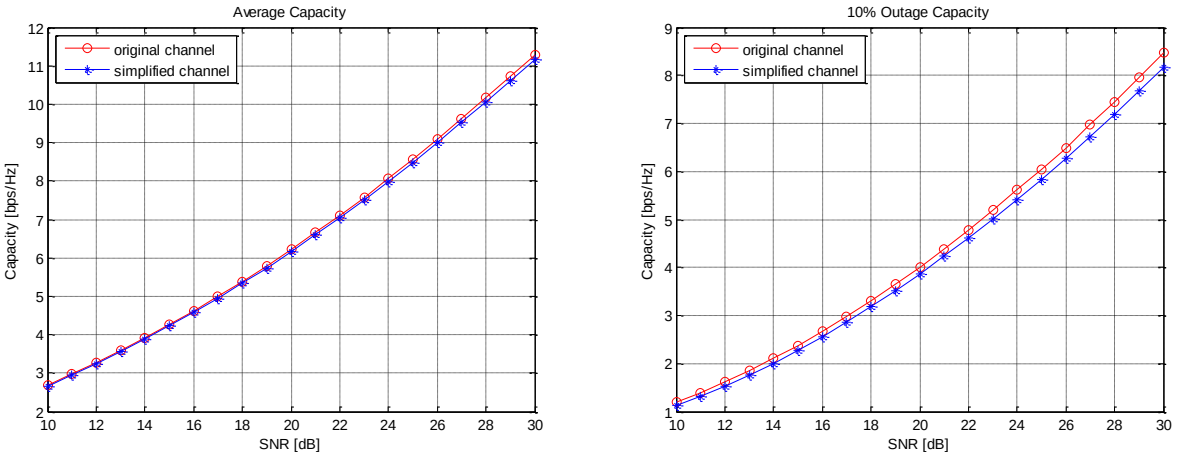

Figure 4.40: Capacities of the original channel and the simplified channel in B1 LOS. The MS with high-correlation antennas are used. In comparison with the original channel, the ergodic capacity and the outage capacity in the simplified channel decrease by 1% and 6%, respectively.

Table 4.13: WINNER II B1 NLOS simplified model.

Cluster #	Delay [ns]	Power [dB]	AoA [°]
1	0	-8.0, -2.7, -8.0	312, 336, 24
2	100	-7.0, -1.7, -7.0	336, 0, 48
3	100	-7.9, -2.6, -7.9	24, 48, 96
4	100	-15.1, -9.8, -15.1	264, 312, 336
5	250	-15.6, -10.3, -15.6	24, 48, 96

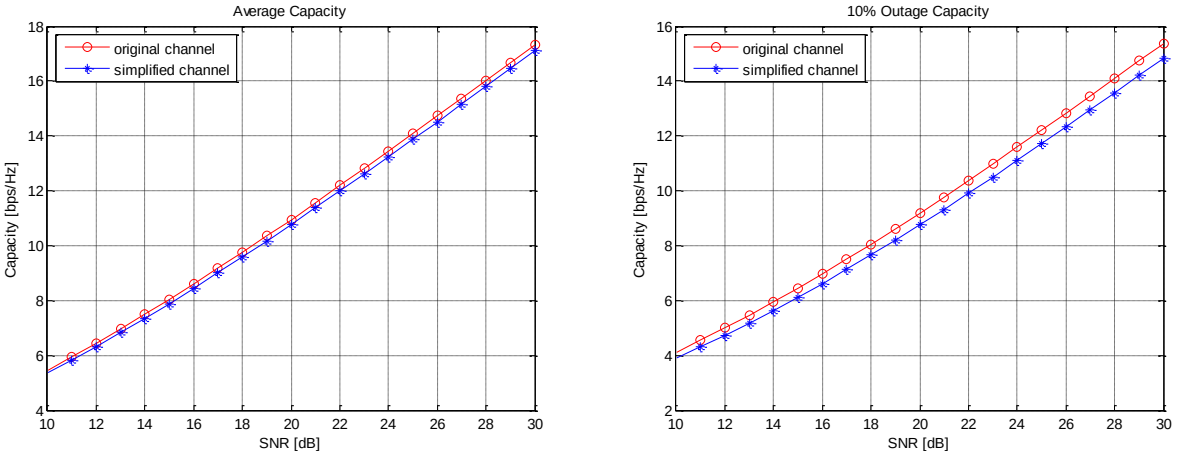

Figure 4.41: Capacities of the original channel and the simplified channel in B1 NLOS. The MS with low-correlation antennas are used. In comparison with the original channel, the ergodic capacity and the outage capacity in the simplified channel decrease by 2% and 5%, respectively.

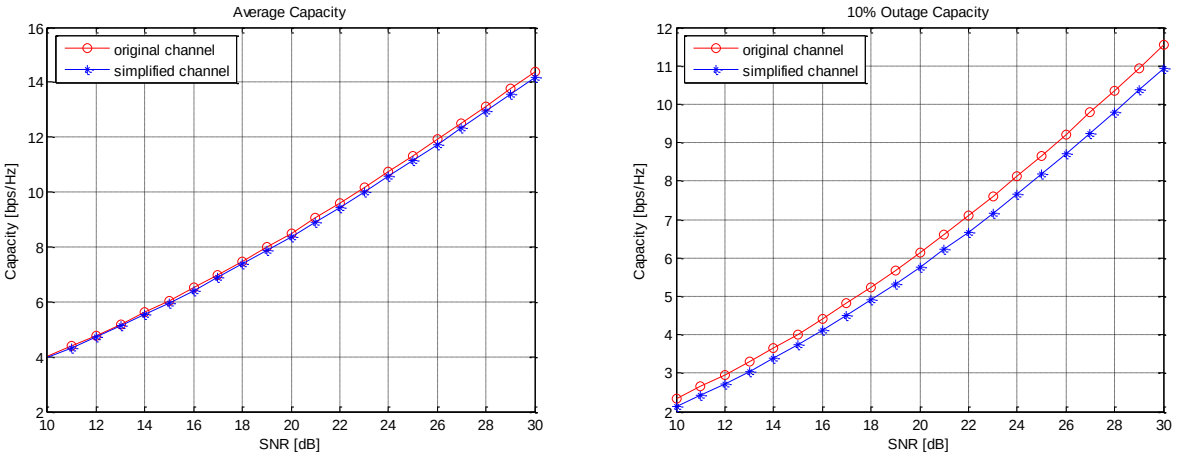

Figure 4.42: Capacities of the original channel and the simplified channel in B1 NLOS. The MS with high-correlation antennas are used. In comparison with the original channel, the ergodic capacity and the outage capacity in the simplified channel decrease by 2% and 9%, respectively.

Table 4.14: WINNER II C1 NLOS simplified model.

Cluster #	Delay [ns]	Power [dB]	AoA [°]
1	0	0.3	0
2	0	-7.2	288
3	50	-2.9	48
4	50	-2.8	288
5	50	-6.1	288
6	50	-2.8	312
7	150	-4.3	312
8	150	-7.7	72
9	200	-6.9	72
10	200	-2.8	312

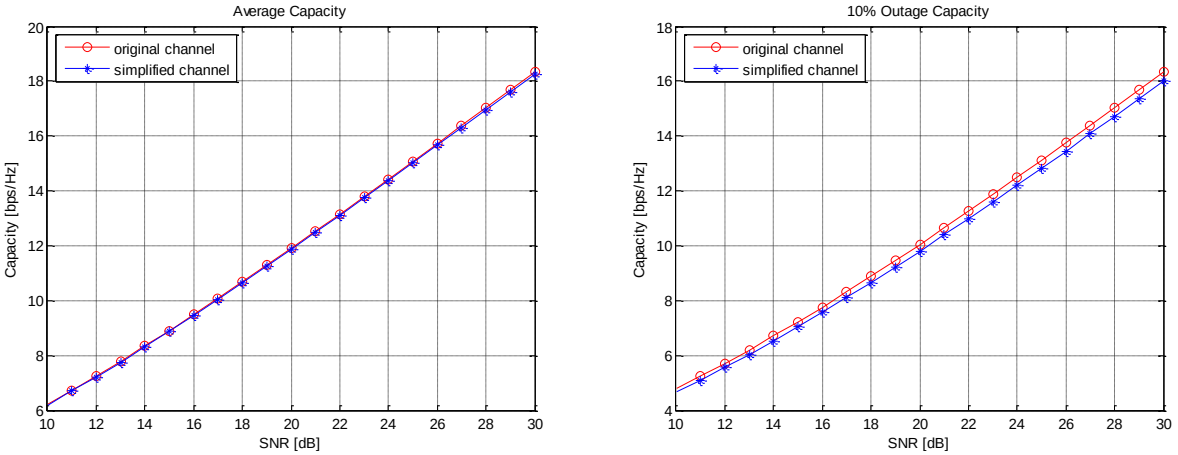

Figure 4.43: Capacities of the original channel and the simplified channel in C1 NLOS. The MS with low-correlation antennas are used. In comparison with the original channel, the ergodic capacity and the outage capacity in the simplified channel decrease by 0% and 3%, respectively.

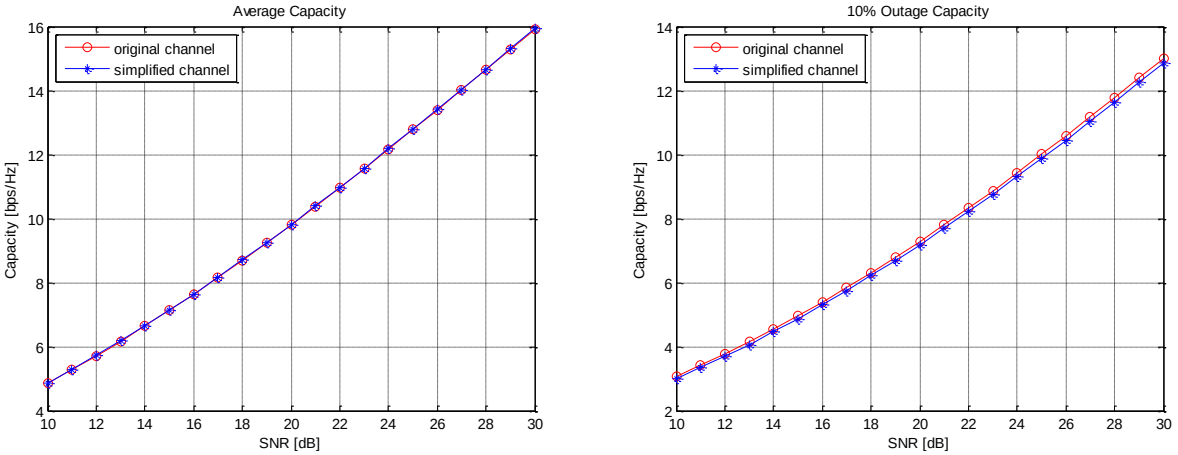

Figure 4.44: Capacities of the original channel and the simplified channel in C1 NLOS. The MS with high-correlation antennas are used. In comparison with the original channel, the ergodic capacity and the outage capacity in the simplified channel decrease by 0% and 2%, respectively.

Table 4.15: WINNER II D1 NLOS simplified model.

Cluster #	Delay [ns]	Power [dB]	AoA [°]
1	0	0.8	0
2	0	-1.0	24
3	0	-2.5	48
4	0	-1.0	312
5	100	-3.4	48

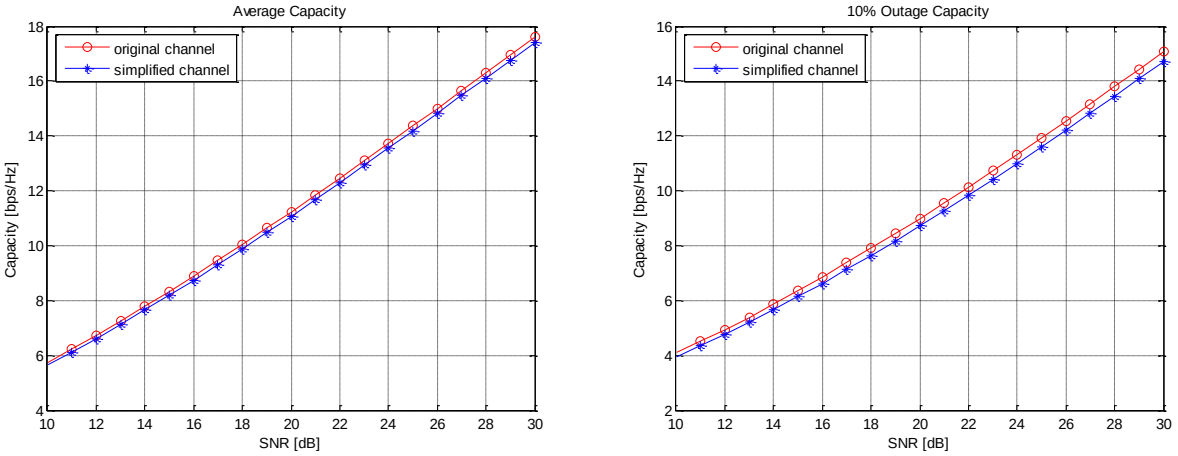

Figure 4.45: Capacities of the original channel and the simplified channel in D1 NLOS. The MS with low-correlation antennas are used. In comparison with the original channel, the ergodic capacity and the outage capacity in the simplified channel decrease by 2% and 3%, respectively.

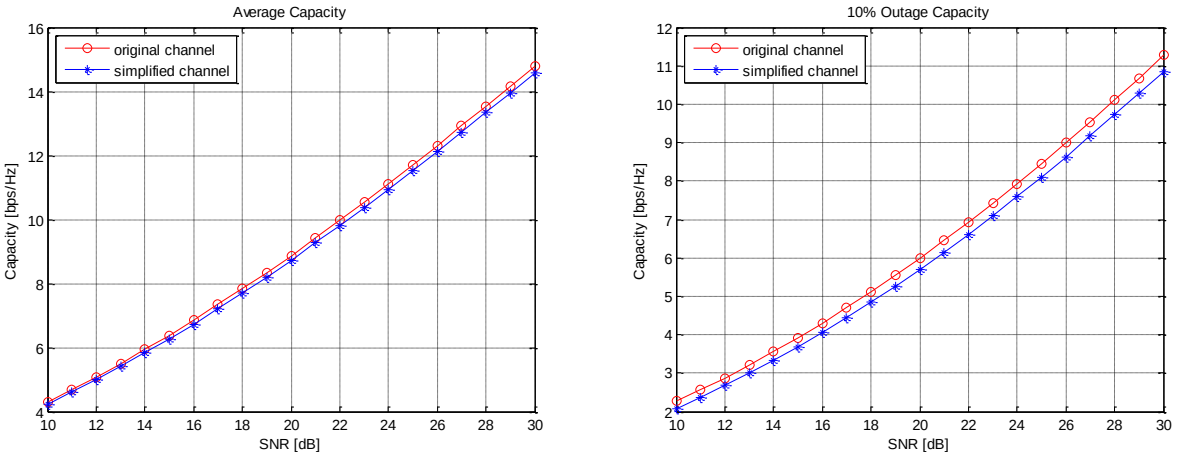

Figure 4.46: Capacities of the original channel and the simplified channel in D1 NLOS. The MS with high-correlation antennas are used. In comparison with the original channel, the ergodic capacity and the outage capacity in the simplified channel decrease by 2% and 8%, respectively.

Chapter 5 Conclusions and Future Work

5.1 Conclusions

The primary goal of this thesis is to provide technical support in the development of a MIMO OTA test system. First, a MIMO OTA test method called the MPS Method is introduced. The focus is to evaluate the OTA performance of MIMO terminals in HSPA and LTE systems. This MPS Method consists of a multipath simulator (MPS) and a spatial fading emulator (SFE), which are combined to generate spatial-temporal multipath propagation channels for MIMO communication systems. To practically implement this method in a MIMO OTA test system, a MATLAB simulation system is built to analyze the channel models and provide the parameters needed in the corresponding hardware setup.

In this thesis, the spatial channel models related to B3G wireless communication systems are described and analyzed. The comparison of features and parameters of these models are tabulated in Section 3.4. As a result, the WINNER II CDL model is suggested to be suitable for the simulation of HSPA and LTE systems, since it supports more scenarios and is based on real channel measurements. Although SCME can also support 100 MHz bandwidth, which satisfies the bandwidth requirement of HSPA and LTE systems, it has several limitations if being used in simulation, including the supported bandwidth being an artificial extension of the 5 MHz bandwidth of the SCM, the indoor channel model is unavailable, and no definite K-factor is specified in the SCME TDL model.

Based on the MATLAB simulation system, 2 x 2 MIMO channels are generated for a set of chosen scenarios and for several MIMO terminals with theoretical (i.e., isotropic) or measured 3-D patterns. In the channel generation, Kronecker model with transmit correlation is used and expressions of Kronecker model for both LOS and NLOS cases are presented. When the channel CIR is calculated, polarizations are also included.

Then, simplifications of the channel model are performed in order to reduce the cost and complexity of the OTA test system. We choose capacity as the dominant criterion to assess the simplifications. The ergodic capacity and outage capacity are calculated and compared between the original channel models and the corresponding simplified channel models. Channel properties such as delay spread, angular spread and MS spatial correlation are also calculated as the support criteria to analyze how the change in channel model parameters influence the channel performance.

The simplifications are performed step by step, and they include bandwidth down-scaling, reduction of the number of rays per cluster, removal of intra-cluster angular spread and cluster discarding. It is pointed out in the thesis that the bandwidth of the channel model can be down-scaled to 20 MHz, since LTE system only supports bandwidth of up to 20 MHz. Thus, the channel models after bandwidth down-scaling to 20 MHz are regarded as the reference models.

In the original CDL model, each cluster is comprised of a vector of 20 sinusoids (or rays), which upon summation with random phases create a Rayleigh fading distribution. However, it is very complicated to realize this using hardware since 20 phase shifters are needed for each cluster. According to [15], the minimum number of sinusoids required to yield a reasonable Rayleigh distribution is 4. This claim is verified by simulation in the thesis. We also illustrate that the number can be further reduced to 1 by pre-fading the amplitude of each cluster. The results of changes in ergodic capacity and outage capacity show that the pre-fading method can be treated as an alternative way to model Rayleigh fading.

When the intra-cluster angular spread is examined, it is noticed that all the scenarios of interest have narrow cluster angular spreads of less than 25 degrees. Therefore, it is intuitive to consider complete removal of the angular spread. The simulation results show that for MSs with isotropic antennas, the capacity changes are below 10% in all the chosen scenarios, which is small enough to be considered negligible. However, for MSs with high correlation antennas, the capacity changes are greater than the capacity change of isotropic antennas. To make the simplified channel model applicable for all kinds of MSs, the MS with high correlation antennas is used as a reference to evaluate this simplification step. Then, for the scenarios with indispensable angular spread, a method of using 3 rays to replace the 20 rays per cluster is described. Simulation results show that this method is a good way to represent the original narrow angular spread with a small number of rays.

In the OTA test system, the number of clusters has a significant influence on the cost and complexity, since it determines the required numbers of attenuators and phase shifters. To reduce the number of clusters, thresholds are determined to discard clusters with low power. Different scenarios need different power threshold upper limits, which are decided through the simulation and given in Table 4.3, together with the number of preserved clusters.

After the simplifications of channel models, the optimal number of antenna probes for the SFE is studied and is found to be 12 or 15 for these simplified channels. The antenna probes are placed evenly in a circular configuration with a radius of 1.4 m, which is restricted to the size of anechoic chamber. In the SFE, the effective area is defined with regards to the change in capacity. In the study of the effective area, the far field distance between the probe antenna and the DUT is considered. In order to keep the validity of far field, the DUT should be tested within a circular area of radius 0.2 m in the middle of the SFE structure. In this far field area, the effective areas for 12 probes and 15 probes are found. Considering that the effective area should support the DUT with 3-wavelength antenna spacing, the number of probes is optimized to 15.

5.2 Future Work

In this thesis, Doppler shift is not simulated. The fading channel is realized by randomly generating ray phases for each realization. However, the fading of the channel is caused by the movement of the receiver, so it is reasonable to generate the Doppler shift by using the AoAs of the MPCs, the MS speed and its direction.

The simulation system is currently based on MATLAB. To control the hardware implementation based on the knowledge acquired, some codes should be transferred into LabVIEW or other kinds of hardware-control software. The software should be able to generate appropriate control signals for the phase shifters and attenuators.

The simplification steps in this thesis are measured by the change of ergodic capacity and outage capacity, on the assumption that the capacity can reflect the system throughput. In future work, the results need to be confirmed by the throughput performance.

Another aspect that needs to be verified is the 3-ray method for DUTs with different antenna spacing. In this thesis, we find that degree of matching depends on the MS antenna spacing. A good match can be obtained for the case of half-wavelength spacing while the deviation is significantly larger for 3-wavelength spacing antennas. It is necessary to specify the antenna spacing range where this matching method can work or to find a more efficient way to model the intra-cluster angular spread.

References

[1] A. Paulraj, R. Nabar, and D. Gore, *Introduction to Space-Time Wireless Communications*, UK: Cambrigde University Press, 2003.

[2] S. Ling, "MIMO OTA measurement campaign planning," Vodafone Group R&D Document, version 8, Mar. 2010.

[3] R4-090369, "Response to LS on status of radiated testing methods for MIMO/multiple receive antenna terminals (COST2100 SWG 2.2, COST2100_LS_Feedback)".

[4] D. Reed, "Experiments in spatial correlation for evaluating OTA techniques," in *COST2100*, TD (09) 856, Valencia, Spain, May 2009.

[5] J. Welinder and L. Fast, "Towards a low cost over the air performance test method," in *COST2100*, TD (09) 807, Valencia, Spain, May 2009.

[6] J. Kallankari, S. Laukkanen, and M. Nurkkala, "OTA HSDPA throughput measurements in a fading channel," in *COST2100*, TD (09) 836, Valencia, Spain, May 2009.

[7] A. Scannavini, L. Durand, M. A. El Anour, N. Gross , J. Nuutinen, P. Heino, and P. Kyösti, "Practical considerations on MIMO OTA testing," in *COST2100*, TD (09) 854, Valencia, Spain, May 2009.

[8] Y. Feng and W. Schroeder, "Extending the definition of TIS and TRP for application to MIMO OTA testing," in *COST2100*, TD (09) 866, Valencia, Spain, May 2009.

[9] S. Ling, "MIMO OTA measurement campaign planning," Vodafone Group R&D Document, version 2, Oct. 2009.

[10] M. Narandzic, C. Schneider, R.Thomä, T.Jämsa, P. Kyösti, and X. Zhao, "Comparison of SCM, SCME, and WINNER channel models," in *Proc. IEEE VTC2007-Spring*, Dublin, Ireland, Apr. 2007, pp. 413-417.

[11] 3GPP TR 25.996, "3rd Generation Partnership Project; Technical Specification Group Radio Access Network; Spatial channel model for MIMO simulations (Release 6)", V6.1.0, Sep. 2003.

[12] T. Jämsä, D. S. Baum, H. El-Sallabi, T. Rautiainen, C. Schneider, and P. Zetterberg, "Overview of WINNER channel modelling activities," in *Proc. 15th Meeting of the Wireless World Research Forum (WWRF)*, Paris, France, Dec. 2005.

[13] https://www.ist-winner.org/

[14] V. Erceg et al., "TGn channel models", IEEE 802.11-03/940r2, Jan. 2004.

[15] D. S. Baum, J. Salo, G. Del Galdo, M. Milojevic, P. Kyösti, and J. Hansen, "An interim channel model for beyond-3G systems", in *Proc. IEEE VTC 2005 Spring*, vol. 5, Stockholm, Sweden, May 2005, pp. 3132-3136.

[16] IST-2003-507581 WINNER D5.4, Final report on Link Level and System Level Channel Models v1.4, https://www.ist-winner.org.

[17] IST-WINNER D1.1.2 P. Kyösti, et al., WINNER II Channel Models, v1.2, Sep. 2007.

[18] EURO-COST 231, "Urban transmission loss models for mobile radio in the 900 and 1800 MHz bands," in *COST231*, TD(90) 119 Rev. 2, Sep. 1991.

[19] D. Gesbert and J. Akhtar, "Breaking the barriers of Shannon's capacity: An overview of MIMO wireless systems," *Telektronikk Telenor Journal*, Jan. 2002.

[20] K. Yu, M. Bengtsson, B. Ottersten, and M. A. Beach, "Narrowband MIMO channel modeling for LOS indoor scenarios," in *Proc. URSI General Assembly (URSI GA'2002)*, Maastricht, The Netherlands, Aug.

2002.

[21] M. Zhu, “On optimal IEEE802.11n schemes for maximum throughput performance of four 6x6 MIMO antenna configurations in measured indoor office environments”, *Master Thesis*, Department of Electrical and Information Technology, Lund University, Lund, Sweden, Apr. 2009.

[22] A. F. Molisch, *Wireless Communications*, Wiley, 2005.

[23] M. B. Knudsen and G. F. Pedersen, “Spherical outdoor to indoor power spectrum model at the mobile terminal,” *IEEE J. Sel. Areas Commun.*, vol. 20, no. 6, pp. 1156-1168. Aug. 2002.

[24] A. Yamamoto, T. Sakata, T. Hayashi, K. Ogawa, K. Sakaguchi, and J. I. Takada, “Procedure of designing the structural parameters of a spatial fading emulator with a Laplacian angular power spectrum of incoming wave,” in *COST2100*, TD(10) 10016, Athens, Greece, Feb. 2010.

Appendix

WINNER II CDL Channel Models

Table 1: Scenario B1 LOS CDL model, urban micro-cell environment.

Cluster #	Delay [ns]			Power [dB]			AoD [°]	AoA [°]	Ray power[dB]		Cluster ASD = 3°	Cluster ASA = 18°	XPR = 9 dB
1	0			0.0			0	0	-0.31*	-24.7**			
2	30	35	40	-10.5	-12.7	-14.5	5	45	-20.5				
3	55			-14.8			8	63	-27.8				
4	60	65	70	-13.6	-15.8	-17.6	8	-69	-23.6				
5	105			-13.9			7	61	-26.9				
6	115			-17.8			8	-69	-30.8				
7	250			-19.6			-9	-73	-32.6				
8	460			-31.4			11	92	-44.4				

* Power of dominant ray,

** Power of each other ray

Table 2: Scenario B1 NLOS CDL model, urban micro-cell environment.

Cluster #	Delay [ns]			Power [dB]			AoD [°]	AoA [°]	Ray power [dB]	Cluster ASD = 10°	Cluster ASA = 22°	XPR = 6 dB
1	0			-1.0			8	-20	-14.0			
2	90	95	100	-3.0	-5.2	-7.0	0	0	-13.0			
3	100	105	110	-3.9	-6.1	-7.9	-24	57	-13.9			
4	115			-8.1			-24	-55	-21.1			
5	230			-8.6			-24	57	-21.6			
6	240			-11.7			29	67	-24.7			
7	245			-12			29	-68	-25			
8	285			-12.9			30	70	-25.9			
9	390			-19.6			-37	-86	-32.6			
10	430			-23.9			41	-95	-36.9			
11	460			-22.1			-39	-92	-35.1			
12	505			-25.6			-42	-99	-38.6			
13	515			-23.3			-40	94	-36.4			
14	595			-32.2			47	111	-45.2			
15	600			-31.7			47	110	-44.7			
16	615			-29.9			46	-107	-42.9			

Table 3: Scenario B3 LOS CDL model, large indoor hall environment.

Cluster #	Delay [ns]			Power [dB]			AoD [°]	AoA [°]	Ray power [dB]		Cluster ASD = 5°	Cluster ASA = 5°	XPR = 9 dB
1	0			0.0			0	0	-0.32*	-24.5**			
2	0	5	10	-9.6	-11.8	-13.6	-23	-53	-19.6				
3	15			-14.5			-34	-79	-27.6				
4	25			-12.8			-32	-74	-25.8				
5	40			-13.7			33	76	-26.8				
6	40	45	50	-14.1	-16.4	-18.1	-35	80	-24.1				
7	90			-12.6			32	-73	-26.6				
8	130			-15.2			-35	80	-28.2				
9	185			-23.3			-43	-100	-36.4				
10	280			-27.7			47	-108	-40.7				

* Power of dominant ray,

** Power of each other ray

Table 4: Scenario B3 NLOS CDL model, large indoor hall environment.

Cluster #	Delay [ns]			Power [dB]			AoD [°]	AoA [°]	Ray power [dB]	Cluster ASD = 6°	Cluster ASA = 13°	XPR = 5 dB
1	0			-6.6			-16	-73	-19.6			
2	5	10	15	-3.0	-3.2	-7.0	0	0	-13.0			
3	5			-11.0			-21	-94	-24.0			
4	10	15	20	-4.3	-6.5	-8.2	-10	-46	-14.3			
5	20			-7.1			17	75	-20.1			
6	20			-2.7			-10	-46	-15.7			
7	30			-4.3			-13	-59	-17.3			
8	60			-14.1			-24	107	-27.1			
9	60			-6.2			-16	71	-19.2			
10	65			-9.1			19	86	-22.1			
11	75			-5.5			-15	67	-18.5			
12	110			-11.1			-21	95	-24.1			
13	190			-11.8			22	98	-24.8			
14	290			-17			-26	117	-30.1			
15	405			-24.9			-32	142	-37.9			

Table 5: Scenario B4 NLOS CDL model, outdoor to indoor environment.

Cluster #	Delay [ns]			Power [dB]			AoD [°]	AoA [°]	Ray power [dB]	Cluster ASD = 5°	Cluster ASA = 8°	XPR=9 dB
1	0	5	10	-3	-5.2	-7	0	0	-13			
2	0			-8.7			32	102	-21.7			
3	5			-3.7			-21	-66	-16.7			
4	10			-11.9			37	-119	-24.9			
5	35			-16.2			−43	139	-29.2			
6	35			-6.9			28	91	-19.9			
7	65	70	75	-3.4	-5.6	-7.3	-49	157	-13.4			
8	120			-10.3			-34	-111	-23.3			

9	125	-20.7	-49	157	-33.7			
10	195	-16	43	138	-29.1			
11	250	-21	49	158	-34			
12	305	-22.9	51	165	-35.9			

* AoD refer to angles of the indoor terminal and AoA refer to outdoor terminal

** Cluster ASD refer to indoor terminal and Cluster ASA refer to outdoor terminal

Table 6: Scenario C1 NLOS CDL mode, suburban environment.

Cluster #	Delay [ns]			Power [dB]			AoD [°]	AoA [°]	Ray power [dB]	Cluster ASD = 2°	Cluster ASA = 10°	XPR=4 dB
1	0	5	10	-3	-5.2	-7	0	0	-13			
2	25			-7.5			13	-71	-20.5			
3	35			-10.5			-15	-84	-23.5			
4	35			-3.2			-8	46	-16.2			
5	45	50	55	-6.1	-8.3	-10.1	12	-66	-16.1			
6	65			-14			-17	-97	-27			
7	65			-6.4			12	-66	-19.4			
8	75			-3.1			-8	-46	-16.1			
9	145			-4.6			-10	-56	-17.6			
10	160			-8			-13	73	-21			
11	195			-7.2			12	70	-20.2			
12	200			-3.1			8	-46	-16.1			
13	205			-9.5			14	-80	-22.5			
14	770			-22.4			22	123	-35.4			

Table 7: Scenario D1 NLOS CDL model, rural environment.

Cluster #	Delay [ns]			Power [dB]			AoD [°]	AoA [°]	Ray power [dB]	Cluster ASD = 2°	Cluster ASA = 3°	XPR=7 dB
1	0	5	10	-3	-5.2	-7	0	0	-13			
2	0			-1.8			-8	28	-14.8			
3	5			-3.3			-10	38	-16.3			
4	10	15	20	-4.8	-7	-8.8	15	-55	-14.8			
5	20			-5.3			13	48	-18.3			
6	25			-7.1			15	-55	-20.1			
7	55			-9			-17	62	-22			
8	100			-4.2			-12	42	-17.2			
9	170			-12.4			20	-73	-25.4			
10	420			-26.5			29	107	-39.5			